7. EXPERIMENTAL RESULTS AND DISCUSSION

The mass and energy balances in the model suppression pool are checked using equations 7.1. The energy increase in the pool is compared with the energy released from the steam generator, in this case the PUMA RPV.

$$\dot{Q}_{in} = \dot{Q}_{cond,pool} + \dot{Q}_{evap} + \dot{Q}_{loss} \tag{7.1}$$

where, $\dot{Q}_{in} = \dot{m}_s h_{fg} t$, $Q_{evap} = h_{evap}\left(T_{ww,g} - T_{ww,f}\right) A_{evap} t$,

and $\dot{Q}_{cond,pool} = M_{final} \cdot c_{p,f}\left(T_{ww,final}\right) \cdot T_{final} - M_{initial} \cdot c_{p,f}\left(T_{ww,initial}\right) \cdot T_{initial}$

In the above equation, h_{evap} is the evaporation heat transfer coefficient and A_{evap} is the area available for evaporation heat transfer form pool surface to gas space. In the actual prototype, $\dot{Q}_{evap}$ determines the steam contribution to the pressure in the SP gas space.

In the following sections the experimental results are discussed based on the test conditions discussed in Chapter 4.

7.1 2-Inch Vent Diameter Data

Experimental results for 2-inch diameter vent pipe injection cases are discussed here. There are 8 preliminary cases of experimental data that were discussed in Chapter 6, and in this report an additional 17 cases of experimental data are provided. The test results for the 2-inch vent pipe cases are summarized in Table 7.1. For all cases, a steam-air mixture is injected. The typical cases of T2-18 and T2-23 are depicted in detail. Cases T2-18 and T2-23 are for the lowest and highest mixture flow rates, respectively.

Case T2-18 has the steam flow rate of 13.8 g/s, the air mass fraction of 1.4%, and the initial pool temperature of 20.8 °C, and its temperature data in the suppression pool are shown in Figures 7.1 through 7.5. The pool water is fully mixed in this case as indicated by the bulk temperature. The injected air is sufficient to mix the entire pool.

However, the pool water temperature near the vent regions of the pool is consistently higher than that towards the far wall of the pool. Figure 7.1 shows the real-time temperature data of thermocouples T_109 and T_117 at the water surface. Their temperatures increase with significant fluctuations. Figures 7.2 and 7.3 show the vertical temperature distributions along the vent side and the pool side centerlines, respectively, for case T2-18. The temperature data of thermocouple T_222 fluctuates with high amplitudes at the injection point of the steam-air mixture and the temperature data of thermocouple T_220, which is at a higher elevation than T_222 (please refer to figure B.13), also fluctuates with lower amplitudes near the injection point. The temperature data of thermocouples T_223 and T_224 below the injection point show a stable profile with slightly lower temperature differences. All temperature data of thermocouples along the pool side centerline show a similar trend but with much reduced amplitudes. Figures 7.4 and 7.5 show the temperature profiles developing at the centerline and pool surface, respectively. Along the centerline, the fluctuation intensity is much higher near the vent exit than away from the vents. The temperatures at the injection point oscillate rapidly and in some cases a violent external chugging phenomenon happens. Chugging is caused by the steam coming into direct contact with the subcooled liquid and condensing so rapidly that it creates low pressure near the vent and the surrounding liquid volume rushes into the vent. A condensation shock occurs and in quick succession the steam venting pressure builds back up and becomes sufficient enough to expel the steam into the pool once again. This process is typically repeated within a time of less than one second. The surface of the pool water maintains a uniform temperature increase with slightly higher temperatures near the vent regions of the pool.

T2-23 is the case where the steam flow rate is 42.8 g/s, the air mass fraction is 11.5%, and the initial pool temperature is 29.1 °C, and its temperature data in the suppression pool are shown in Figures 7.6 through 7.10. The pool is fully mixed in this case also, and the presence of the high non-condensable mass fraction causes the pool to mix homogeneously. The overall temperature increase is higher in this case compared with the case T2-18 due to the higher injected steam-air mixture flow rate. Furthermore its temperature data of thermocouples T_222 and T_220 show higher values than those of

case T2-18. This may be due to the fact that the steam-air mixture provides a larger buoyancy flux to heat more the water nearer the injection point with higher steam-air mixture flow rate.

7.2 3-Inch Vent Diameter Data

Experimental results for 3-inch diameter vent pipe injection cases are discussed here. Fifty-five cases of experimental data are provided in this report. The test results for the 3-inch diameter vent pipe are summarized in Table 7.2. Experimental results are separately described for injection cases of pure steam and steam-air mixture. Both for the pure steam and for the steam-air mixture injection cases the phenomena of mixing, mixing-to-stratification transition, stratification, and stratification degradation are all observed under specific conditions. With an orifice in the vent pipe both single and double vent tests are performed. For the single vent case, partial stratification phenomenon is investigated under specific conditions. The transition from the mixing to stratification conditions are described quantitatively on a flow regime map for pure steam and steam-air mixture injection cases, separately, which are described in section 7.2.4.

7.2.1 *Pure Steam Injection*

The typical cases of T3-23, T3-24, T3-42, T3-27, T3-43, T3-47, and T3-50 are described here in detail. All of these cases show a common feature of vent oscillations indicated by the temperature response at the vent exit, which are shown by the response of nearby thermocouples such as T_222 and by flow visualization. T_222 is located at the vent exit where the steam comes into contact directly with the subcooled water.

Case T3-23 shows the typical result of a fully mixed case. It has the steam flow rate of 17.8 g/s, and the initial pool temperature of 31.1°C, and temperature data in the suppression pool are shown in Figures 7.11 through 7.15. Case T3-23 shows the similar

trend with the previous cases of T2-18 and T2-23. However, the affected region by the injected fluid is wider than the previous 2-inch diameter vent cases along the horizontal direction. Sometimes the hot temperature region is formed away from the vent exit due to the ejected hot water through the horizontal vent pipe as shown in Figure 7.14 (t =1000 seconds).

Case T3-24 shows the typical result of the mixing to stratification transition phenomenon. It has the steam flow rate of 16.4 g/s, and the initial pool temperature of 46.6 °C, and temperature data in the suppression pool are shown in Figures 7.16 through 7.20. The pool volume can be divided by the following three regimes; the upper volume above the injection point, the middle volume between the injection point and level 2, and the lower volume around level 1 to the bottom of the pool. The relative locations of each defined level within the pool are shown in Figure 4.4. In this case the pool water temperature begins to be sharply stratified within 1827 seconds. During this period only the upper volume of the pool above the injection vent removes the steam energy. This is indicated by the change in the slope of the temperature-time responses of thermocouples T_222, T_220 and T_219 as shown in Figure 7.17. The middle volume of the pool remains approximately constant at 66 °C as indicated by thermocouple T_223. The temperature of the lower volume of the pool below elevation 16.9 cm remains at approximately 61 °C, which is indicated by thermocouple T_223, until the termination of the experiment at 3166 seconds. The surface temperature shows little variation and is homogeneous due to the mixing processes within the pool as shown in Figure 7.16. The transition from mixing to stratification is shown in Figure 7.19.

Case T3-42 shows the typical result of the stratification phenomena. A steam flow rate of 13.0 g/s is used, with the initial pool temperature being 62.5 °C. The temperature data, for this case, inside the suppression pool are shown in Figures 7.21 through 7.25. The lower pool volume remains thermally inactive and remains at a constant temperature of about 62.5 °C throughout the run. The middle pool volume is also stratified after around 400 seconds at a temperature of around 65.5 °C.

Case T3-27 shows the typical result of a scenario in which the pool interior begins to stratify and after some time a stratification degradation phenomenon ensues. A steam flow rate of 19.5 g/s is used, and the initial pool temperature is 55.9 °C, and its temperature data for the suppression pool interior are shown in Figures 7.26 through 7.30. At 684 seconds the middle volume around level 2 begins to remain at a constant temperature of about 63.2 °C until around 1594 seconds when it gradually increases in temperature and once more participates in heat removal at around 2179 seconds, which is shown in Figure 7.28. However, for the remainder of the experiment some mild stratification between the upper pool volume above the vent and the middle pool volume is observed. Throughout the entire experiment the lower pool volume (elevation 16.9 cm) remains thermally inactive. The surface temperature, as shown in Figure 7.30, shows a high degree of homogeneity.

Case T3-43 also shows another typical result which exhibits the stratification and stratification degradation phenomena. It has the steam flow rate of 32.1 g/s, and the initial pool temperature of 49.1 °C, and its temperature data in the suppression pool are shown in figures 3.31 through 3.35. Case T3-43 show similar results with case T3-27 except for the larger fluctuation of temperature data due to the increased steam flow rate.

Case T3-47 shows the typical result which shows mixing, stratification, and stratification degradation phenomena altogether. It has the steam flow rate of 27.2 g/s, and the initial pool temperature of 42.3 °C, and temperature data in the suppression pool are shown in Figures 7.36 through 7.40. This case includes all of the phenomena that may be expected to happen during the suppression pool test. At the beginning of the experiment, the pool water is entirely mixed, and is stratified with the increase of the pool temperature due to the heat addition from the injected steam-air mixture. Finally the stratification is degraded due to the conduction of higher temperature region to lower temperature region.

Case T3-50 also shows another typical result which shows mixing, stratification, and stratification degradation phenomena. This case has a steam flow rate of 29.3 g/s, and

an initial pool temperature of 61.6 °C, and its temperature data in the suppression pool are shown in Figures 7.41 through 7.45. Case T3-50 show similar results with case T3-47.

7.2.2 *Steam-Air Mixture Injection*

The typical steam-air mixture injection test cases of T3-30, T3-51, T3-26 and T3-38 are described in detail in this section.

Case T3-30 shows a typical result of the full mixed phenomenon. This has a steam flow rate of 17.6 g/s, an air mass fraction of 2.86 %, and an initial pool temperature of 26.7 °C, with temperature data in the suppression pool shown in Figures 7.46 through 7.50. Case T3-30 is one in which the mixing is predominant in the vertical plane. However, across the width of the pool, there is more heating of the liquid nearer to the vent side than that away from the vent side or towards the pool side.

Case T3-51 shows the typical result of mixing to stratification transition phenomena. The steam flow rate is 12.3 g/s, the air mass fraction is 0.99 %, and the initial pool temperature is 27.2 °C. The temperature data inside the suppression pool are shown in Figures 7.51 through 7.55. In this case the pool water temperature is not as clearly stratified as case T3-24, which shows the typical mixing to stratification transition phenomenon for pure steam injection case. Also the middle pool volume is not stratified but following the mixing trend of the upper pool volume.

Case T3-26 shows the typical result of the stratification phenomena. The steam flow rate is 20.7 g/s, the air mass fraction is 0.33 %, and the initial pool temperature is 50.9 °C. The temperature data in the suppression pool are shown in Figures 7.56 through 7.60. The lower pool volume remains thermally inactive and remains at a temperature of about 51 °C throughout the run. The middle volume removes heat at the same rate as the upper volume above the injection vent. However, there is a constant temperature difference of around 1.4 °C between the upper volume and the middle volume, as shown

in Figure 7.22. The regions near the vent side show a higher temperature than towards the pool side, which can be seen in the vertical temperature profile development indicated by the temperature contour maps of Figures 7.59 and 7.60.

Case T3-38 shows the typical result of the stratification and stratification degradation phenomena. A steam flow rate of 11.6 g/s is used and the air mass fraction is 0.48 %. The initial pool temperature of 52.9 °C, and temperature data in the suppression pool are shown in figures 3.61 through 3.65. Case T3-38 depicts another scenario in which the lower pool volume does not participate in heat removal until the middle and upper pool starts to become saturated and a heat transfer from the upper volume begins to propagate down towards the bottom of the pool. From 3354 to 4587 seconds, the stratification degradation occurs. The stratification degradation is neither smooth nor gradual, but unsteady oscillations are predominant with no fixed amplitude, as the lower part of the pool heats up. This phenomenon can be seen in Figure 7.63. Figures 7.61 through 7.65 show the real-time temperature data and instantaneous temperature maps for the vertical centerline plane and pool surface.

7.2.3 *Double Venting of Steam and Steam-Air Mixtures*

Cases T-53, T-54 and T-55 are experiments that were performed with an orifice inserted in the vent lines just upstream of the pool (Figure 4.8). Typical results for single top vent injection (case T3-53) and double vent injection (case T3-55) are shown.

Case T3-53 shows the typical result of partial stratification phenomenon. A steam flow rate of 12.8 g/s is used, and the initial pool bulk temperature is 25.7 °C. The temperature data of the suppression pool interior are shown in Figures 7.66 through 7.70. The temperature data of thermocouple T_223 show that they are fluctuating and go between those of T_222 and T_224.

Case T3-55 shows the typical result of double venting case which shows full mixing. A steam flow rate of 12.5 g/s is used, and the initial pool bulk temperature is 52.9°C. In this case the pool mixing shows the similar phenomenon described previously with the single vent case except that the temperatures around two vent locations are high with fluctuating amplitudes. The temperature data of the suppression pool interior are shown in Figures 7.71 through 7.75. For the double venting case, it was observed that there were in fact two continuous injection streams. However, under the flow rates indicated, there still existed periods of violent external chugging when the condensing effluent near the vent was forced back into the vent pipe but were prevented from completely backing into the vent pipe due to the restriction of the small area of the orifice. Therefore, unwanted vibrations were introduced but were not too large to cause any significant effect on the mixing phenomenon observed inside the pool. The temperature profile maps show that in some instances, two continuous venting did not always occur and only during brief periods venting synchronization occurred. The top venting was characterized by a two-phase steam mixture effluent whilst the condition of effluent from the lower venting was periodically changed between two phase mixture and single phase hot liquid.

7.2.4 *Regime Transition Maps*

The transition from the mixed to stratified conditions for pure steam cases are described in Figure 7.76. The transition conditions are defined in test cases where transition from mixed to stratified condition occurs. Although the pool water was fully mixed at the beginning, the temperatures in layers 1 and 2 become stratified or show very little changes with the variation of time as the pool temperature increases due to the condensation of the injected steam. At the low steam mass fluxes of around 2.5 kg/m^2s the pool temperatures in layers 1 and 2 become stratified at temperatures of around 64 and 70 °C, respectively. However it is more easily stratified at higher steam mass flux when the pool temperature is at the same condition. In general for the pure steam

injection case transition easily occurs when the steam mass flux is higher and the initial pool temperature is lower.

The transition from the mixed to stratified conditions for steam-air injection cases are described in Figures 7.77 and 7.78. In the steam-air injection cases level 2 is always mixed with a certain temperature gap from the level above the injection point, which is different from the phenomena occurred in pure steam injection cases where two layers are stratified with a certain time delay. Figure 7.77 shows the mixing to stratification transition in terms of steam mass flux and air mass flow rate of the injected mixture. When the air mass flow rate is above 0.12 g/s with the steam mass flux of around 2.5 kg/m^2-s, the pool water temperature always maintains a mixing condition throughout the test period, while it maintains a stratified condition below the air mass flow rate of 0.1 g/s. As the steam mass flux increases, the air mass flow rate at the transition point to stratification increases a little to 0.2 g/s. Figure 7.78 shows the mixing to stratification transition in terms of pool water temperature and air mass flow rate of the injected mixture. It shows that both the minimum air mass flow rate for the cases of mixing and the maximum value for the cases of stratification are around 0.12 g/s. In general for steam-air mixture injection case the transitional behavior is mainly dependent on the air mass flow rate of the injected mixture but the dependency on the pool water temperature can not be found with the present data.

7.2.5 *Flow Visualization*

Figures 7.79 and 7.80 show images acquired from the high speed camera, taken at window number 8, for pure steam injection (17.8 g/s mass flow rate) and steam-air injection (17.8 g/s mass flow rate and 0.5 % air) cases respectively. Refer to Figure 4.3 which indicates the location of windows 8 and 10 where the flow visualization images using a high speed camera are reported. The pure steam case shows that an inertia-dominated jet-plume forms and propagates towards the far wall of the pool where a 'semi-toroidal' ring forms around the jet-plume comprising of condensing vapor in the upper half of the torroidal cell. When steam-air is injected, the toroid forms and persists

for certain duration and is more symmetric at the periphery. Due to the larger buoyancy introduced by the air, it propagates upwards to the pool surface and never reaches the pool far wall. In the 2-inch case, when a large buoyancy flux is introduced, a vortex pair forms under certain conditions (Figures 6.18 and 6.20). However, this was not observed for the 3-inch case since in this larger vent diameter case the effluent has more width to spread and only a single vortex or toroid forms.

7.3 Thermal-Hydraulic Calculations at Vent Exit

For flow of a compressible fluid in a conduit, the steam partial pressure can be obtained from the following relation (Holland et al., 1995):

$$\int_1^2 \frac{dP}{V} + G^2\left[\ln\left(\frac{V_2}{V_1}\right) + \frac{2fL}{D}\right] \tag{7.2}$$

where 1 and 2 represent inlet and exit conditions respectively of the piping system (see Figure 4.6). G is the steam mass flux in kg/m^{2}s, f is friction factor, and D is the pipe diameter (2" routing pipe). For isothermal conditions we have:

$$\int_1^2 \frac{dP}{V} = \frac{P_2^2 - P_1^2}{2P_1V_1} \tag{7.3}$$

and since PV = constant, then

$$\ln\left(\frac{V_2}{V_1}\right) = \ln\left(\frac{P_1}{P_2}\right) \tag{7.4}$$

For steam:

$$P_1V_1 = \frac{RT}{M} = \frac{8314.3\dfrac{J}{kmol.K} \times T^oK}{18\dfrac{kg}{kmol}} \tag{7.5}$$

Then, equation 7.2 can be written:

$$\ln\left(\frac{P_1}{P_2}\right) = \frac{1}{G^2}\left[\frac{P_1^2 - P_2^2}{2P_1V_1}\right] - \frac{2fL}{D} \tag{7.6}$$

The friction factor, based on the Moody chart, for turbulent flow is given by:

$$f = \frac{1.325}{\left[\ln\left(\frac{e}{3.7D} + \frac{5.74}{\mathrm{Re}^{0.9}}\right)\right]^2} \tag{7.7}$$

In equation 3.7, e is the roughness parameter for a stainless steel conduit taken to be 4.5 x 10^{-5} m, Re is the steam Reynolds number, and the total length of the steam supply line to the vent exit is L = 8.84 m (see isometric drawing Figure 4.6, for pipe length information).

The total mixture pressure is obtained from the following (Norman, et al., 2005)

$$P_m = P_s\left[\sqrt{\frac{R_a}{R_s}\left(\frac{x}{1-x}\right)} + 1\right] \tag{7.8}$$

where R_a = 286.9 J/kgK, and R_s = 455 J/kgK, and x is the non-condensable mass fraction. The steam outlet pressure and mixture pressure are given in Tables 7.1 and 7.2 for all cases.

In calculating the average pool temperature, the pool was divided in to 3 regions defined by 3 heights. The regions are defined from by height as region 1 = 0 to 0.304 m; region 2 = 0.304 m to 0.738 m; and region 3 = 0.738 m to 1.211 m; where 0 m represents the zero water level or bottom of the pool. The temperatures in these 3 volumes were then averaged. The initial and final average temperatures are summarized for each experiment in Tables 7.1 and 7.2.

Table 7.1 Summary of SP tests using 2 inch injection pipe*

CASE	Duration (sec)	steam mass flow rate (g/s)	air mass flow rate (g/s)	Pool init average Temp (°C)	Pool final average Temp (°C)	Pool final water level (m)	Steam Reynolds number	Steam Inlet Temp (°C)	Steam Inlet Pressure (kPa)	Steam Outlet Pressure (kPa)	Steam Outlet Vol. rate (m^3/s)	Gas Mixture Pressure (kPa)
T2-09	1860	17.0	1.207	37.6	50.5	1.257	23839	101.7	107.6	106.8	0.0271	129.4
T2-10	1888	23.6	0.302	18.7	36.2	1.273	24409	101.7	107.7	106.1	0.0378	115.6
T2-11	1790	24.2	0.302	35.8	54.1	1.280	23986	104.0	116.7	115.1	0.0359	125.3
T2-12	1845	23.6	7.499	24.3	39.7	1.251	23784	101.8	108.1	106.6	0.0377	154.3
T2-13	1848	23.4	7.499	39.1	57.3	1.270	23992	102.9	112.4	110.9	0.0360	160.8
T2-14	1795	24.4	7.499	55.7	72.7	1.270	25176	103.8	115.8	114.3	0.0365	164.6
T2-15	1804	23.4	0.302	52.4	66.1	1.273	26190	102.2	109.8	108.3	0.0368	118.0
T2-16	1848	42.9	0.504	21.5	57.3	1.330	21479	104.6	119.2	114.8	0.0639	124.7
T2-17	1264	43.3	0.526	55.9	80.0	1.299	24187	108.5	136.3	132.4	0.0564	143.9
T2-18	1815	13.8	0.202	20.8	30.1	1.241	23991	101.3	106.0	105.4	0.0222	115.6
T2-19	1812	13.4	5.000	25.2	33.2	1.243	23643	101.2	106.0	105.4	0.0216	156.6
T2-20	1799	12.9	5.000	33.0	41.8	1.235	26605	102.4	110.4	109.9	0.0200	164.3
T2-21	1794	13.9	0.202	32.7	42.9	1.251	26777	101.3	106.2	105.6	0.0224	115.7
T2-22	1806	13.8	0.202	42.7	52.9	1.248	37597	102.2	109.8	109.2	0.0215	119.7
T2-23	1857	42.8	5.549	29.1	61.6	1.316	18113	101.9	108.4	103.6	0.0701	133.2
T2-24	1048	42.5	5.549	59.8	79.9	1.286	25793	104.1	117.2	112.8	0.0643	145.1
T2-25	1866	14.8	5.000	39.5	50.2	1.248	21237	101.4	106.7	106.1	0.0237	155.0

* In all these cases the pool was mixed and no notable thermal stratification was observed.

Table 7.2 Summary of SP tests using 3 inch injection pipe

CASE	Duration (sec)	steam mass flow rate (g/s)	air mass flow rate (g/s)	Pool init average Temp (°C)	Pool final average Temp (°C)	Pool final water level (m)	Steam Reynolds number	Steam Inlet Temp (°C)	Steam Inlet Pressure (kPa)	Steam Outlet Pressure (kPa)	Steam Outlet Vol. rate (m^3/s)	Gas Mixture Pressure (kPa)
T3-01	1852	12.1	0.000	22.7	31.5	1.226	23839	101.2	105.7	105.3	0.0195	105.3
T3-02	1924	12.4	0.089	26.8	34.2	1.248	24409	101.5	106.9	106.4	0.0198	113.6
T3-03	1824	12.2	0.089	40.4	49.6	1.245	23986	101.9	108.6	108.1	0.0192	115.5
T3-04	1873	12.1	0.456	47.3	58.6	1.283	23784	102.0	108.9	108.4	0.0190	125.1
T3-05	1782	12.2	0.456	57.6	66.1	1.239	23992	101.8	108.2	107.8	0.0193	124.3
T3-06	1874	12.8	0.180	35.9	42.1	1.239	25176	101.8	108.0	107.5	0.0203	117.6
T3-07	1832	13.3	0.135	29.8	37.1	1.235	26190	101.4	106.4	105.9	0.0214	114.3
T3-08	1581	10.9	0.108	29.3	36.0	1.248	21479	101.1	105.5	105.1	0.0176	113.4
T3-09	1839	12.3	0.000	44.6	55.2	1.251	24187	101.9	108.3	107.9	0.0194	107.9
T3-10	1805	12.2	0.000	48.9	58.5	1.248	23991	101.9	108.3	107.8	0.0193	107.8
T3-11	1778	12.0	0.089	48.3	58.9	1.248	23643	101.2	105.7	105.2	0.0194	112.4
T3-12	1781	13.5	0.089	57.7	66.9	1.243	26605	101.1	105.4	104.8	0.0219	111.6
T3-13	1973	13.6	0.065	21.1	28.1	1.246	26777	101.4	106.6	106.1	0.0218	111.9
T3-14	1806	19.1	0.086	22.5	36.0	1.241	37597	101.5	106.9	105.9	0.0307	111.5
T3-15	1806	9.2	0.125	34.8	40.6	1.260	18113	101.4	106.7	106.4	0.0147	116.3
T3-16	1805	13.1	0.948	36.0	44.5	1.251	25793	101.4	106.6	106.1	0.0210	128.7
T3-17	1800	10.8	0.970	48.6	57.8	1.251	21237	101.9	108.3	108.0	0.0170	133.7

CASE	Duration (sec)	steam mass flow rate (g/s)	air mass flow rate (g/s)	Pool init average Temp (°C)	Pool final average Temp (°C)	Pool final water level (m)	Steam Reynolds number	Steam Inlet Temp (°C)	Steam Inlet Pressure (kPa)	Steam Outlet Pressure (kPa)	Steam Outlet Vol. rate (m^3/s)	Gas Mixture Pressure (kPa)
T3-18	1804	22.4	0.086	24.8	41.5	n/a	43945	102.7	111.6	110.2	0.0346	115.6
T3-19	1805	21.6	0.086	43.4	60.8	n/a	42270	103.6	115.2	113.9	0.0324	119.6
T3-20	1809	24.4	0.151	34.3	52.8	1.311	47943	102.1	109.4	107.8	0.0385	114.5
T3-21	1811	25.4	0.000	22.7	43.9	1.267	49904	102.2	109.5	107.8	0.0401	107.8
T3-22	1822	25.4	0.000	42.6	61.9	1.308	49806	102.9	112.3	110.6	0.0392	110.6
T3-23	1835	17.8	0.000	31.1	46.4	1.260	34930	102.6	111.2	110.3	0.0275	110.3
T3-24	3166	16.4	0.000	46.4	68.1	1.295	32150	103.0	112.6	111.9	0.0250	111.9
T3-25	2119	20.6	0.129	27.9	47.8	1.286	40432	102.5	111.0	109.8	0.0320	116.7
T3-26	1749	20.7	0.069	50.9	65.6	1.276	40629	102.5	110.9	109.7	0.0321	114.8
T3-27	3045	19.5	0.000	55.9	76.3	1.299	38365	101.7	107.6	106.5	0.0311	106.5
T3-28	1824	25.7	0.181	27.4	49.3	1.283	50496	102.2	109.5	107.6	0.0406	114.8
T3-29	3696	13.5	0.000	55.8	75.6	1.270	26510	102.4	110.3	109.7	0.0210	109.7
T3-30	2176	17.6	0.517	26.6	42.2	1.264	34648	101.5	106.8	105.9	0.0283	120.3
T3-31	2013	12.1	0.000	43.7	54.0	1.264	23792	101.9	108.5	108.0	0.0191	108.0
T3-32	1819	11.1	0.056	41.7	50.0	1.248	21824	101.9	108.5	108.1	0.0175	114.2
T3-33	3008	12.4	0.000	40.3	55.6	n/a	24381	101.9	108.5	108.0	0.0195	108.0
T3-34	4126	15.8	0.000	53.2	71.6	1.289	31080	101.7	107.9	107.1	0.0251	107.1
T3-35	4355	12.5	0.000	43.4	65.7	1.318	24455	103.7	115.6	115.1	0.0186	115.1
T3-36	1881	12.2	0.196	32.8	43.4	1.251	23974	102.1	109.3	108.8	0.0191	119.8

CASE	Duration (sec)	steam mass flow rate (g/s)	air mass flow rate (g/s)	Pool init average Temp (°C)	Pool final average Temp (°C)	Pool final water level (m)	Steam Reynolds number	Steam Inlet Temp (°C)	Steam Inlet Pressure (kPa)	Steam Outlet Pressure (kPa)	Steam Outlet Vol. rate (m^3/s)	Gas Mixture Pressure (kPa)
T3-37	1825	12.6	0.052	42.9	51.9	1.251	24764	102.1	109.1	108.6	0.0198	114.1
T3-38	4827	11.6	0.056	52.9	77.2	1.305	22791	102.2	109.5	109.1	0.0181	115.1
T3-39	1908	11.2	0.101	30.3	40.0	1.248	22035	101.7	107.6	107.2	0.0178	115.3
T3-40	1862	12.1	0.151	40.9	51.5	1.251	23778	102.1	109.3	108.8	0.0189	118.5
T3-41	2357	12.2	0.116	50.4	63.6	1.264	23952	102.4	110.5	110.1	0.0189	118.6
T3-42	1625	13.0	0.000	63.1	68.5	1.248	25560	101.9	108.5	108.0	0.0205	108.0
T3-43	1477	32.1	0.000	49.1	67.6	1.292	62985	102.6	111.4	108.7	0.0503	108.7
T3-44	1384	15.1	0.101	41.1	49.7	1.260	29699	101.8	108.0	107.4	0.0239	114.3
T3-45	1467	10.1	0.050	50.3	57.1	1.241	19882	101.5	106.9	106.5	0.0161	112.4
T3-46	2019	9.3	0.026	55.3	60.6	1.238	18301	101.6	107.3	107.1	0.0148	111.5
T3-47	2455	27.2	0.000	42.2	70.6	1.321	53378	102.6	111.2	109.2	0.0424	109.2
T3-48	5443	12.4	0.082	47.3	75.8	1.318	24394	101.7	107.7	107.3	0.0197	114.2
T3-49	2675	27.0	0.000	25.3	61.3	1.327	52736	104.3	118.0	116.2	0.0398	116.2
T3-50	1720	29.3	0.000	61.5	84.7	1.311	57134	104.9	120.5	118.4	0.0424	118.4
T3-51	3201	12.3	0.123	26.9	43.4	1.267	24206	101.6	107.3	106.8	0.0196	115.3
T3-52	2312	28.6	0.123	43.3	73.7	1.308	55876	104.2	117.6	115.5	0.0423	121.5
T3-53	1823	12.8	0.000	25.7	34.1	1.248	24482	112.0	153.1	152.7	0.0146	152.7
T3-54	4032	12.1	0.123	34.4	57.4	1.289	23097	112.7	156.9	156.5	0.0135	169.1
T3-55	2336	12.5	0.123	52.9	65.3	1.289	24316	105.8	124.2	123.7	0.0174	133.5

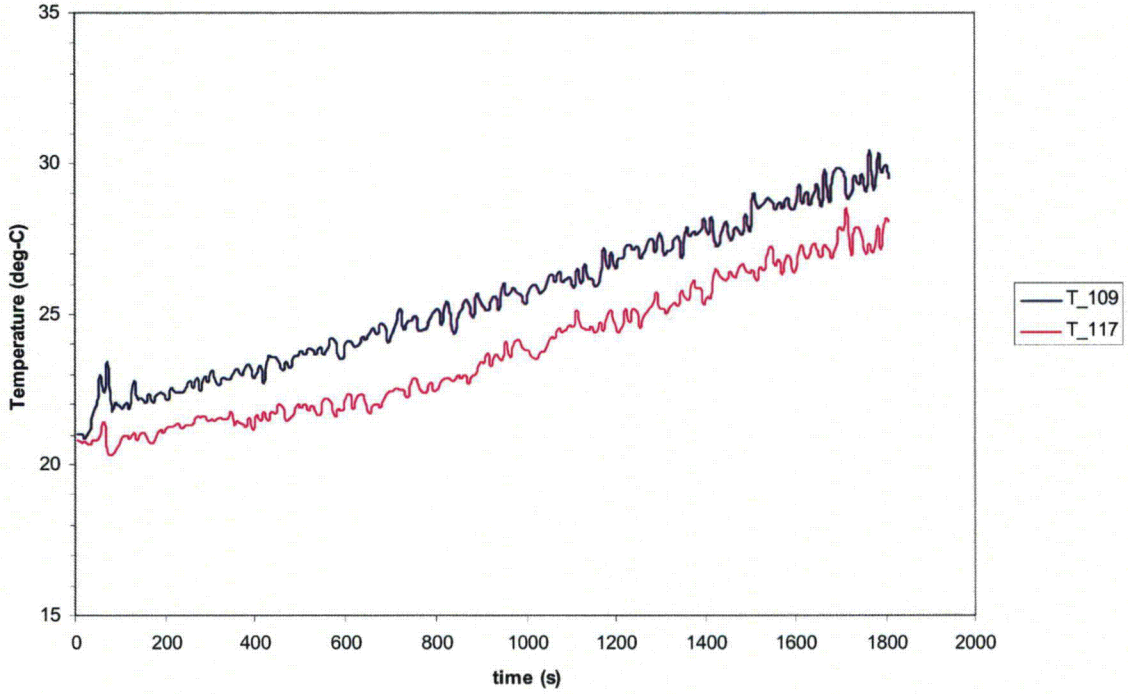

Figure 7.1 Real-time temperature data at the water surface for case T2-18†
†Refer to Table 7.1 for test conditions

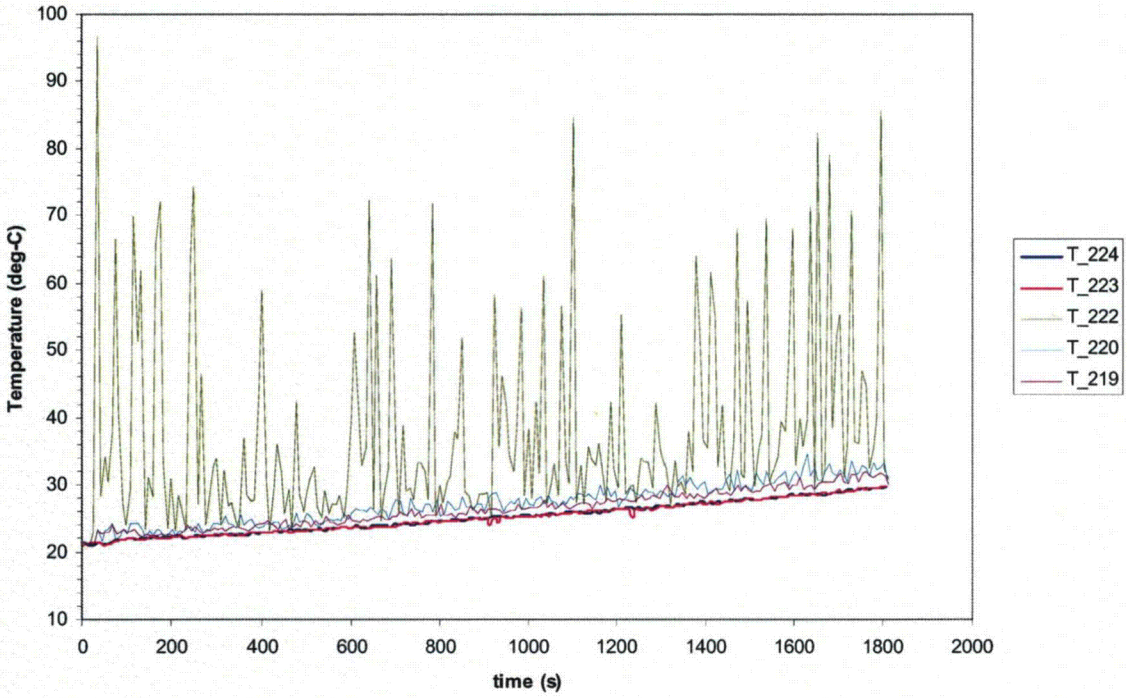

Figure 7.2 Vertical temperature distribution along the vent side centerline for case T2-18†

†Refer to Table 7.1 for test conditions

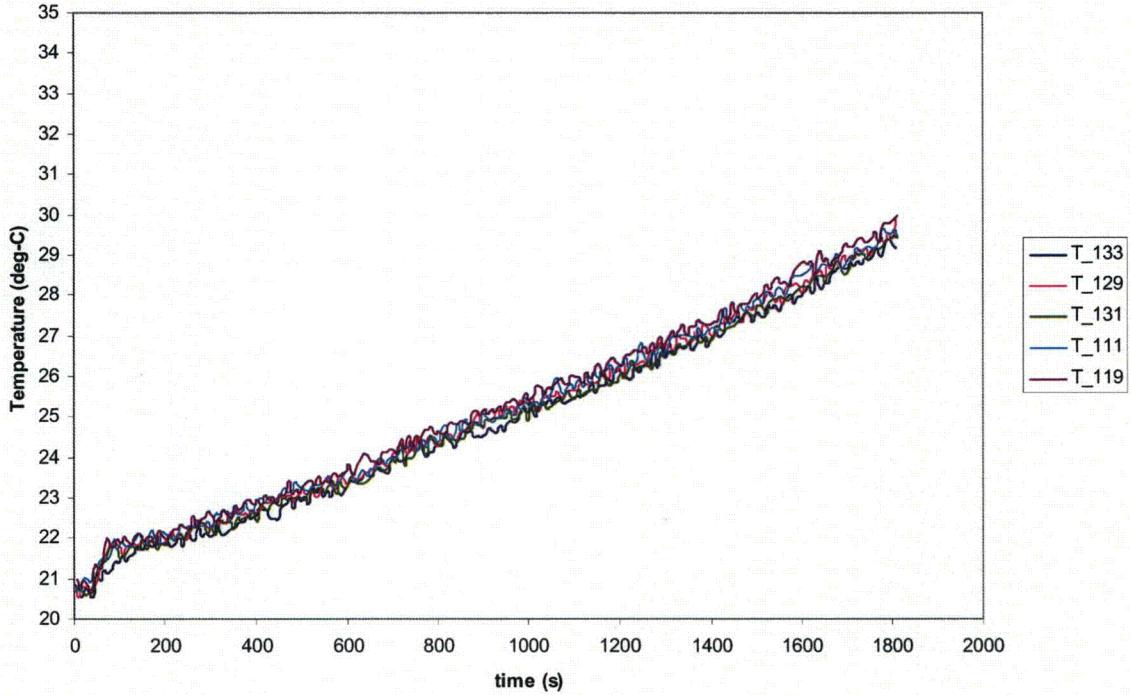

Figure 7.3 Vertical temperature distribution along the pool side centerline for case T2-18†

†Refer to Table 7.1 for test conditions

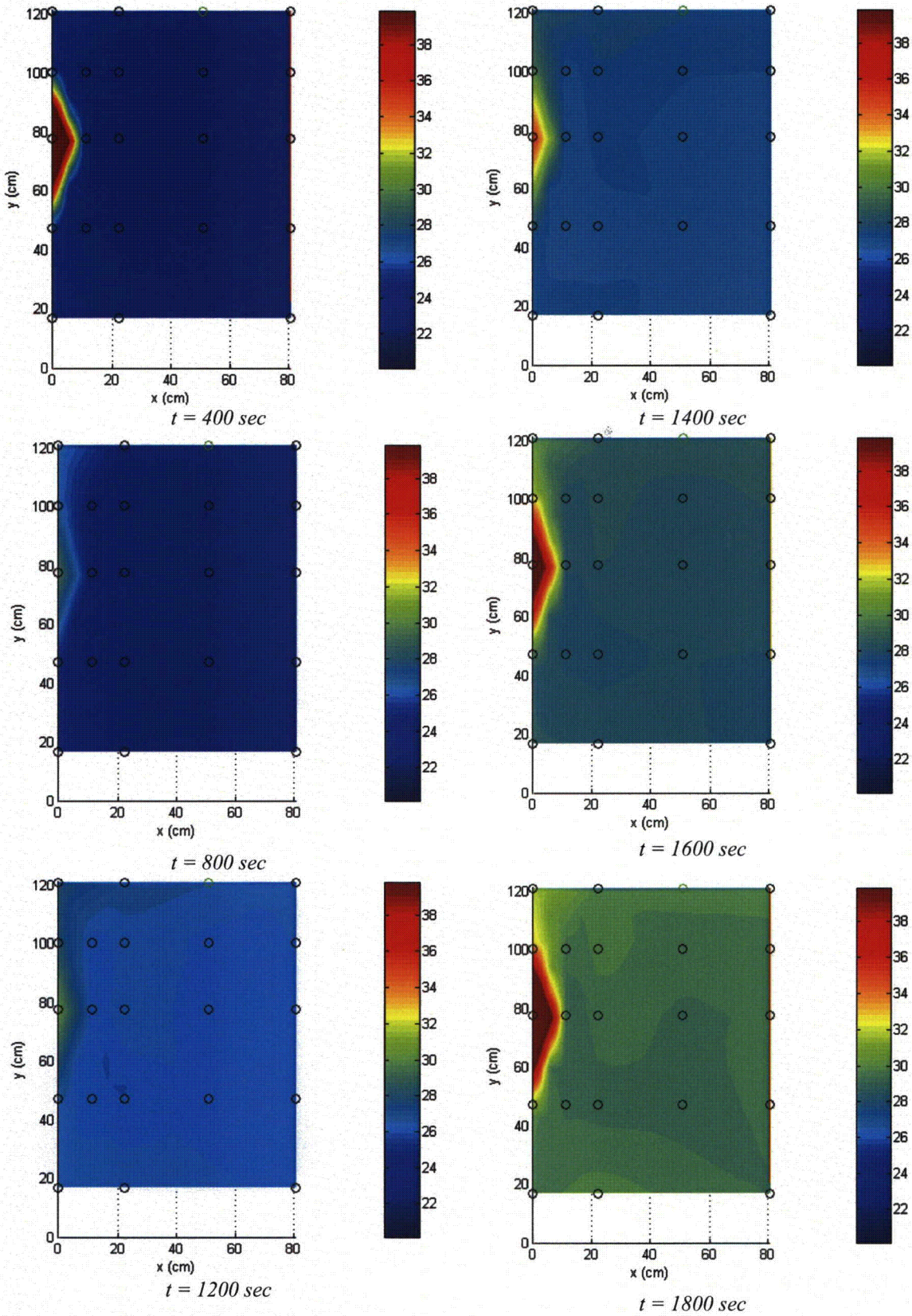

Figure 7.4 Temperature profile development along the pool vertical center plane for case T2-18

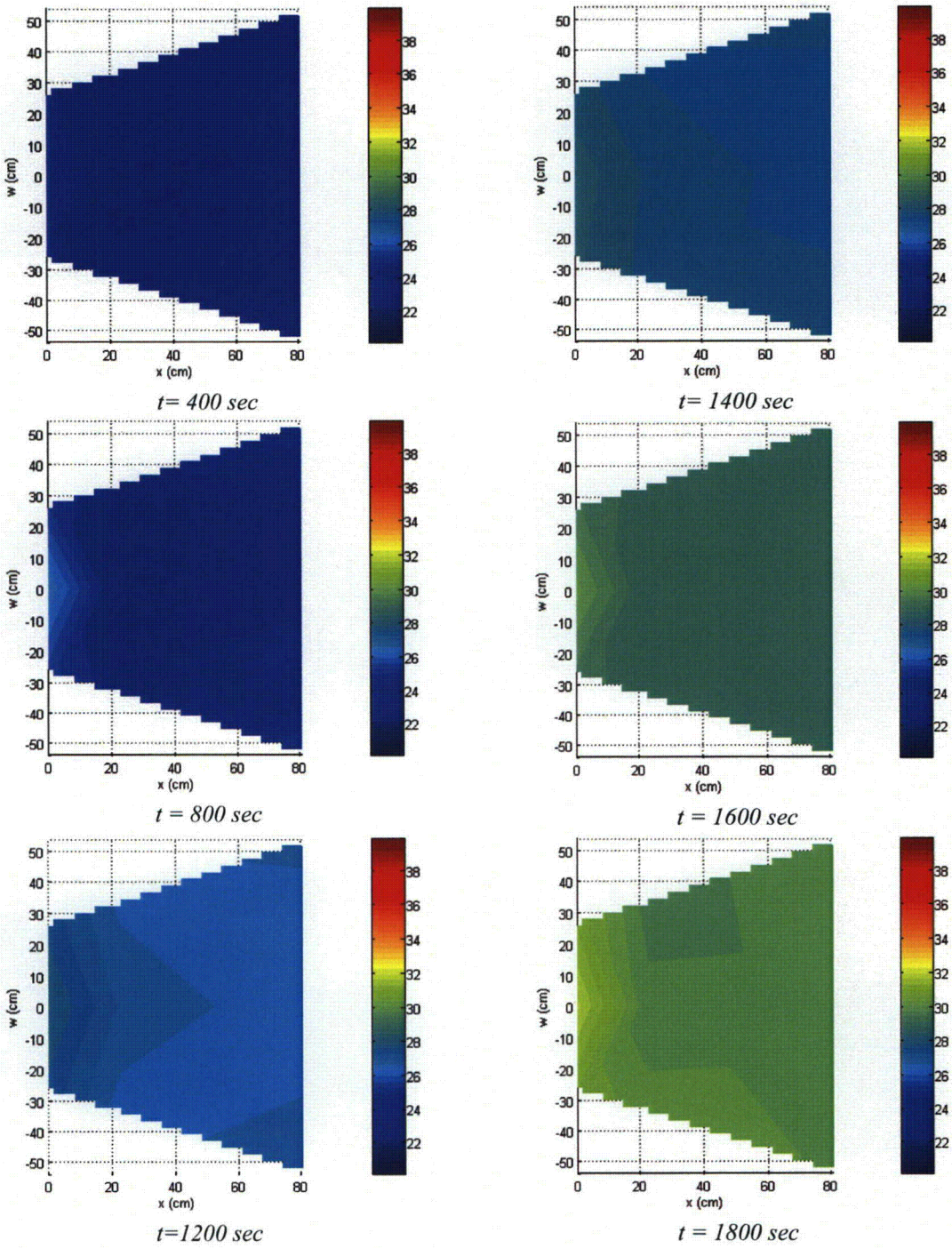

Figure 7.5 Temperature profile development along the pool surface for case T2-18

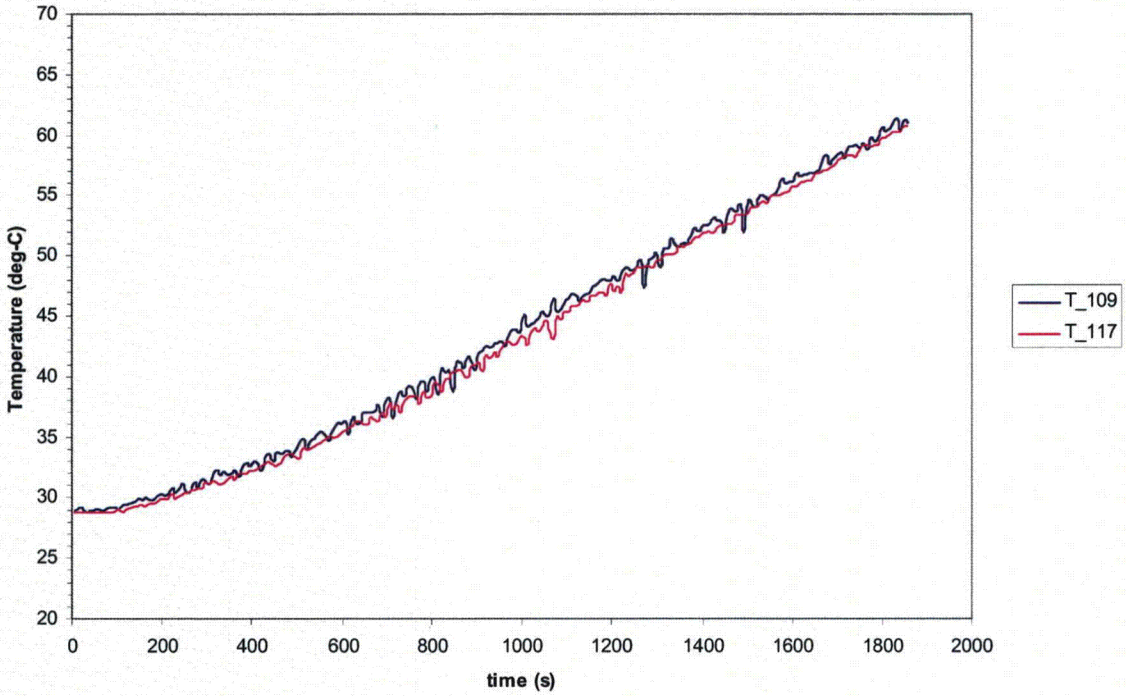

Figure 7.6 Real-time temperature data at the water surface for case T2-23†
†Refer to Table 7.1 for test conditions

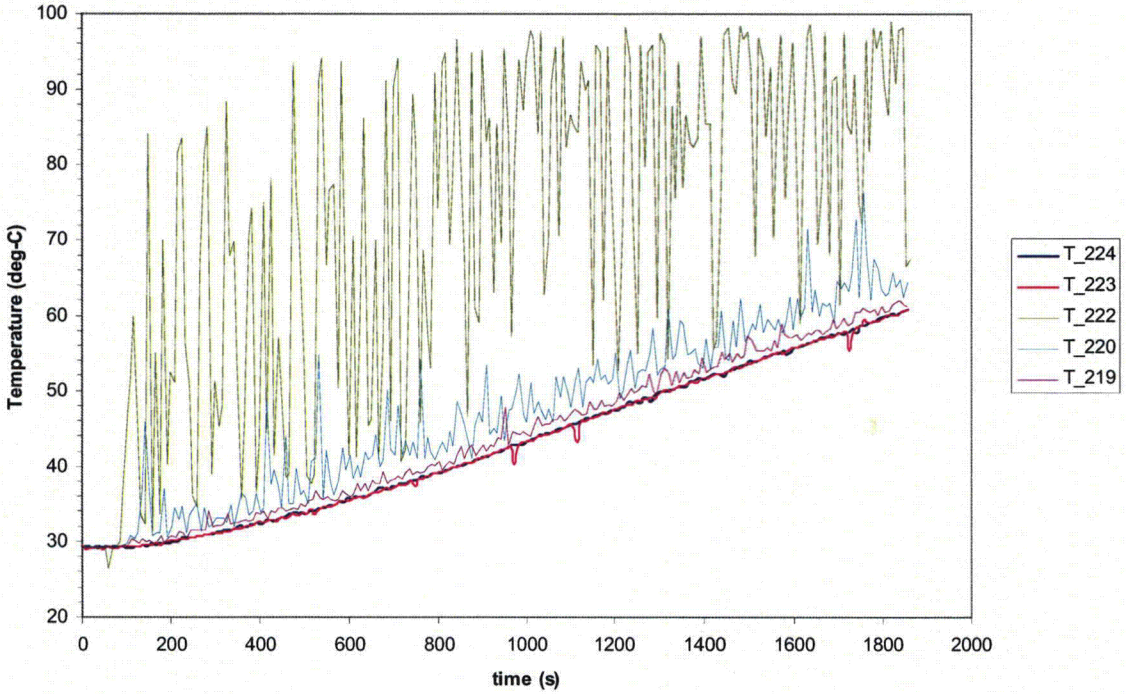

Figure 7.7 Vertical temperature distribution along the vent side centerline for case T2-23†

†Refer to Table 7.1 for test conditions

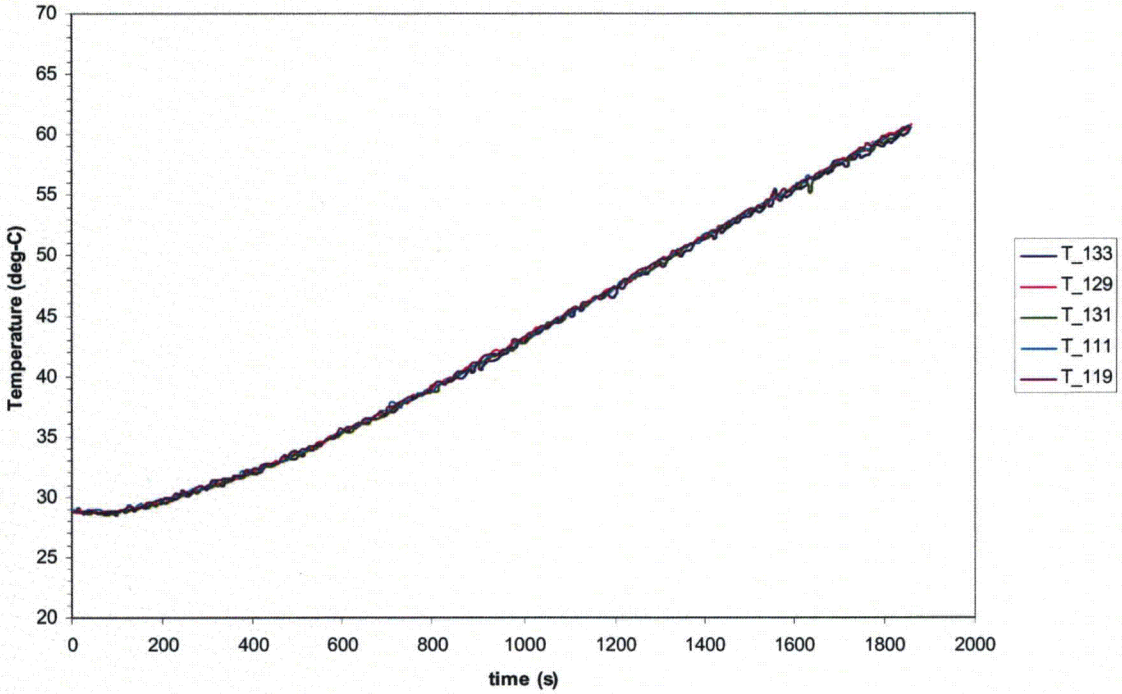

Figure 7.8 Vertical temperature distribution along the pool side centerline for case T2-23†

†Refer to Table 7.1 for test conditions

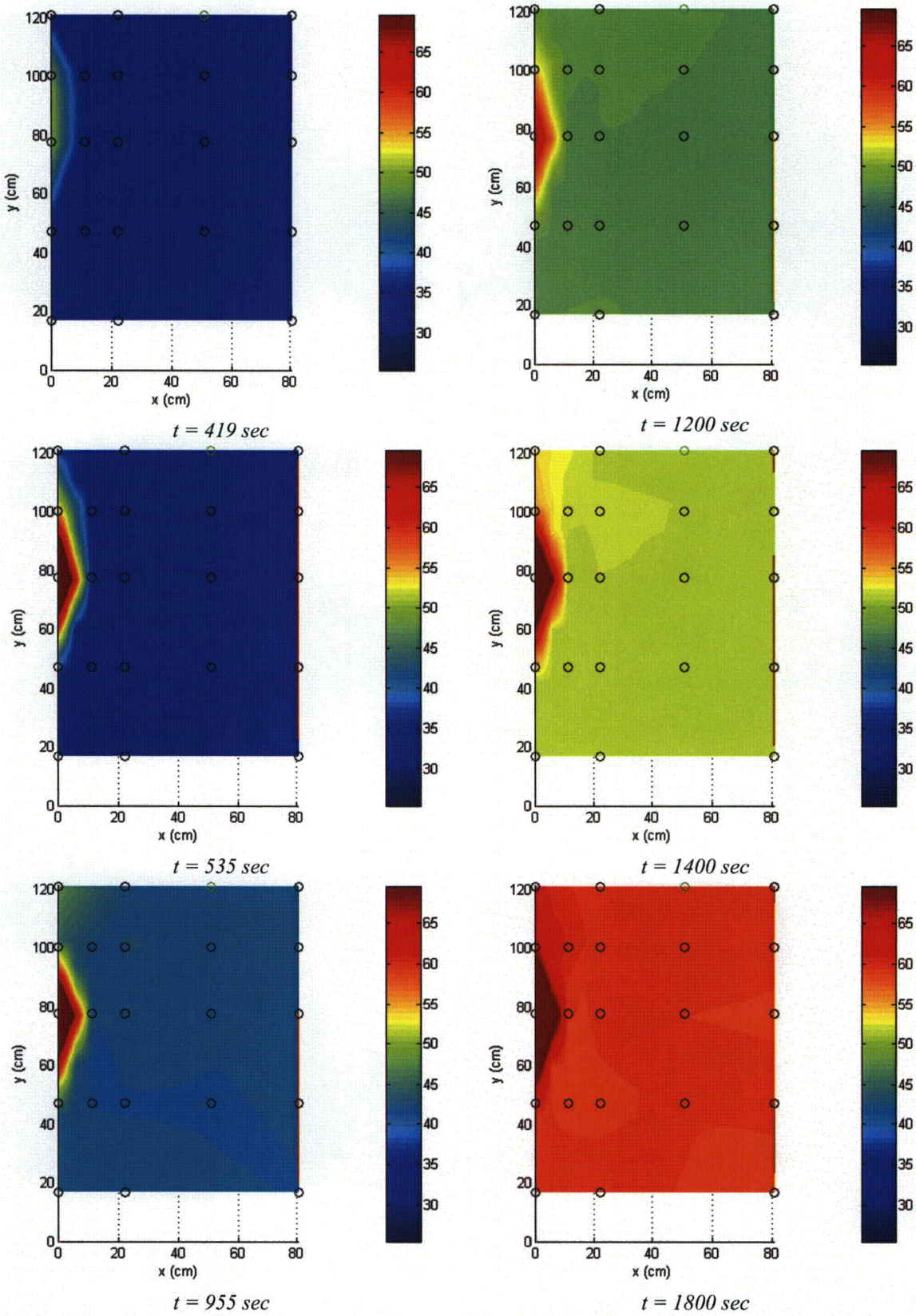

Figure 7.9 Temperature profile development along the pool vertical center plane for case T2-23

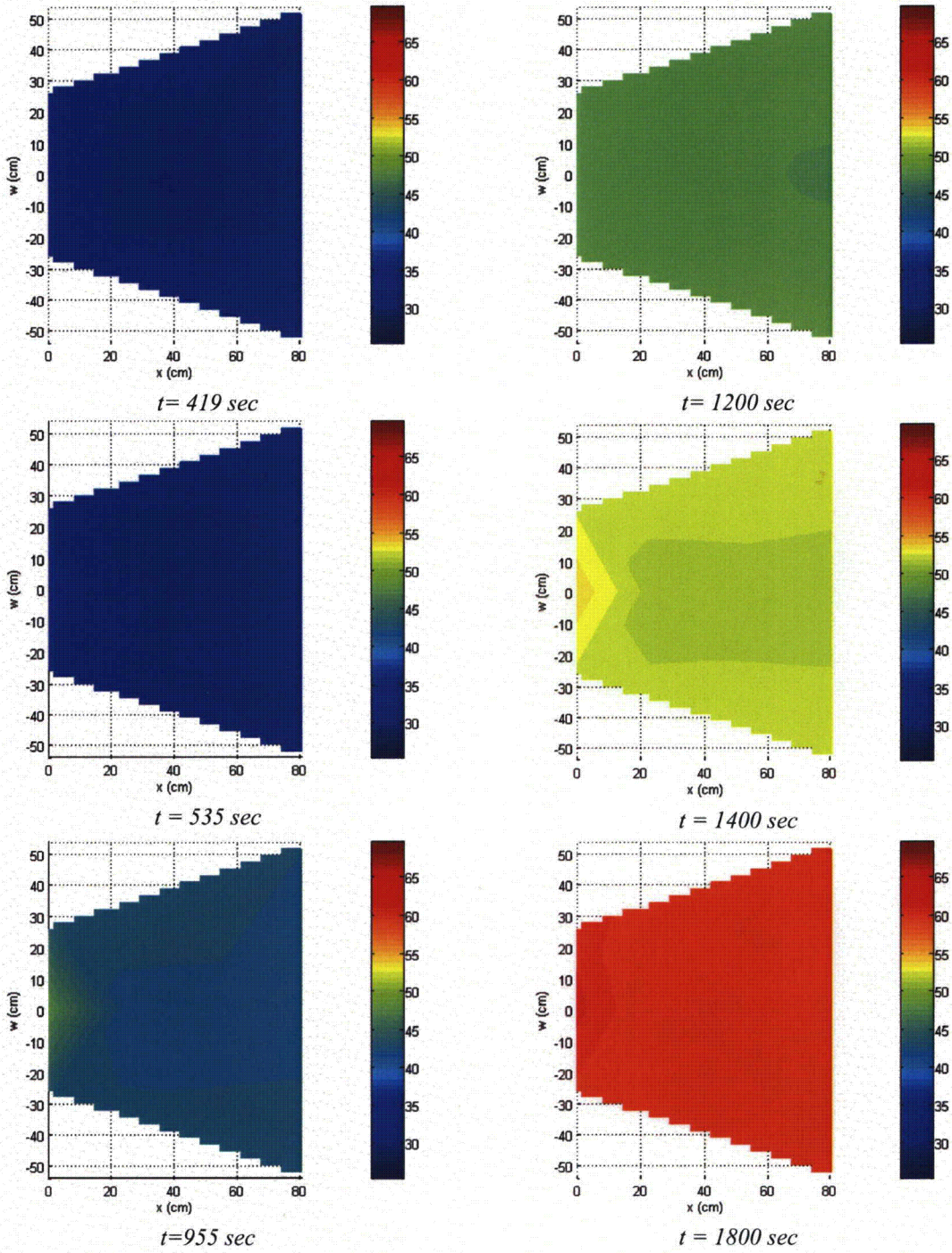

Figure 7.10 Temperature profile development along the pool surface for case T2-23

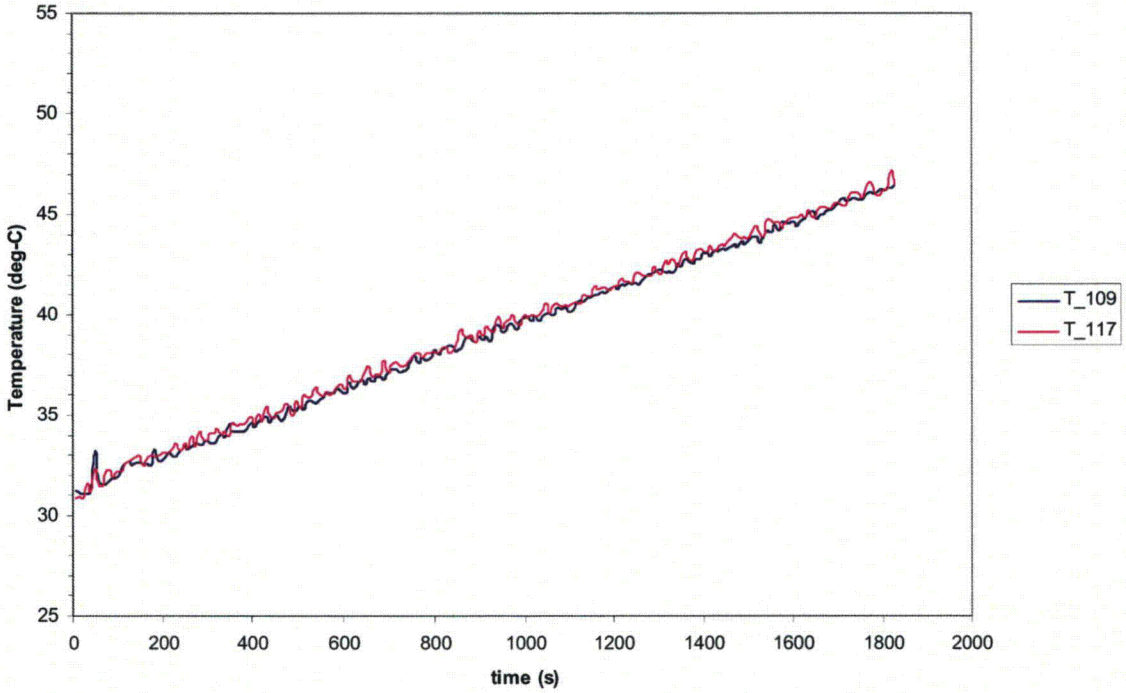

Figure 7.11 Real-time temperature data at the water surface for case T3-23†
†Refer to Table 7.2 for test conditions

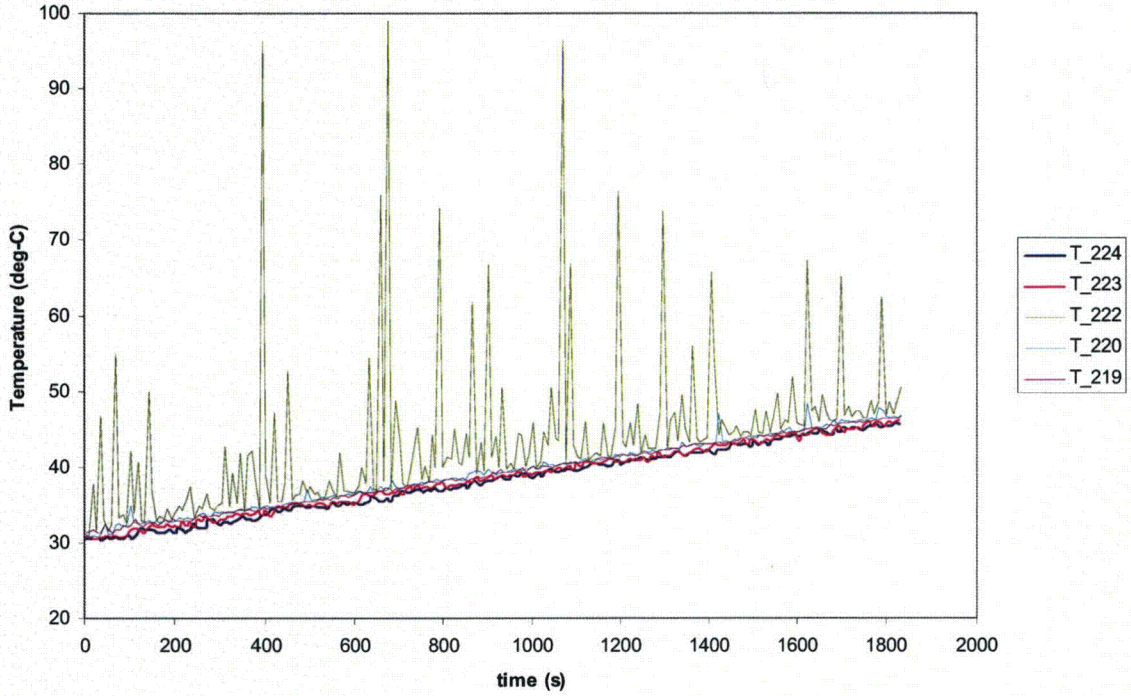

Figure 7.12 Vertical temperature distribution along the vent side centerline for case T3-23†

†Refer to Table 7.2 for test conditions

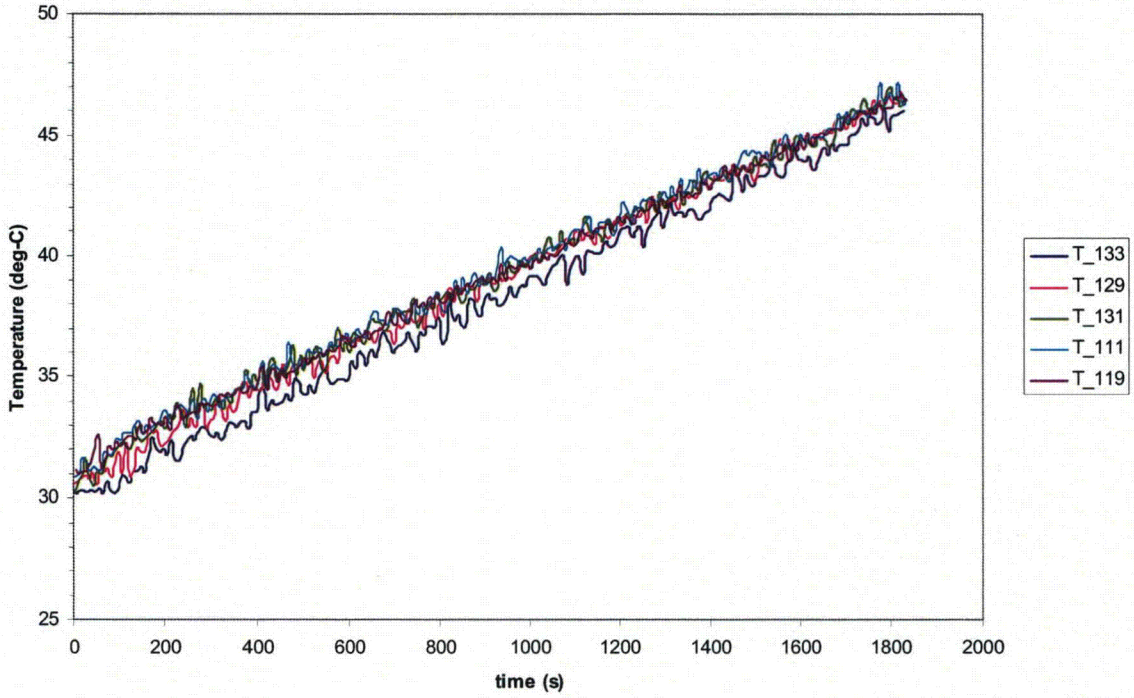

Figure 7.13 Vertical temperature distribution along the pool side centerline for case T3-23†

†Refer to Table 7.2 for test conditions

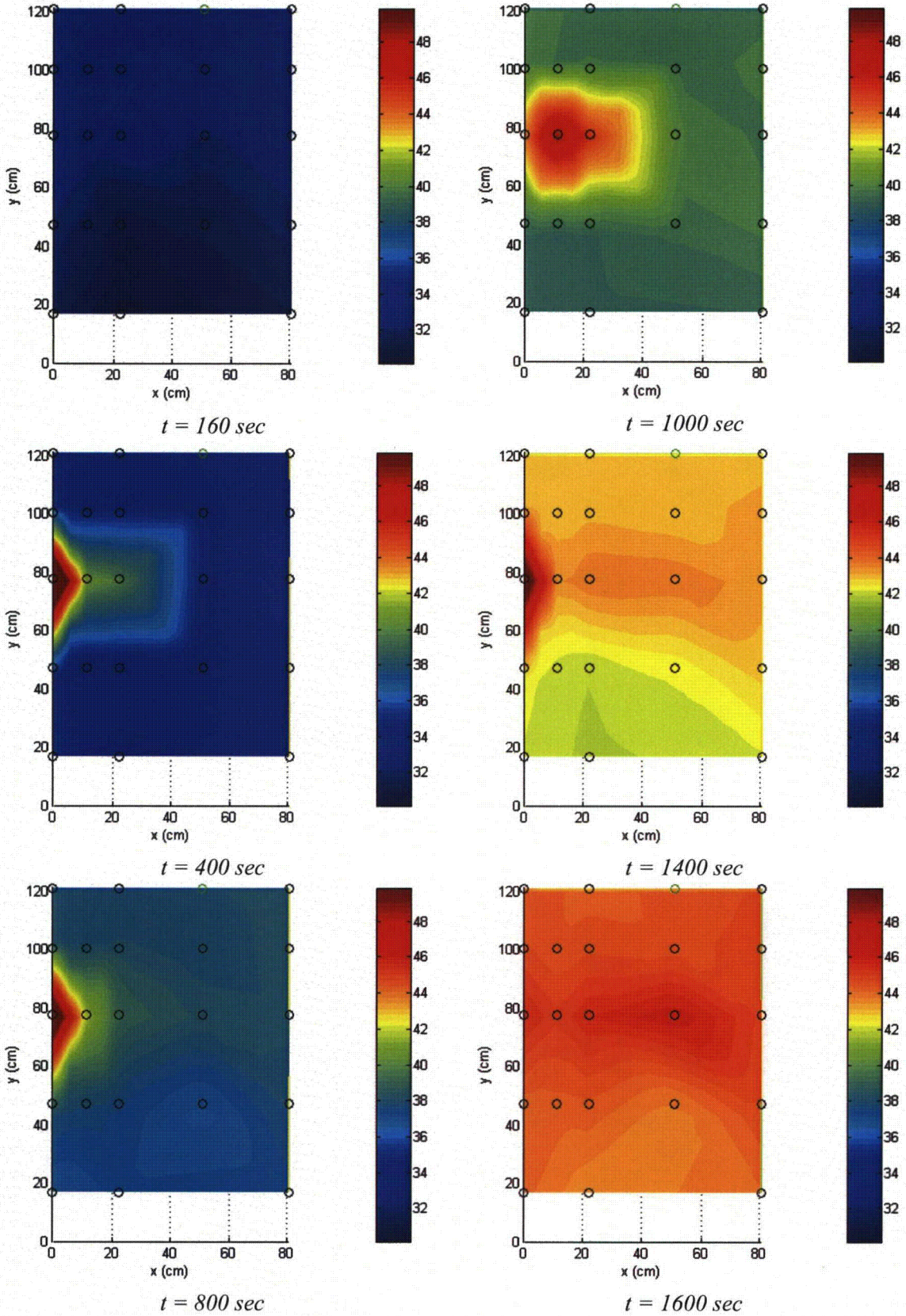

Figure 7.14 Temperature profile development along the pool vertical center plane for case T3-23

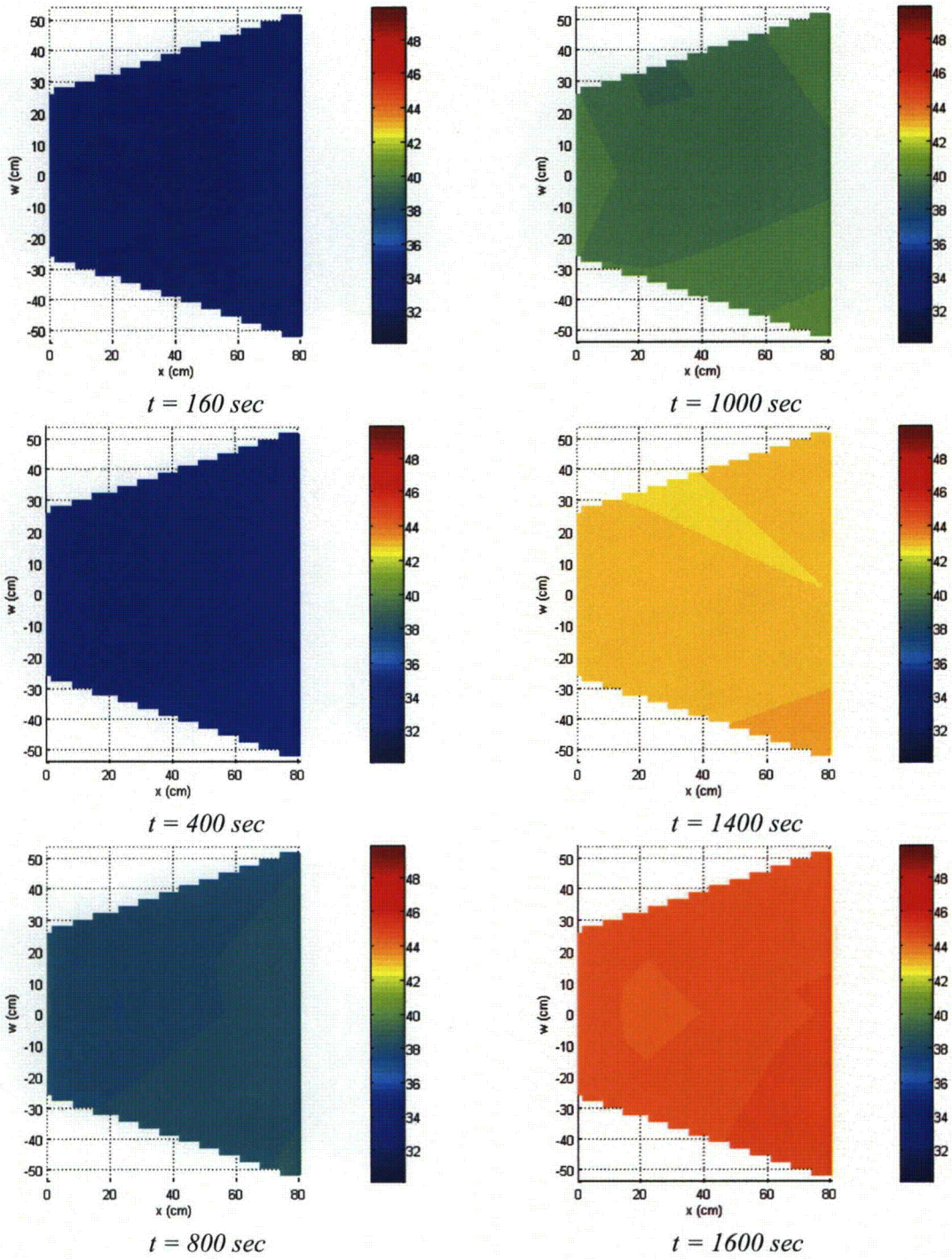

Figure 7.15 Temperature profile development along the pool surface for case T3-23

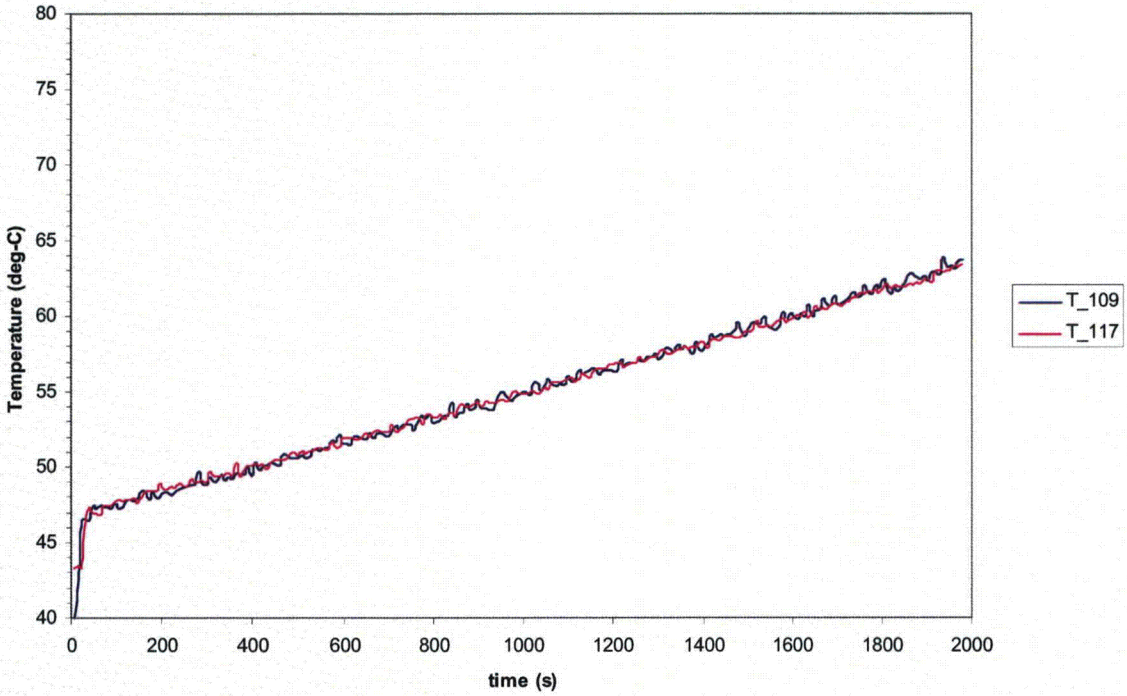

Figure 7.16 Real-time temperature data at the water surface for case T3-24†
†Refer to Table 7.2 for test conditions

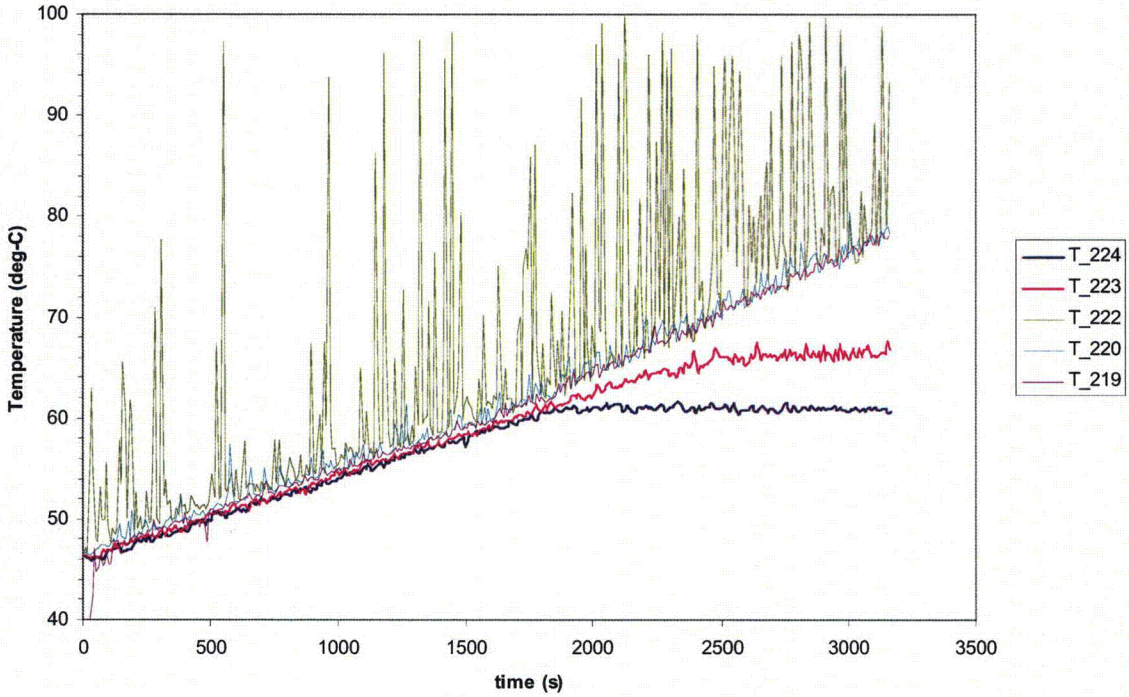

Figure 7.17 Vertical temperature distribution along the vent side centerline for case T3-24†

†Refer to Table 7.2 for test conditions

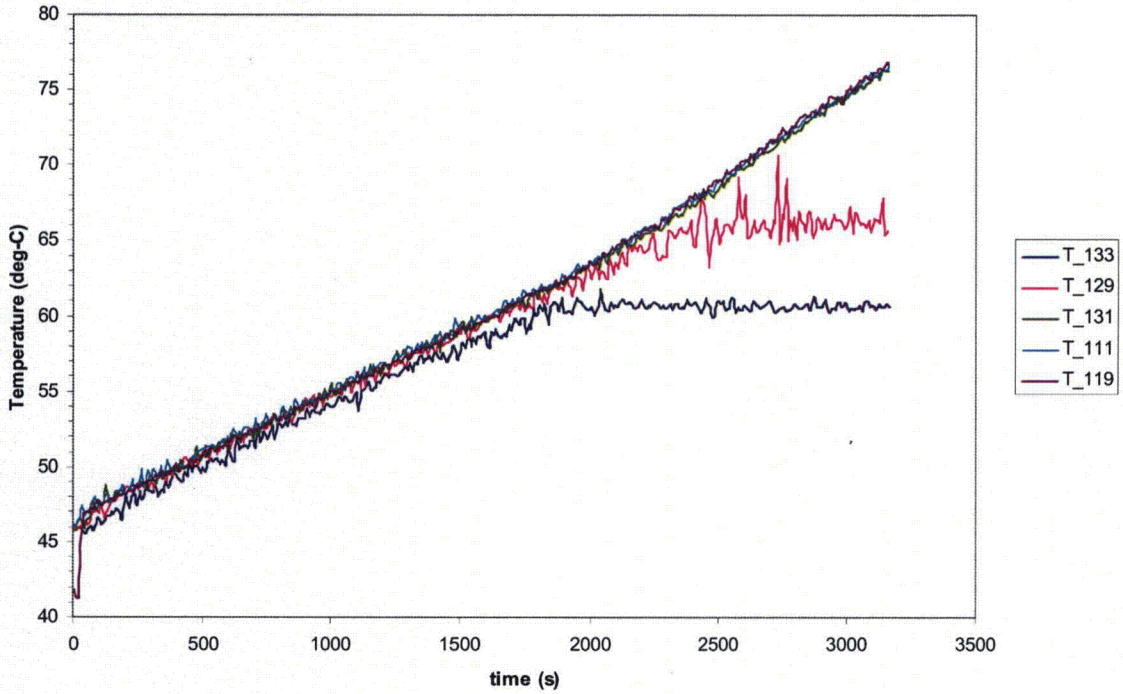

Figure 7.18 Vertical temperature distribution along the pool side centerline for case T3-24†

†Refer to Table 7.2 for test conditions

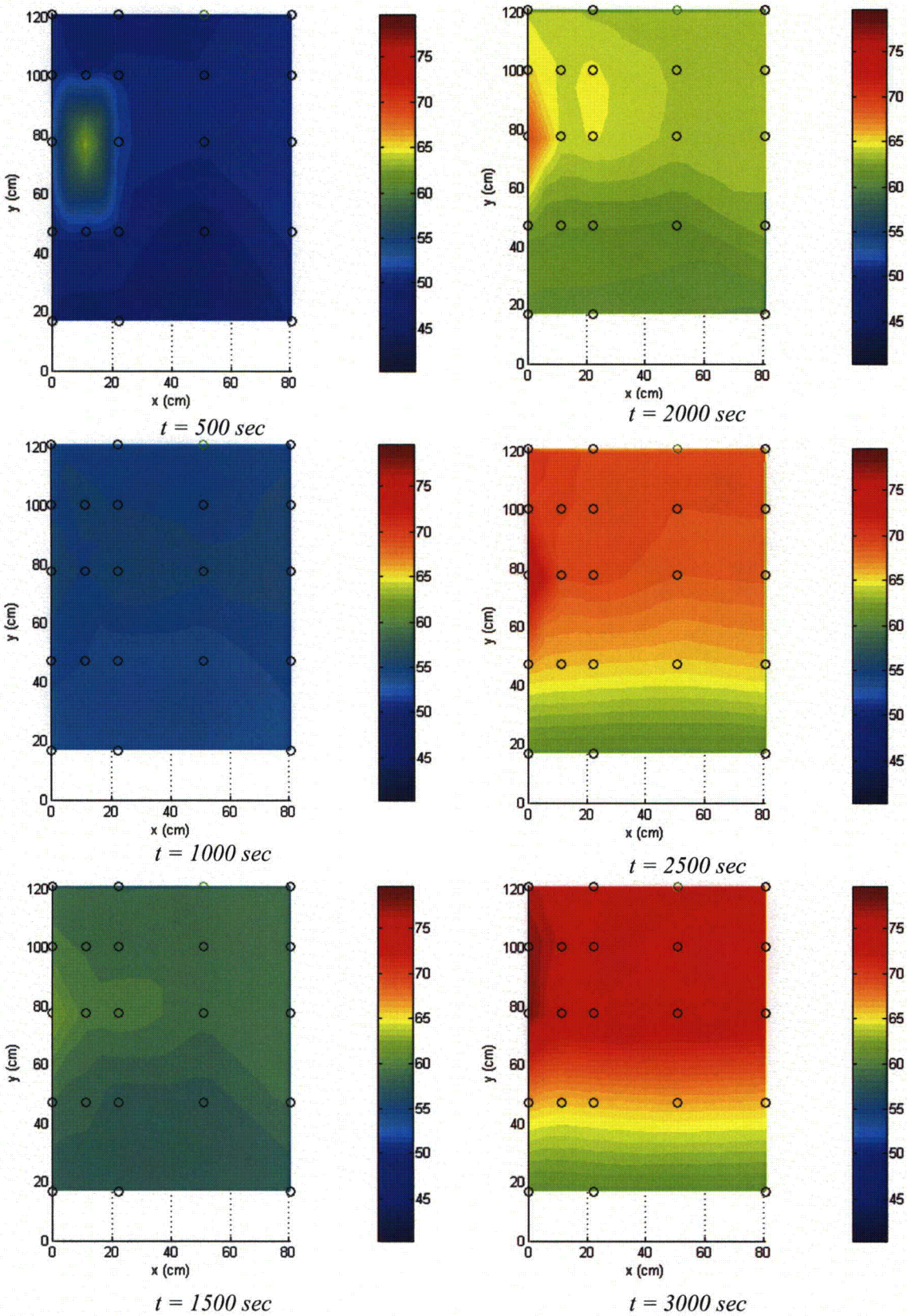

Figure 7.19 Temperature profile development along the pool vertical center plane for case T3-24

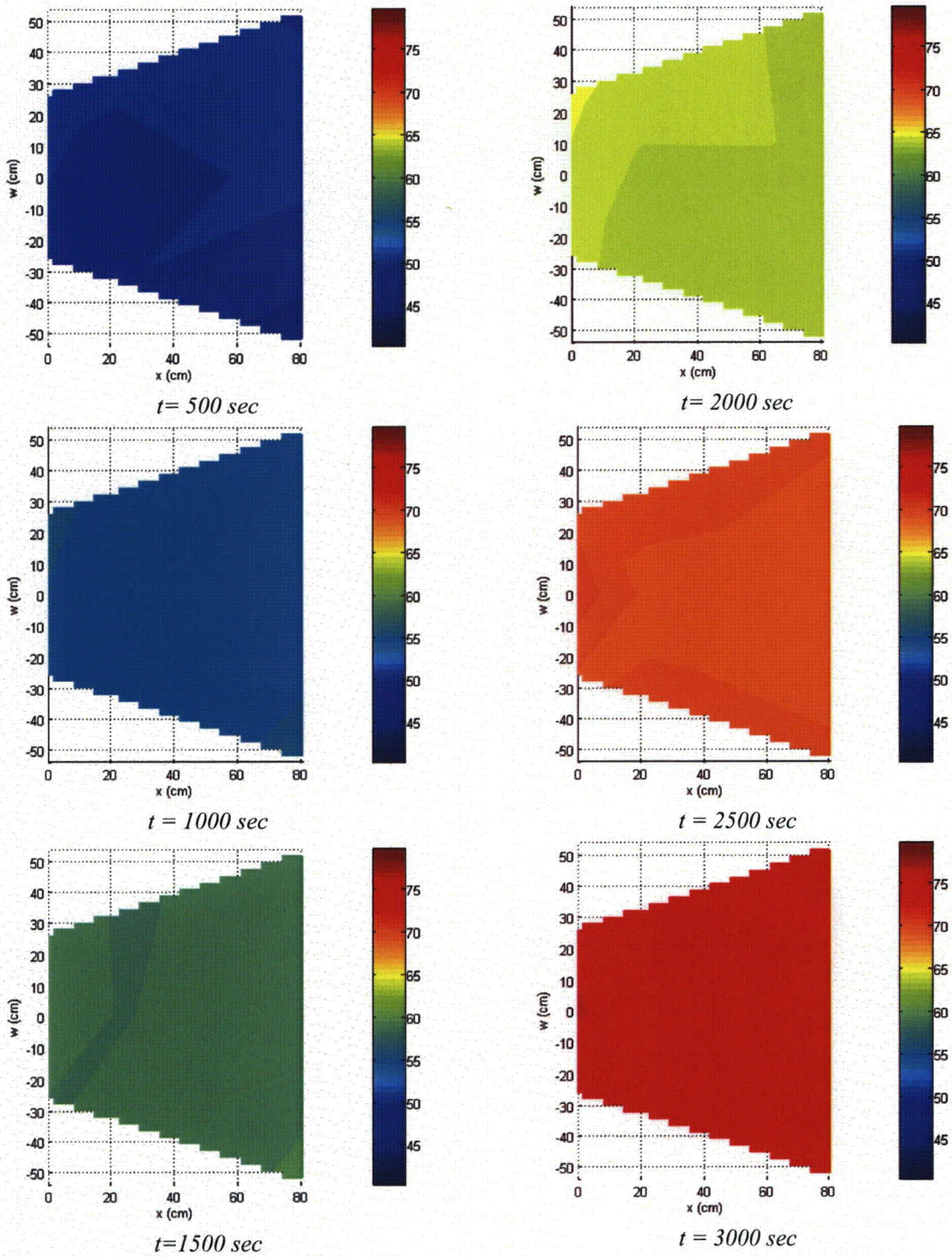

Figure 7.20 Temperature profile development along the pool surface for case T3-24

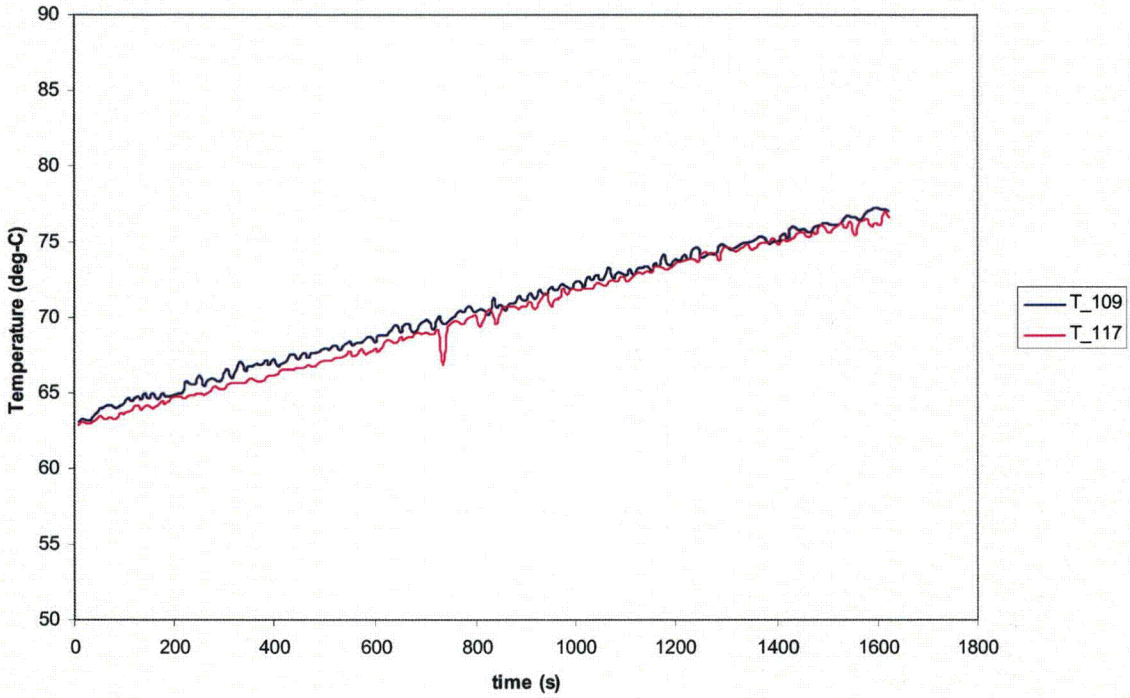

Figure 7.21 Real-time temperature data at the water surface for case T3-42†
†Refer to Table 7.2 for test conditions

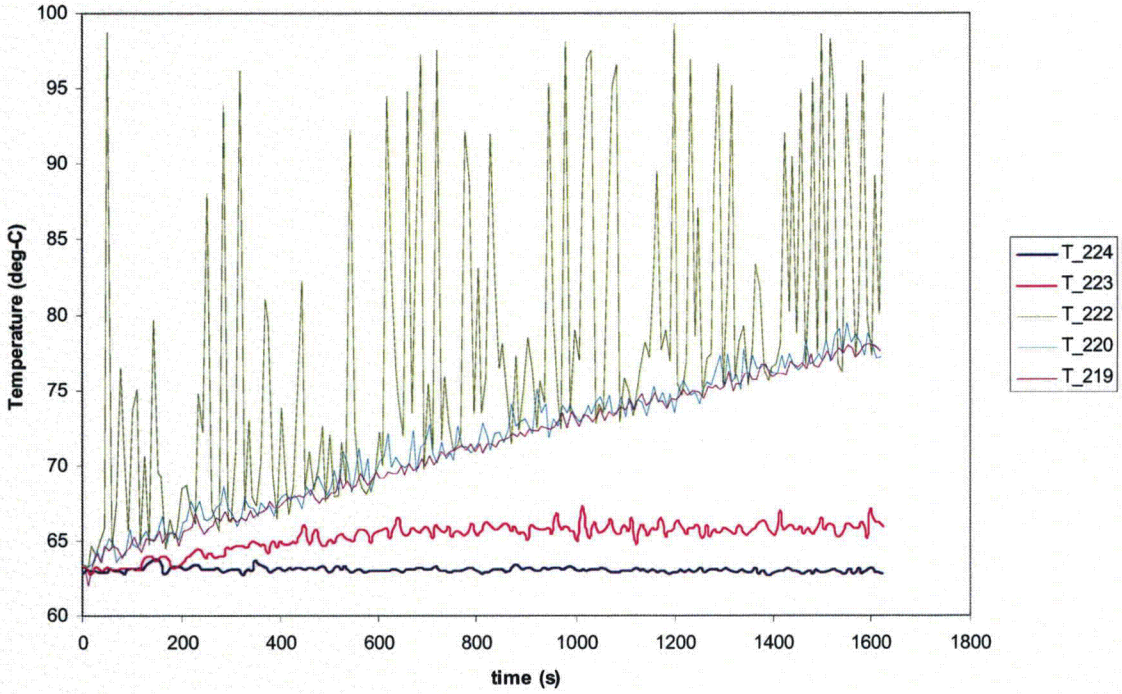

Figure 7.22 Vertical temperature distribution along the vent side centerline for case T3-42†

†Refer to Table 7.2 for test conditions

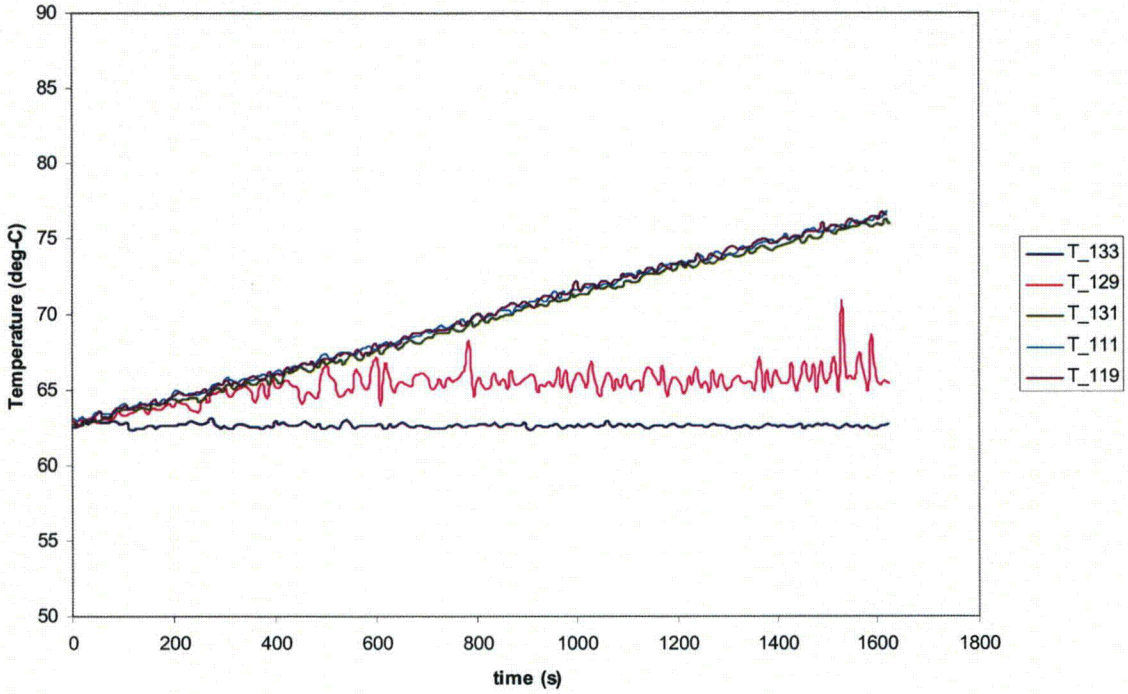

Figure 7.23 Vertical temperature distribution along the pool side centerline for case T3-42†

†Refer to Table 7.2 for test conditions

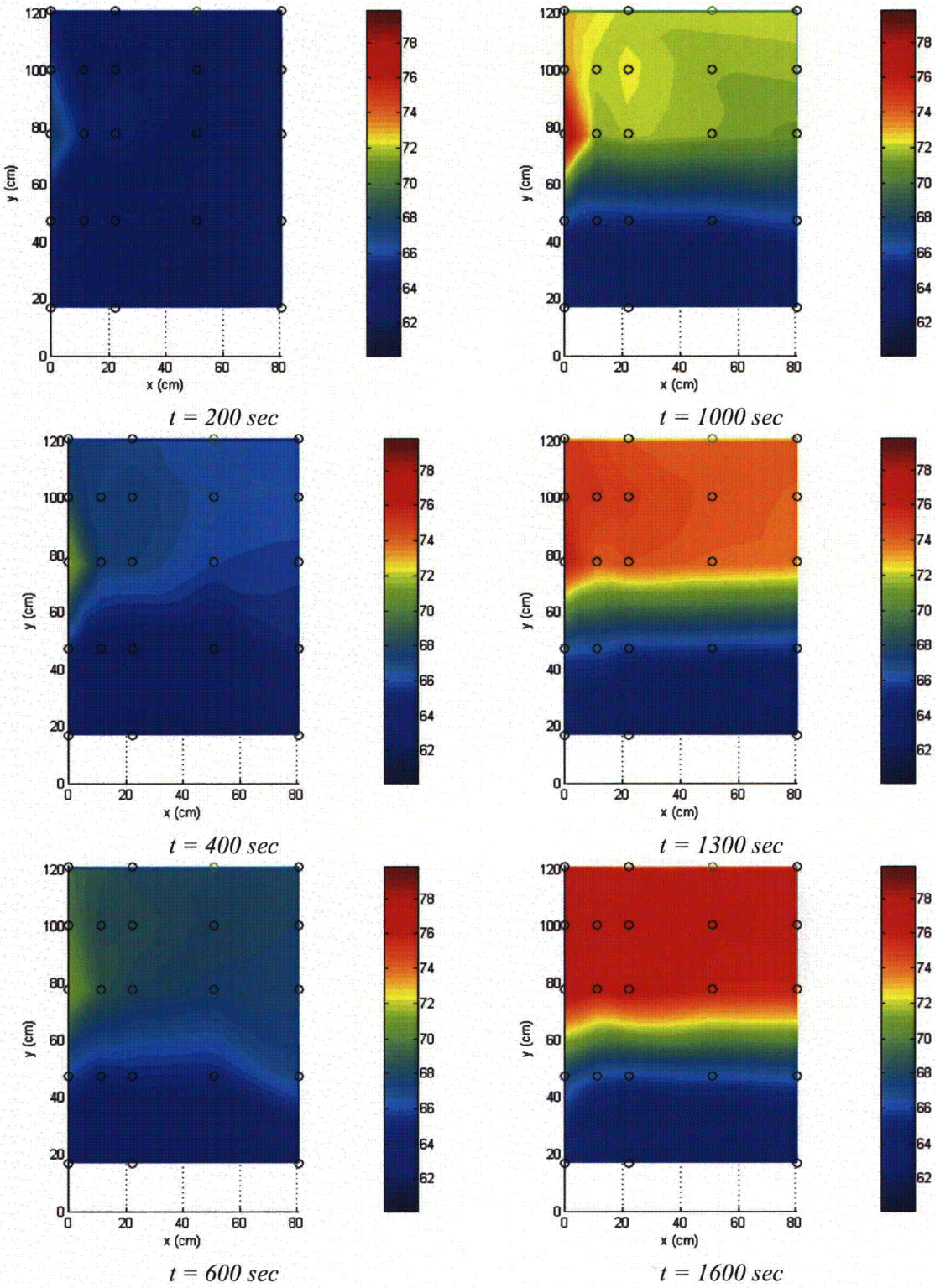

Figure 7.24 Temperature profile development along the pool vertical center plane for case T3-42

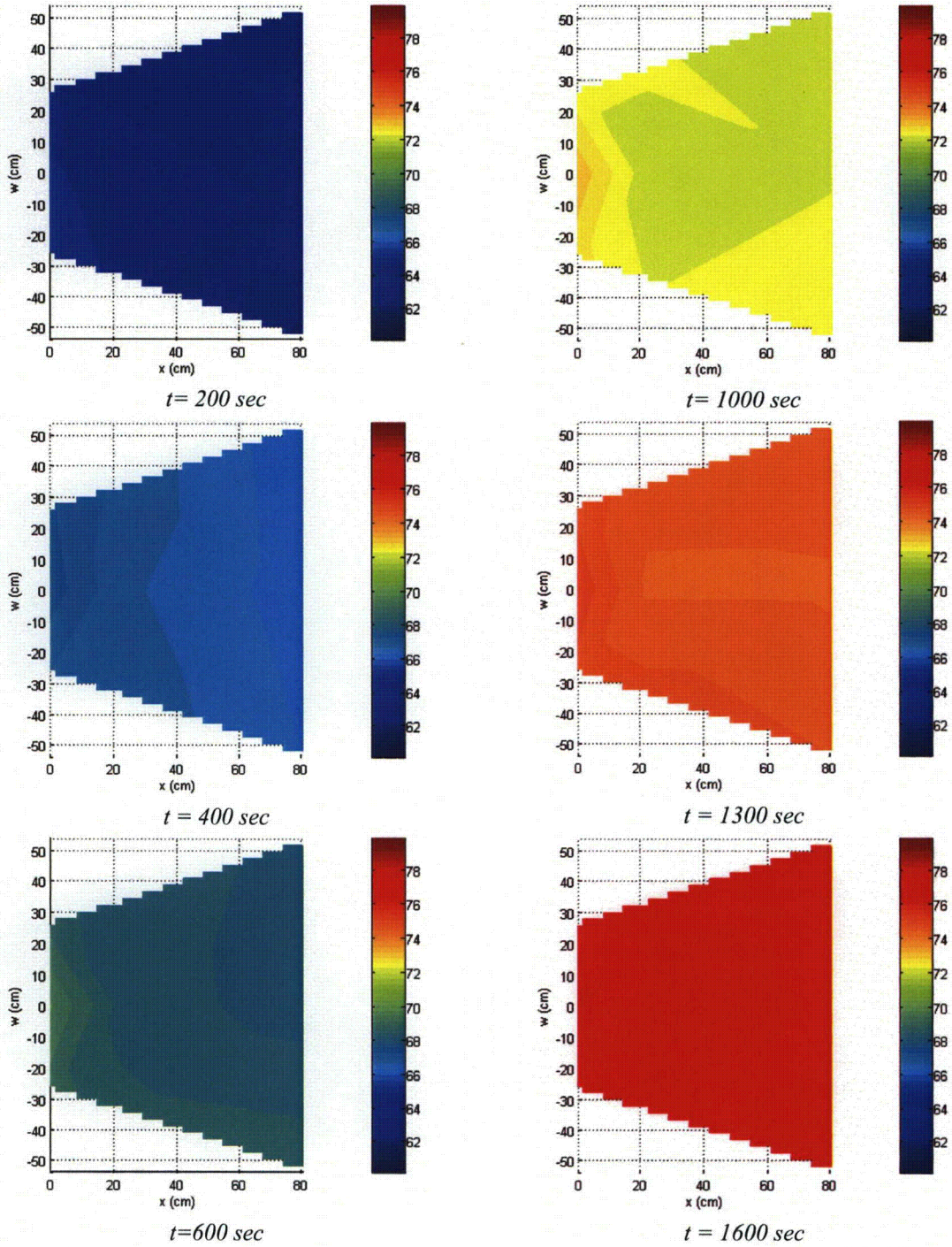

Figure 7.25 Temperature profile development along the pool surface for case T3-42

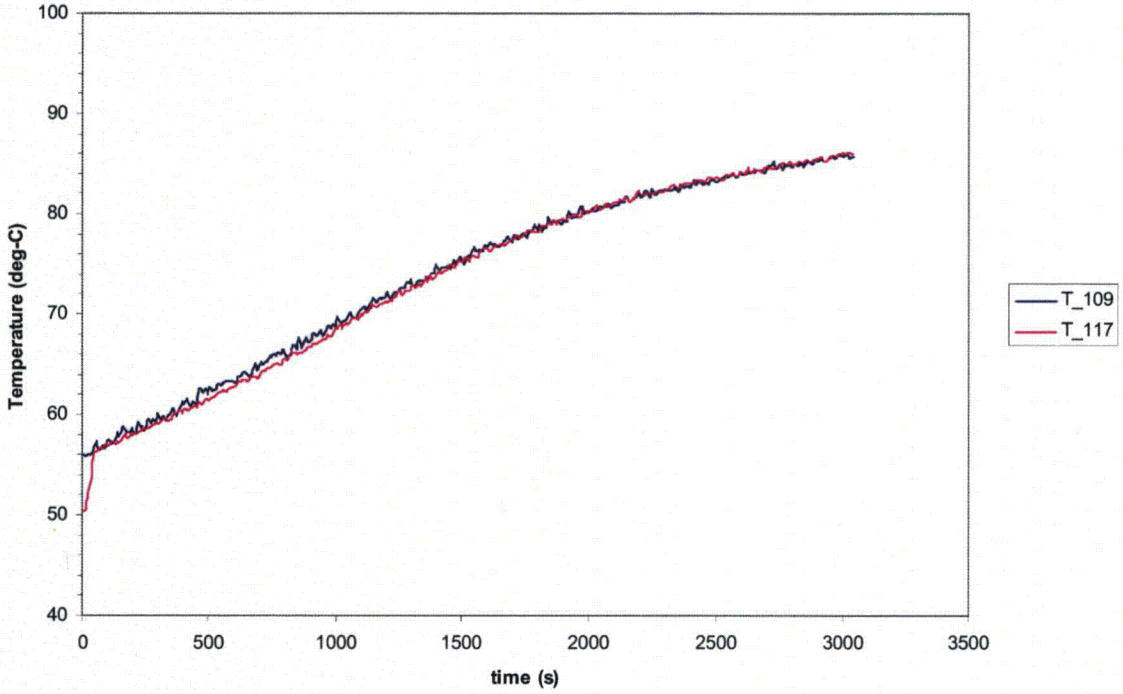

Figure 7.26 Real-time temperature data at the water surface for case T3-27†
†Refer to Table 7.2 for test conditions

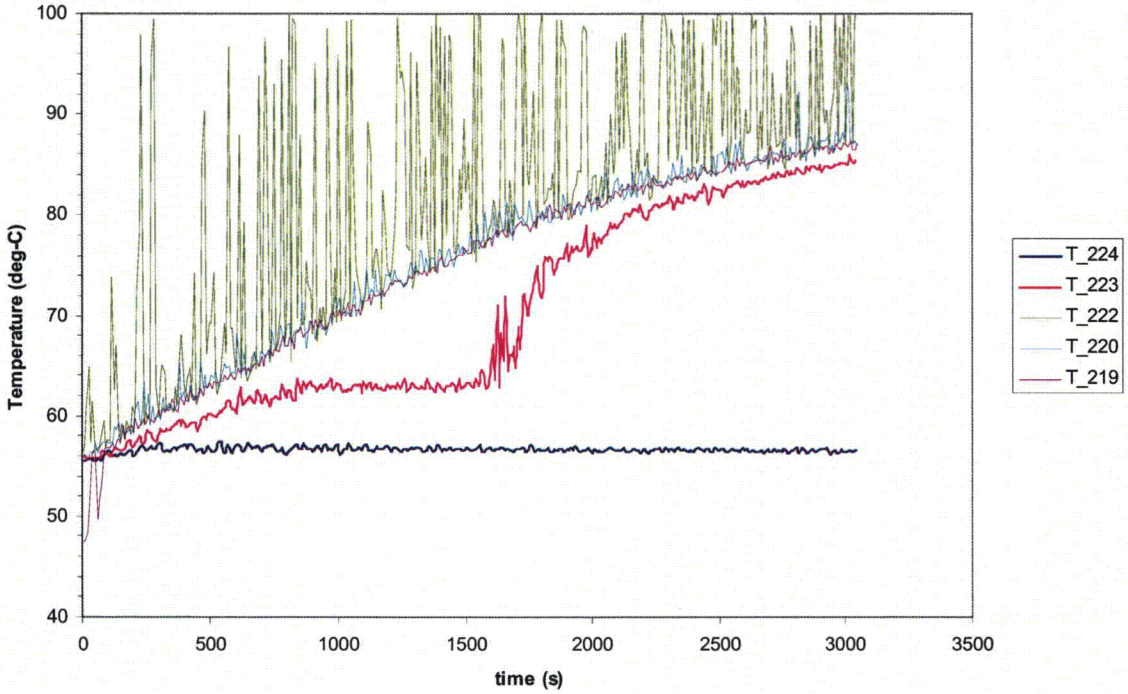

Figure 7.27 Vertical temperature distribution along the vent side centerline for case T3-27†

†Refer to Table 7.2 for test conditions

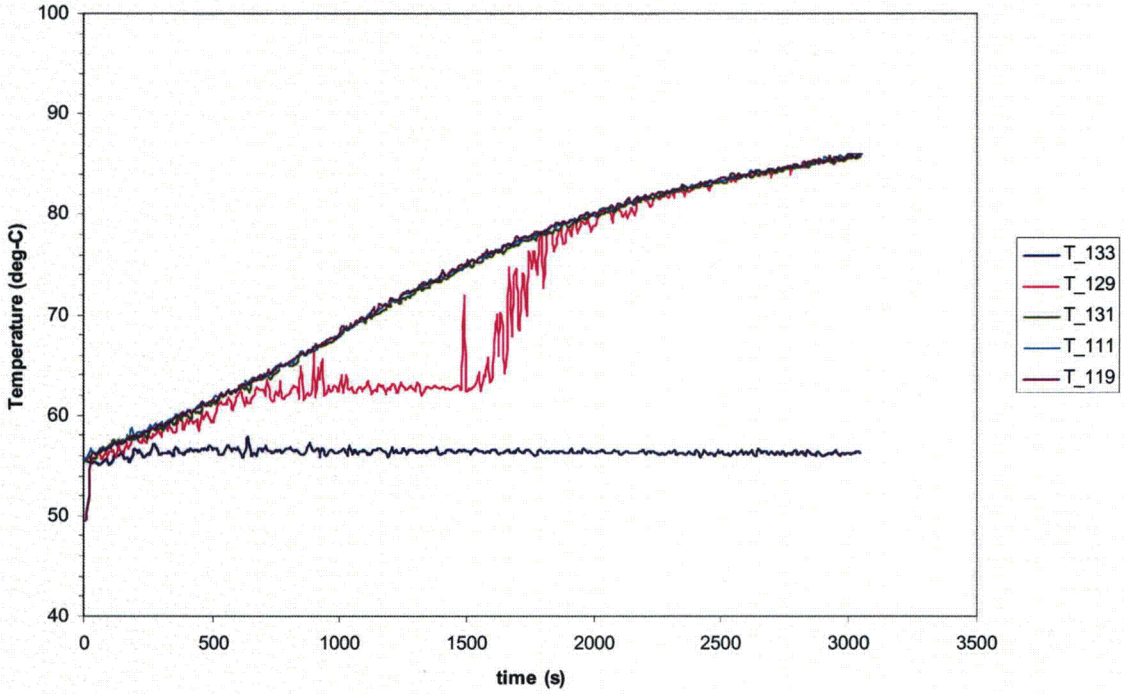

Figure 7.28 Vertical temperature distribution along the pool side centerline for case T3-27†

†Refer to Table 7.2 for test conditions

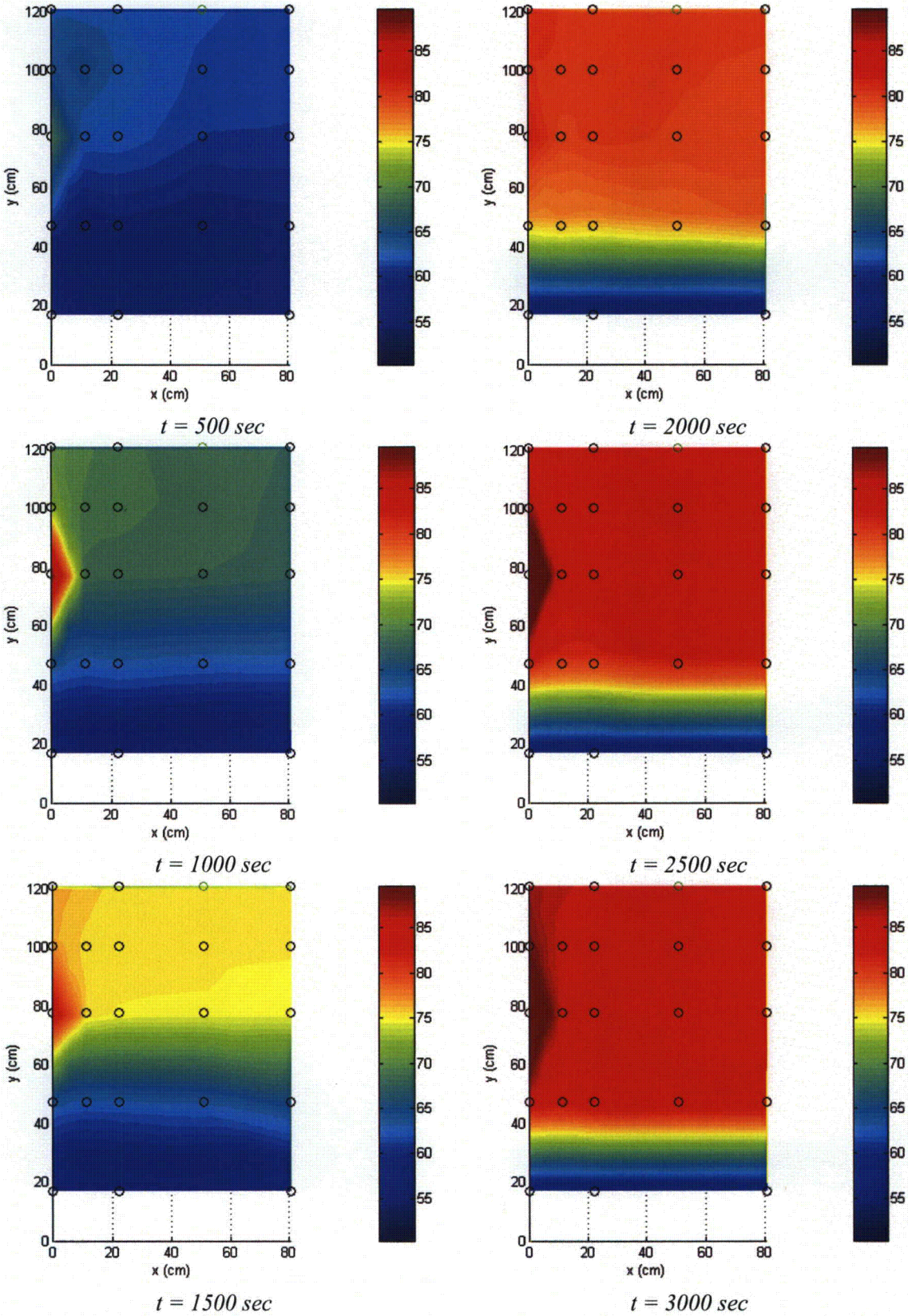

Figure 7.29 Temperature profile development along the pool vertical center plane for case T3-27

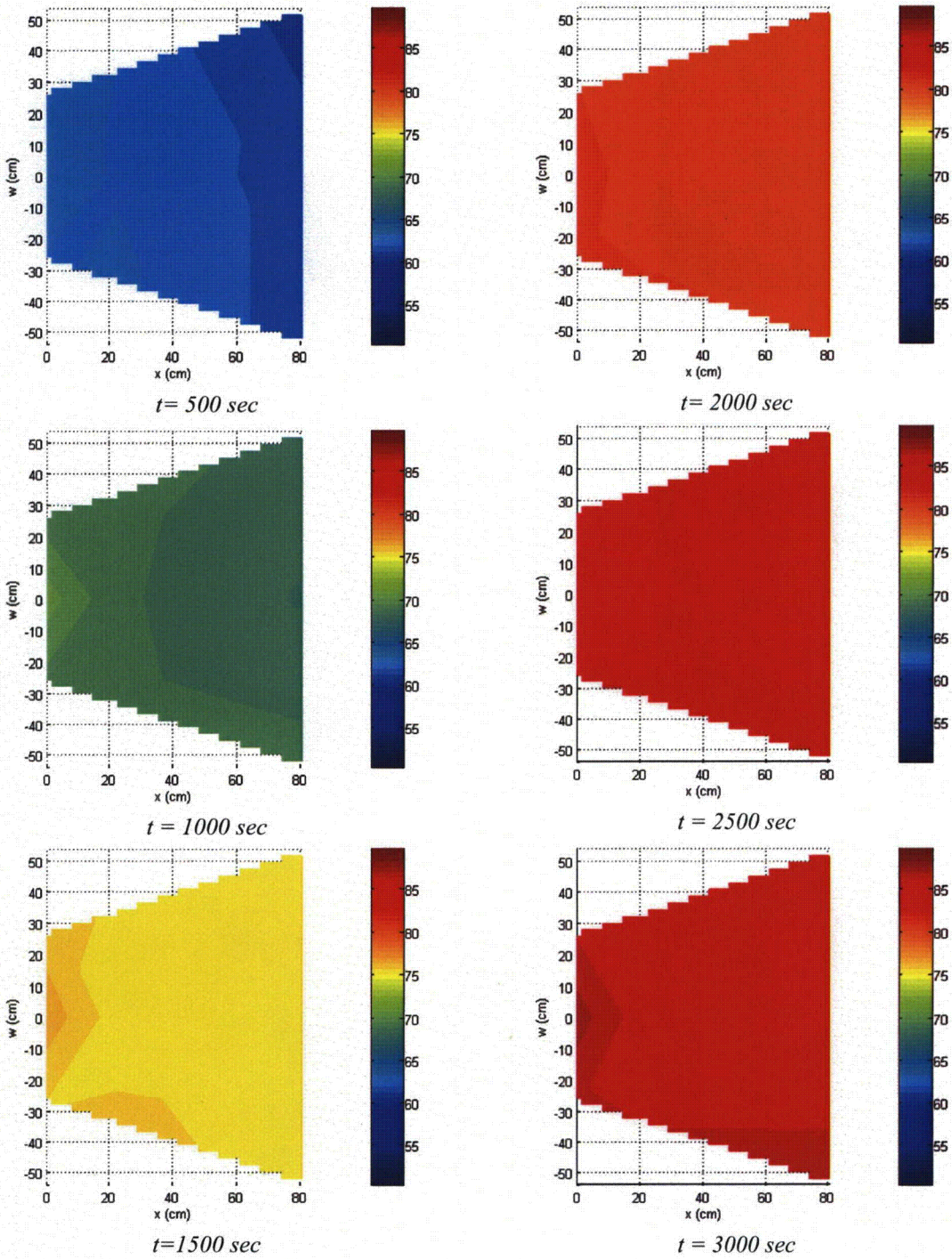

Figure 7.30 Temperature profile development along the pool surface for case T3-27

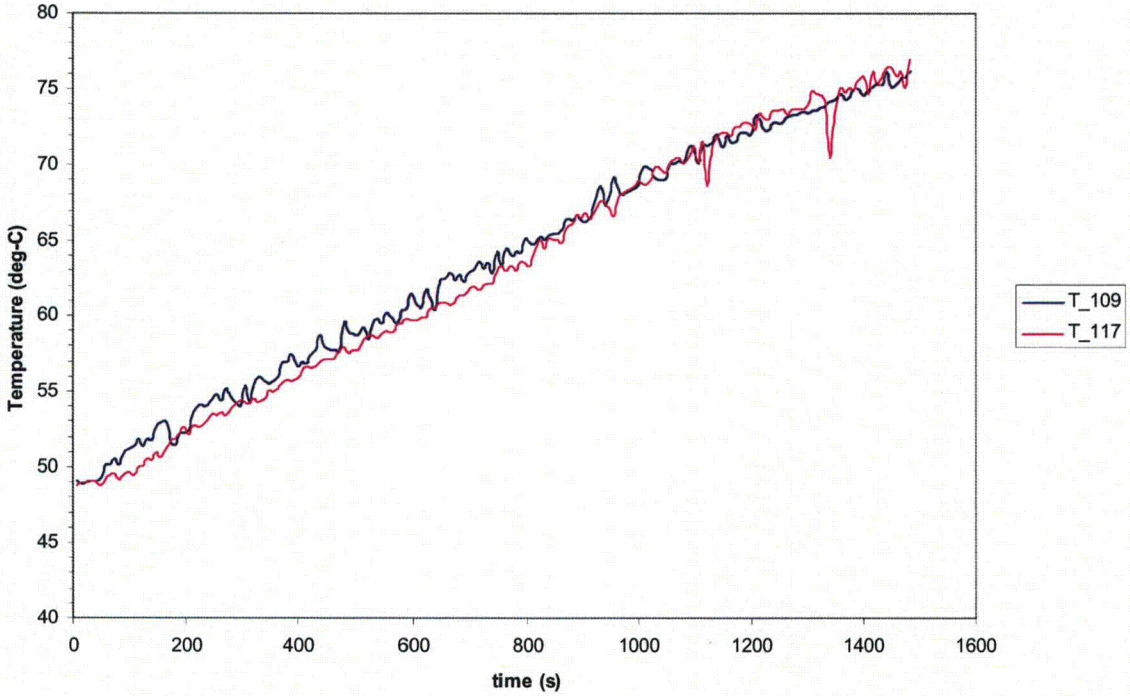

Figure 7.31 Real-time temperature data at the water surface for case T3-43†
†Refer to Table 7.2 for test conditions

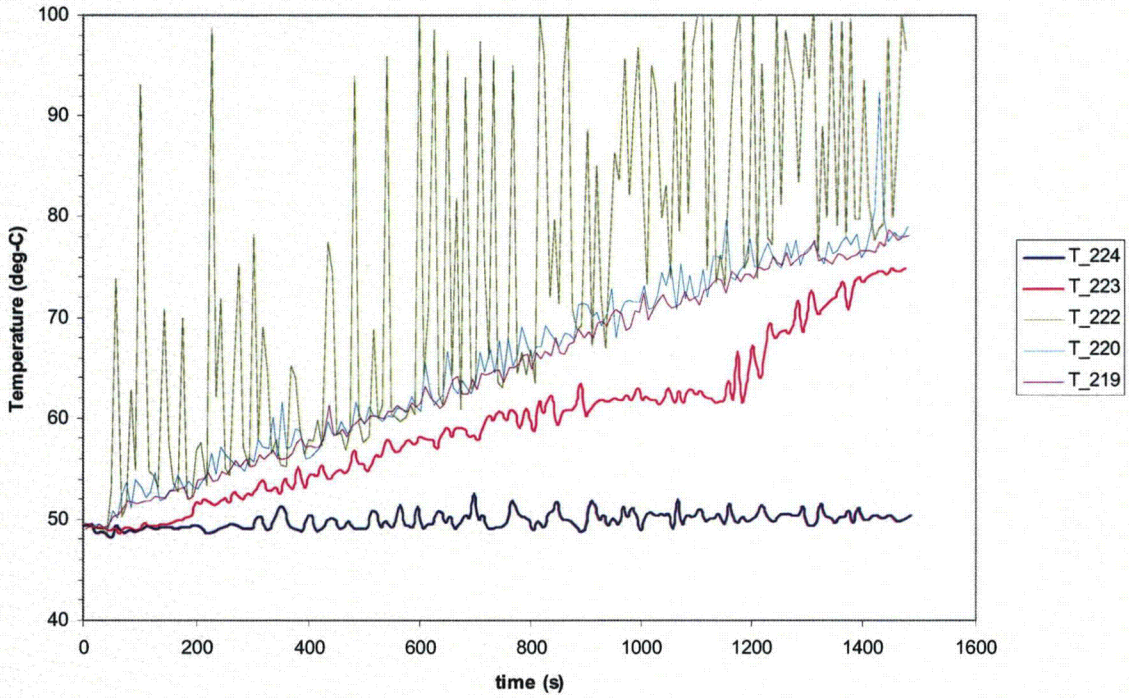

Figure 7.32 Vertical temperature distribution along the vent side centerline for case T3-43†

†Refer to Table 7.2 for test conditions

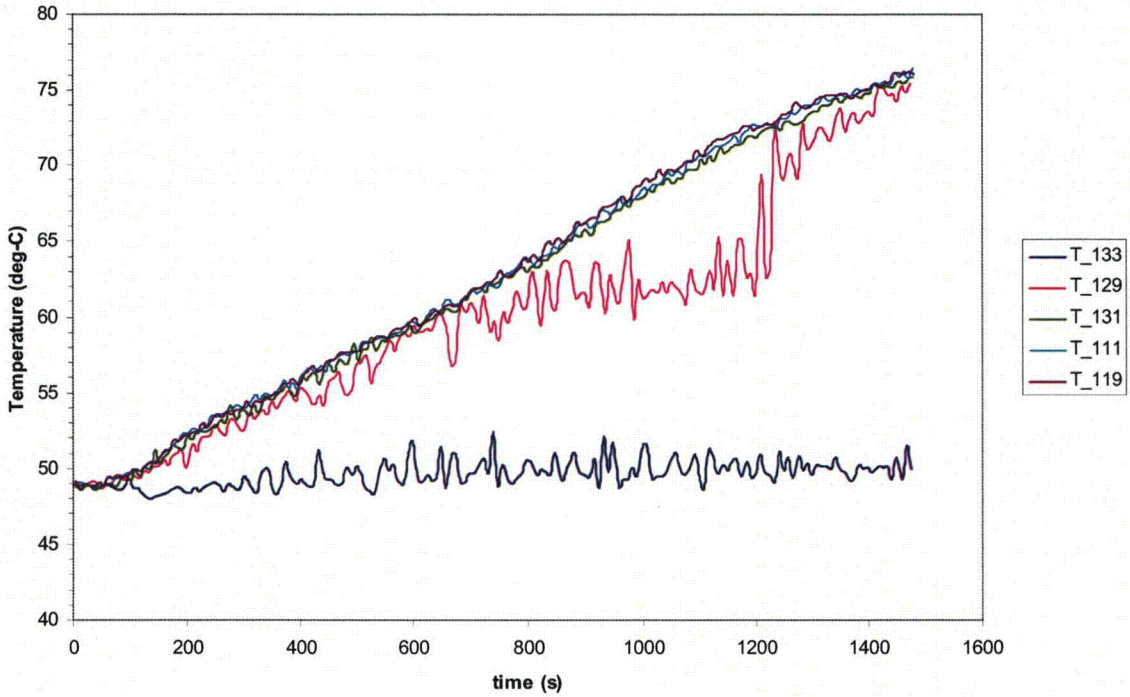

Figure 7.33 Vertical temperature distribution along the pool side centerline for case T3-43†

†Refer to Table 7.2 for test conditions

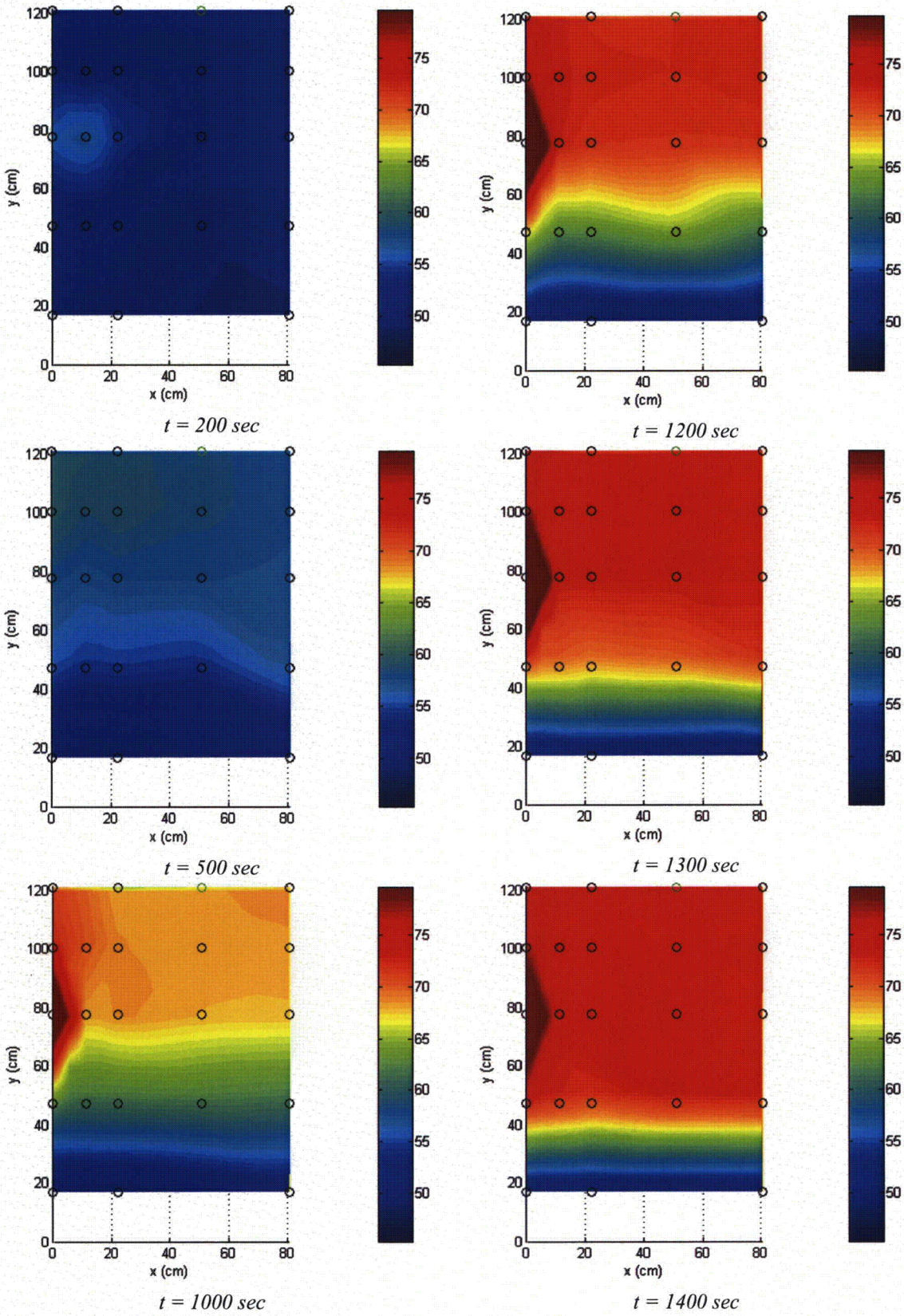

Figure 7.34 Temperature profile development along the pool vertical center plane for case T3-43

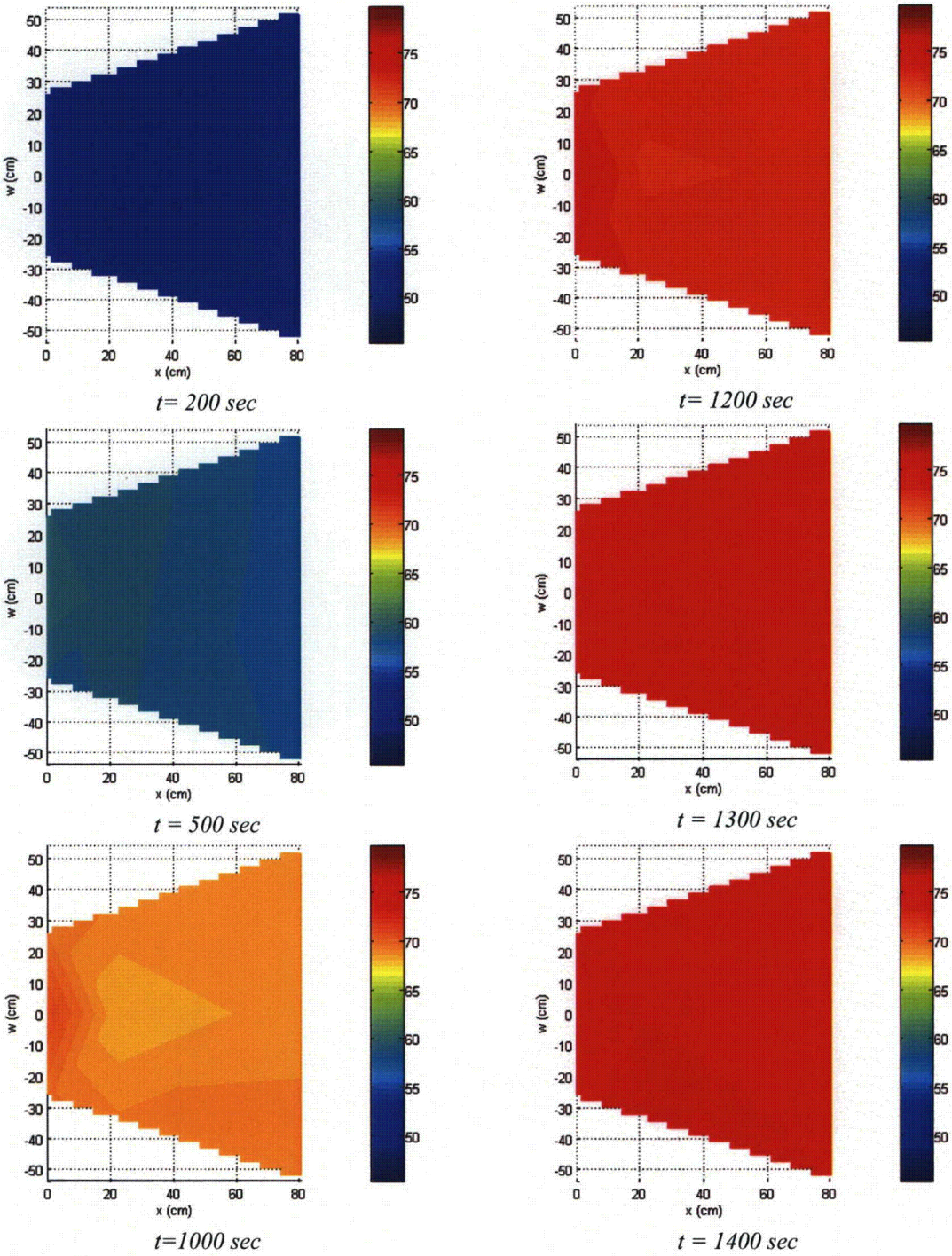

Figure 7.35 Temperature profile development along the pool surface for case T3-43

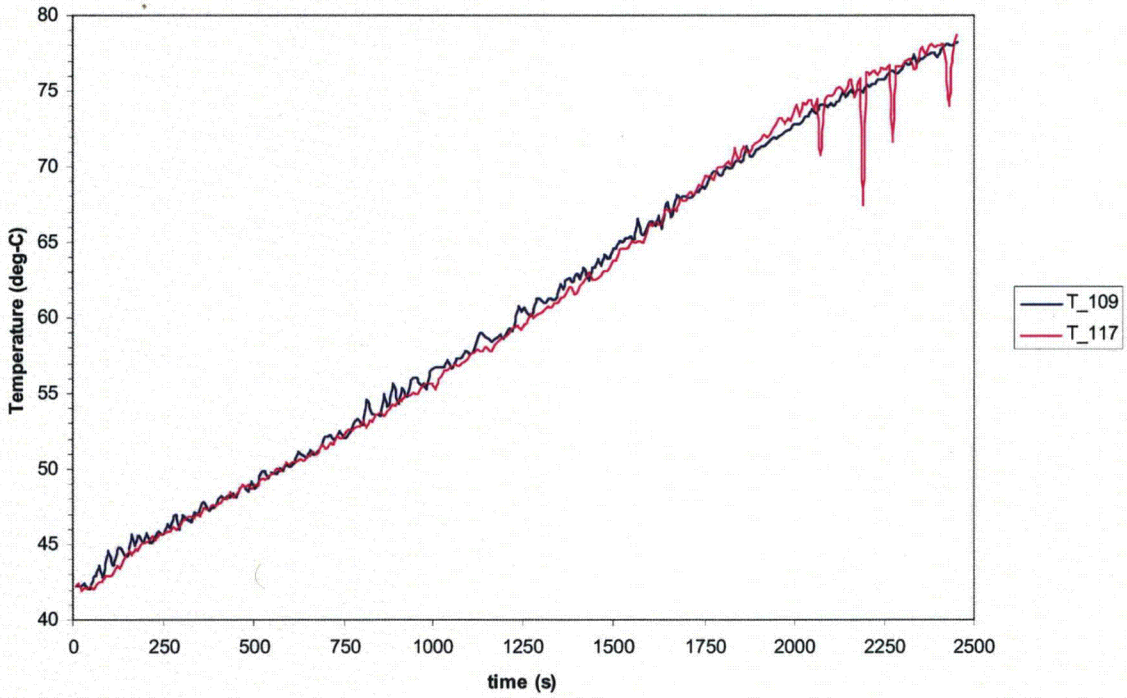

Figure 7.36 Real-time temperature data at the water surface for case T3-47†
†Refer to Table 7.2 for test conditions

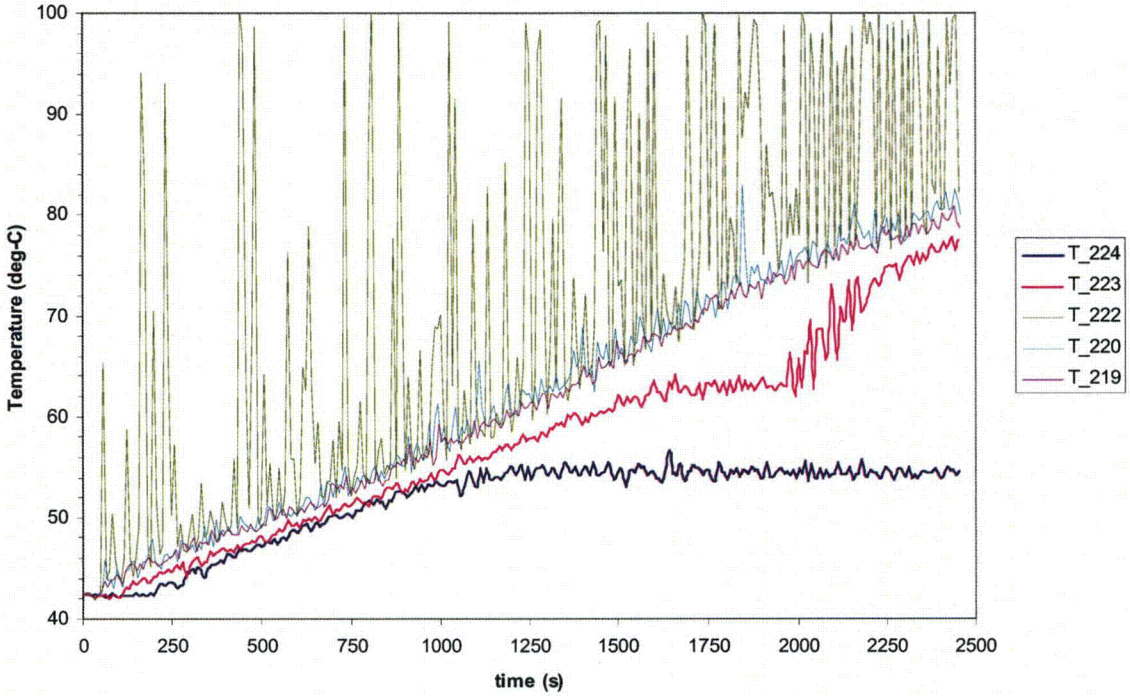

Figure 7.37 Vertical temperature distribution along the vent side centerline for case T3-47†

†Refer to Table 7.2 for test conditions

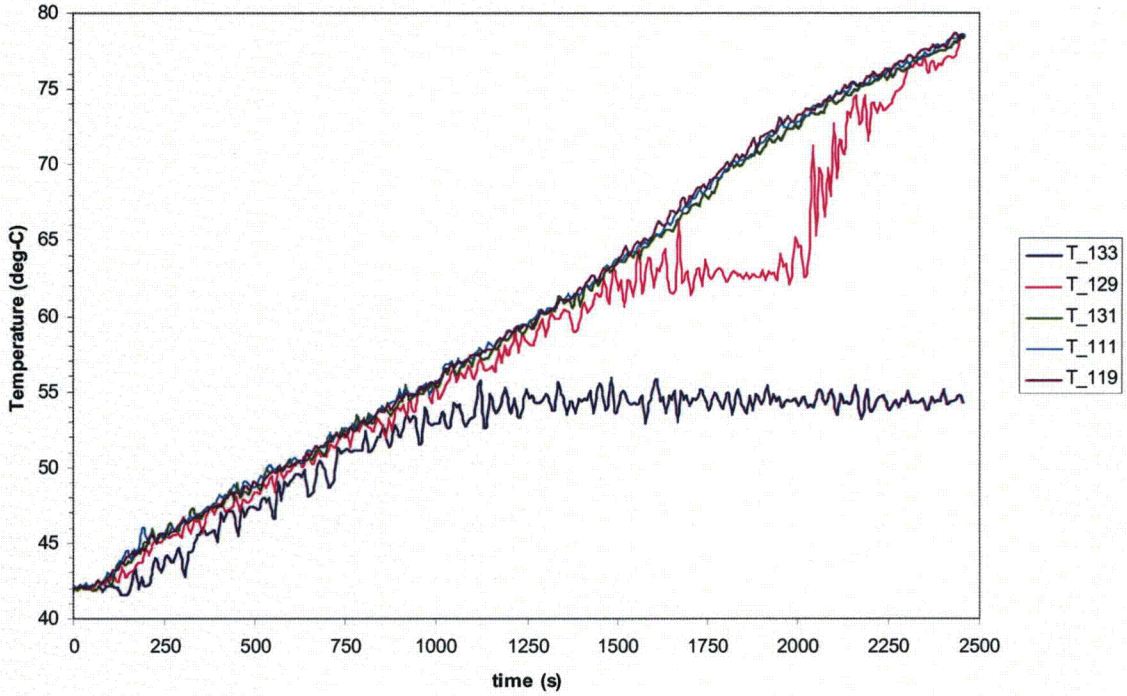

Figure 7.38 Vertical temperature distribution along the pool side centerline for case T3-47†

†Refer to Table 7.2 for test conditions

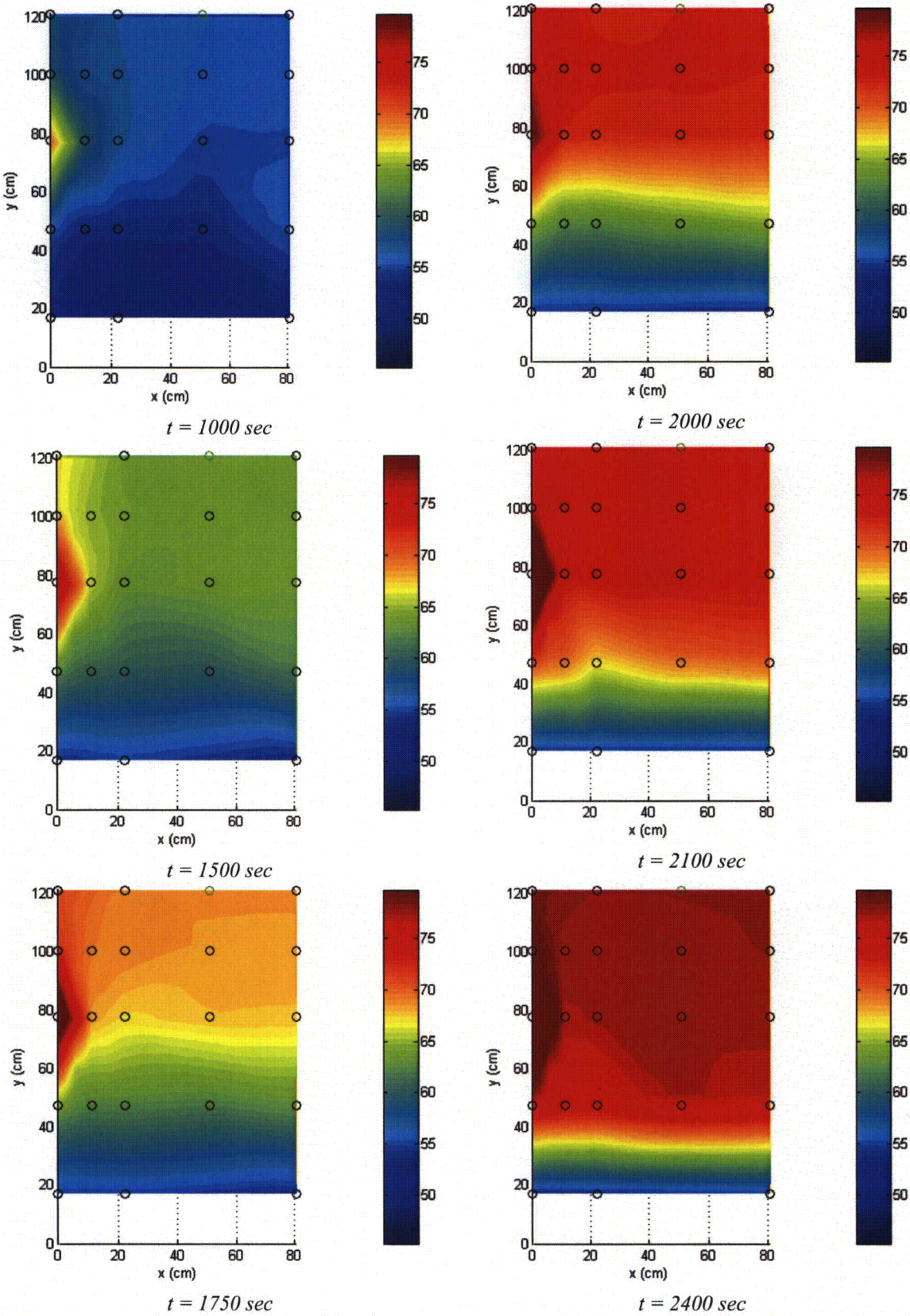

Figure 7.39 Temperature profile development along the pool vertical center plane for case T3-47

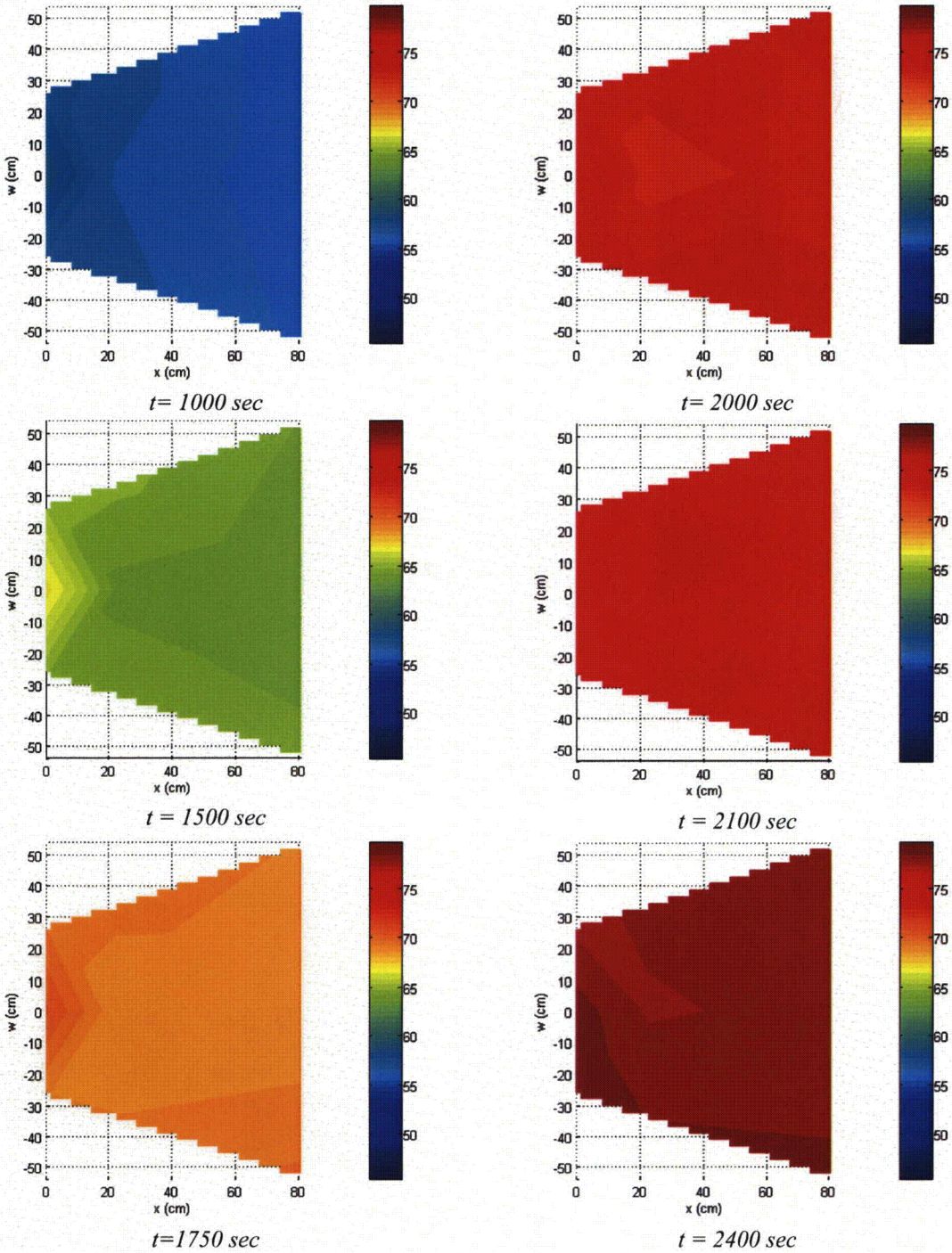

Figure 7.40 Temperature profile development along the pool surface for case T3-47

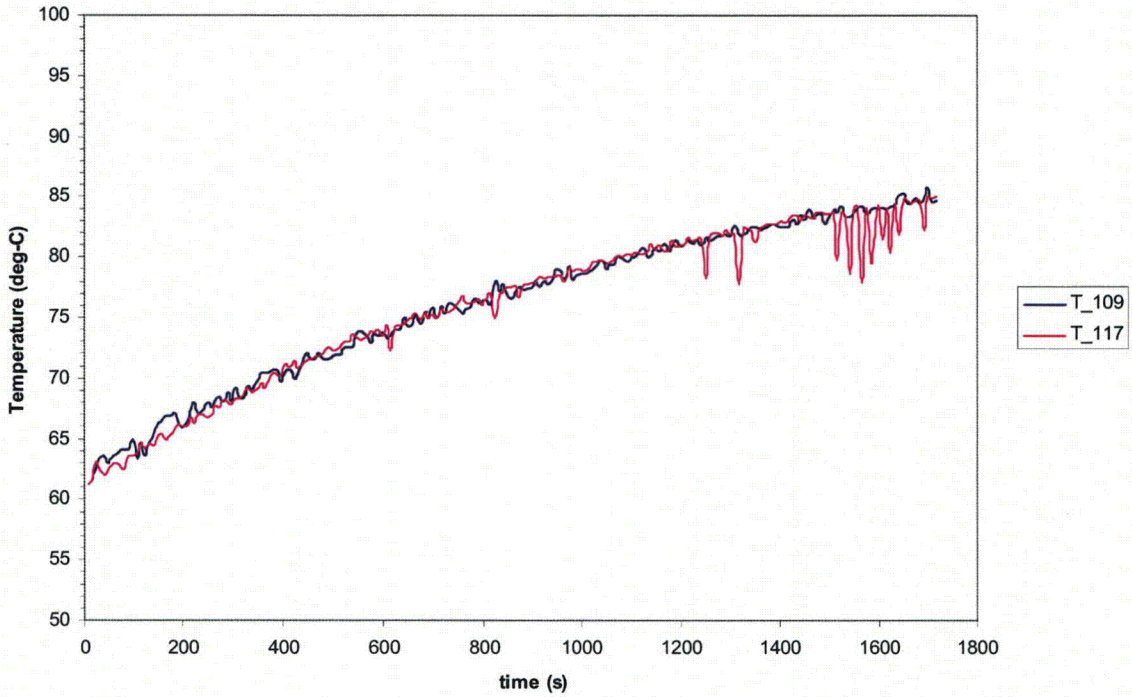

Figure 7.41 Real-time temperature data at the water surface for case T3-50†
†Refer to Table 7.2 for test conditions

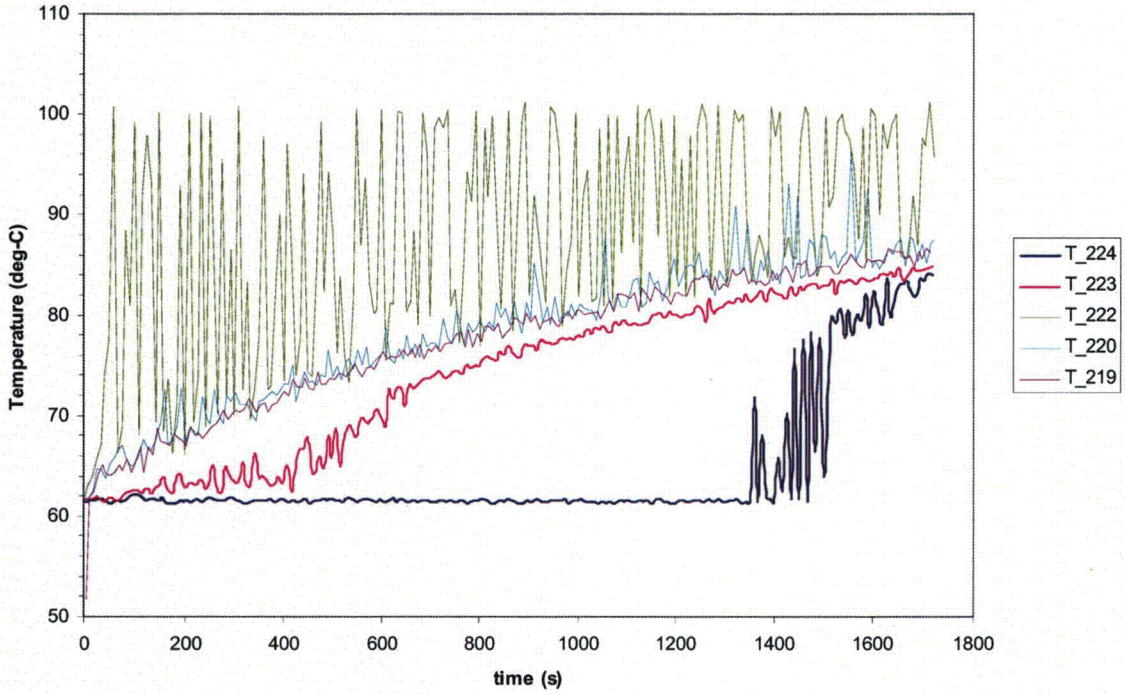

Figure 7.42 Vertical temperature distribution along the vent side centerline for case T3-50†

†Refer to Table 7.2 for test conditions

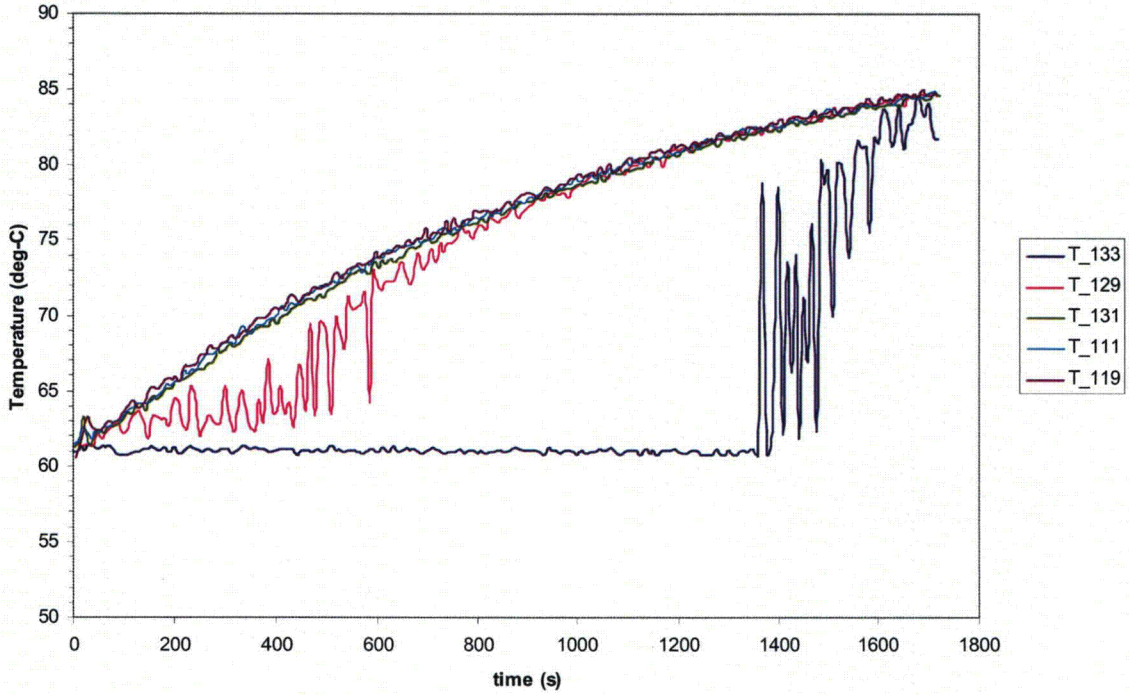

Figure 7.43 Vertical temperature distribution along the pool side centerline for case T3-50†

†Refer to Table 7.2 for test conditions

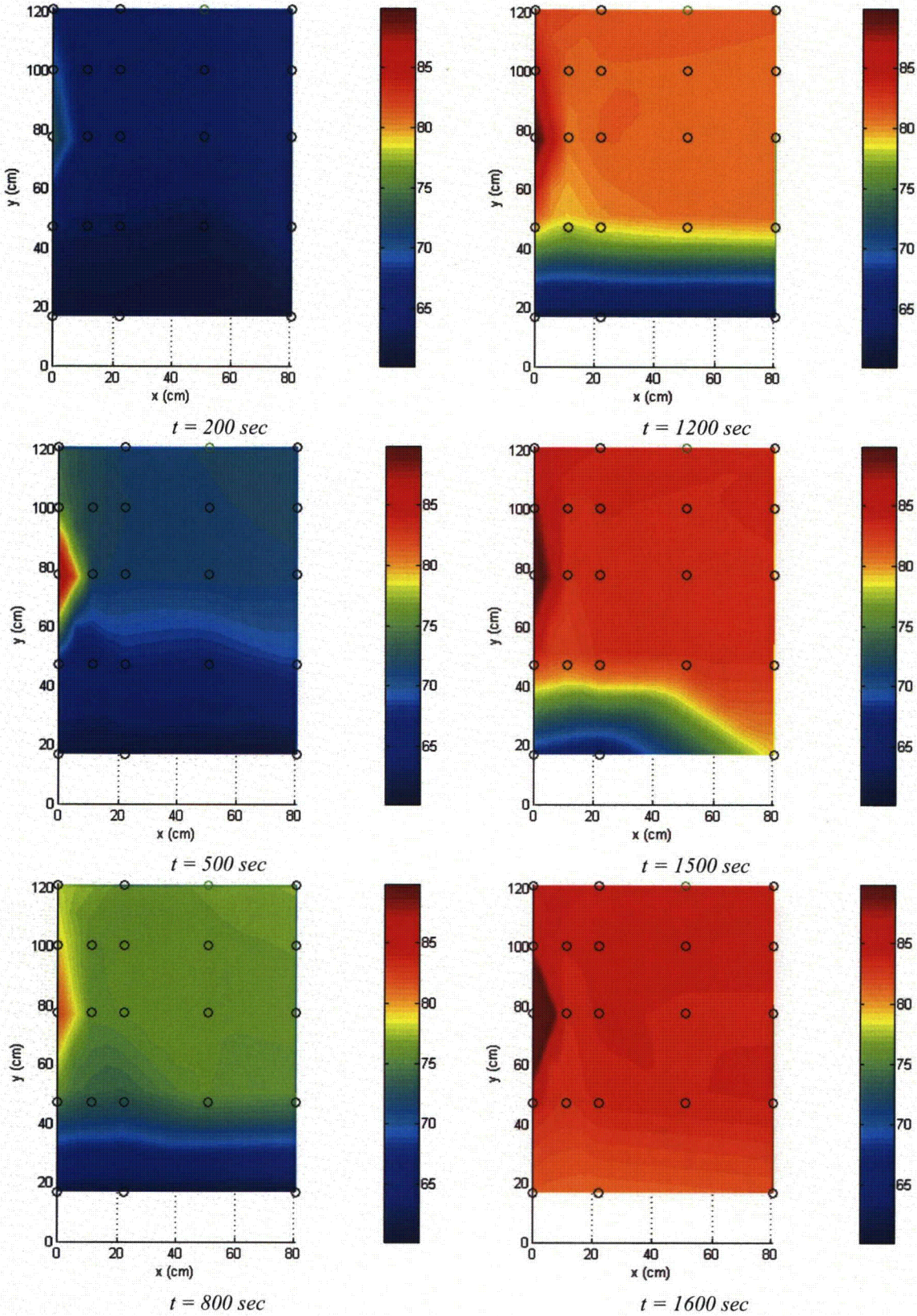

Figure 7.44 Temperature profile development along the pool vertical center plane for case T3-50

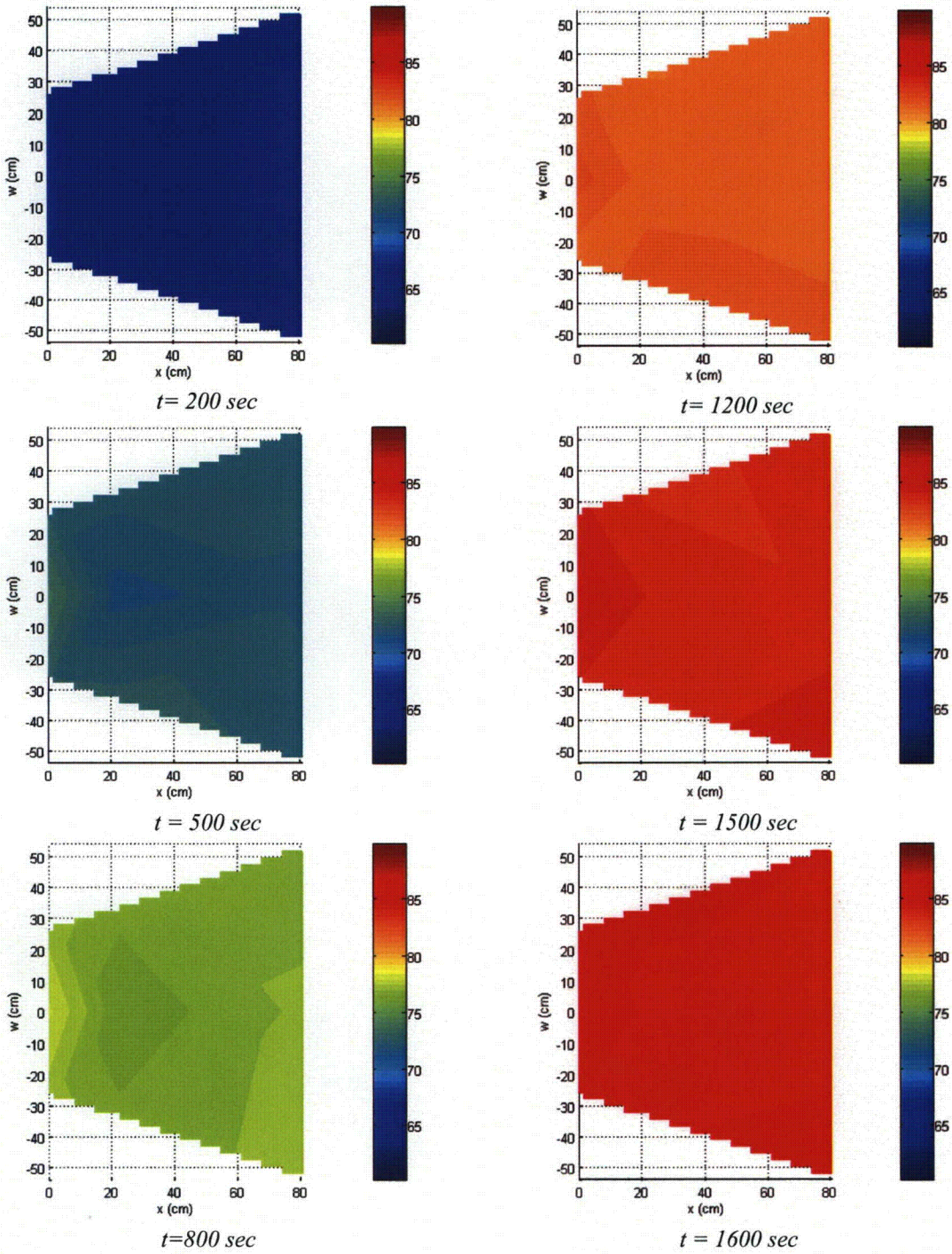

Figure 7.45 Temperature profile development along the pool surface for case T3-50

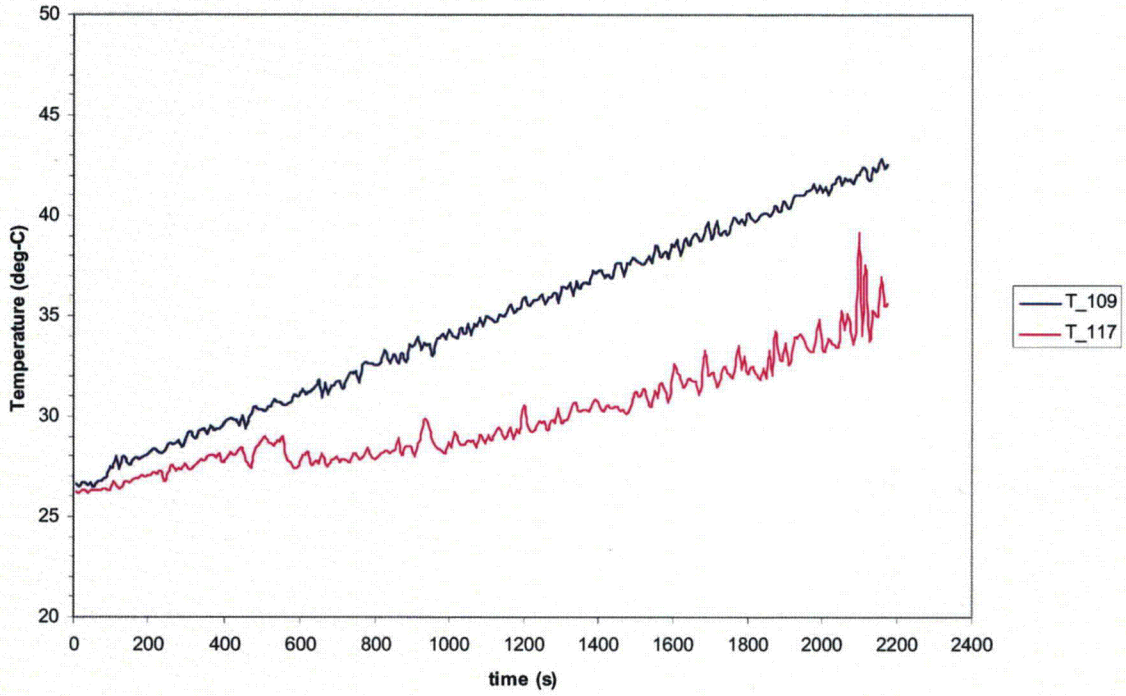

(In this cases, the floating thermocouple T_117 was twisted on its float and was slightly into the gas space. T_117 is located at the back wall of the pool and T_109 is located near the front).

Figure 7.46 Floating thermocouple data for case T3-30†
†Refer to Table 7.2 for test conditions

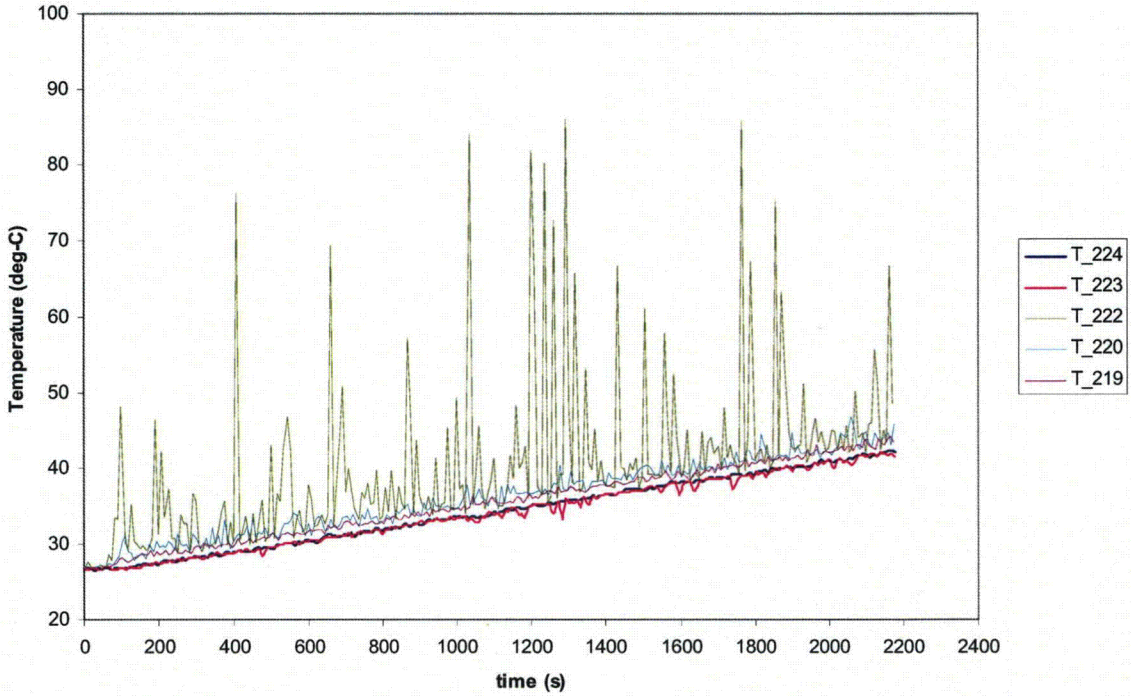

Figure 7.47 Vertical temperature distribution along the vent side centerline for case T3-30†

†Refer to Table 7.2 for test conditions

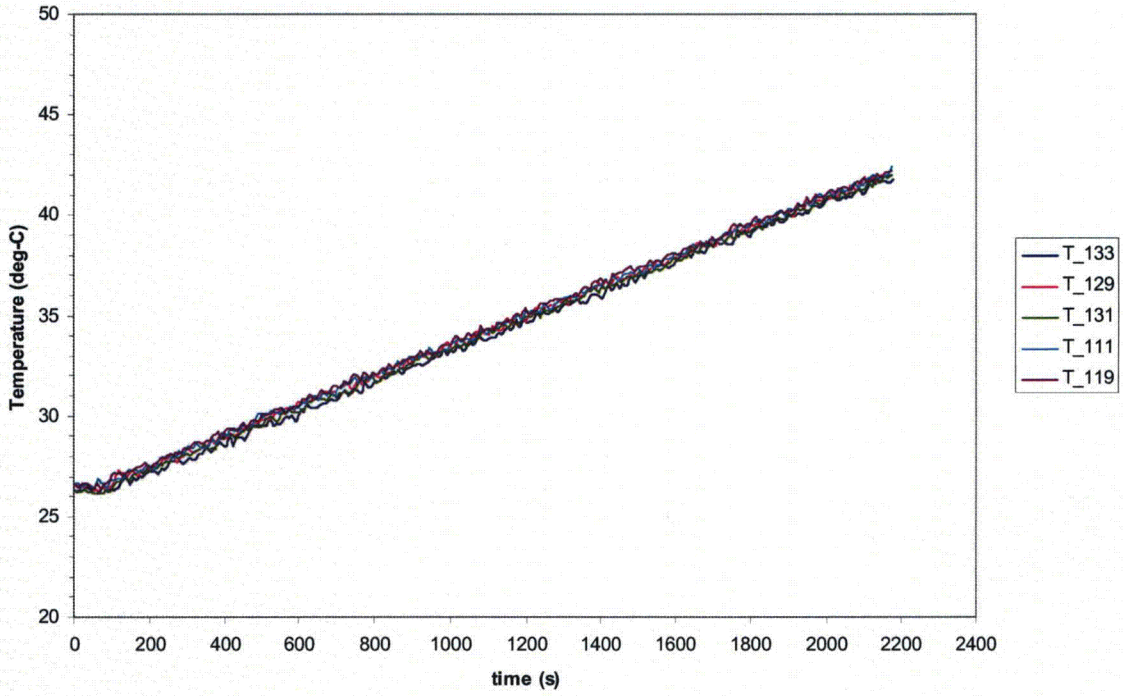

Figure 7.48 Vertical temperature distribution along the pool side centerline for case T3-30†

†Refer to Table 7.2 for test conditions

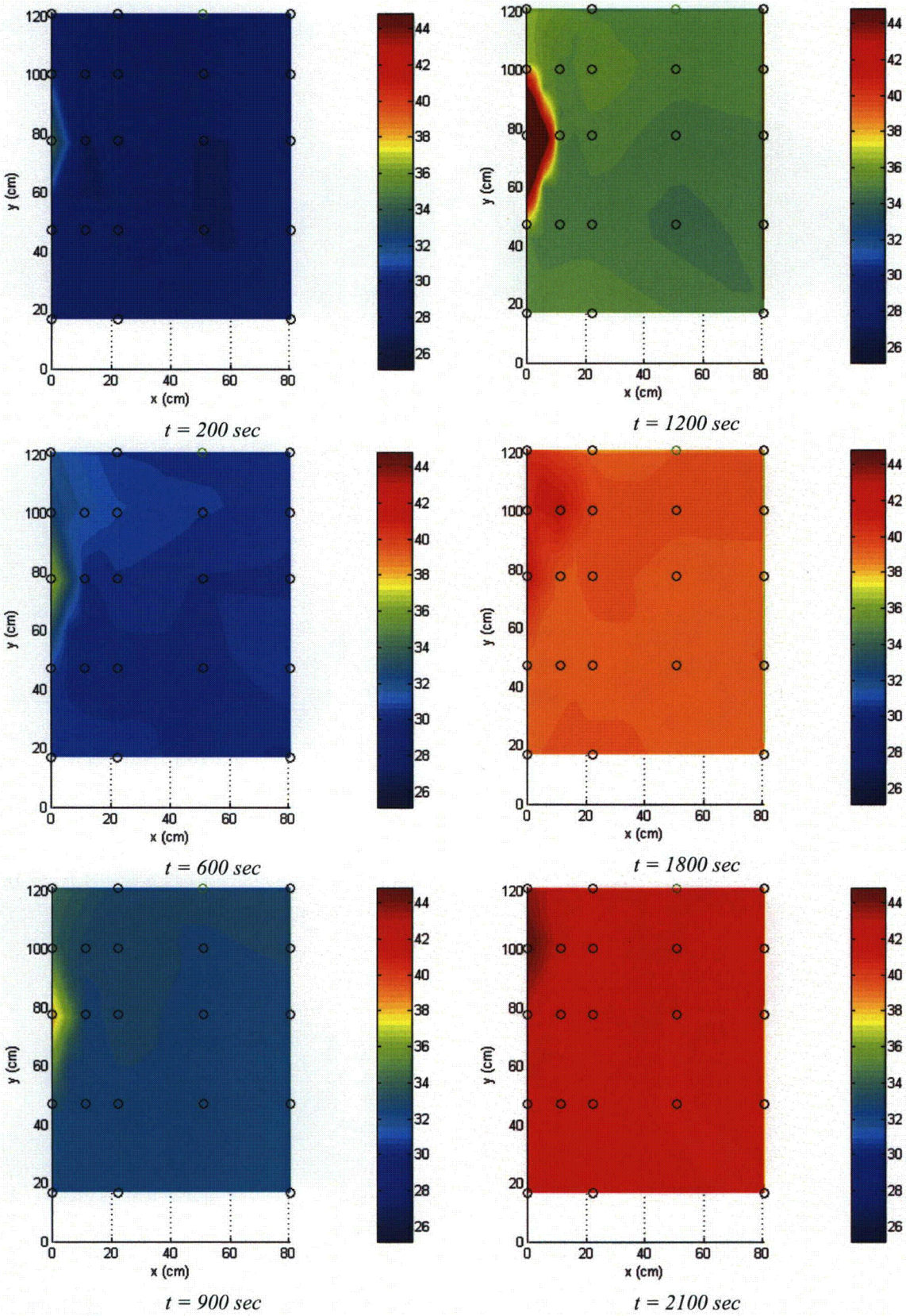

Figure 7.49 Temperature profile development along the pool vertical center plane for case T3-30

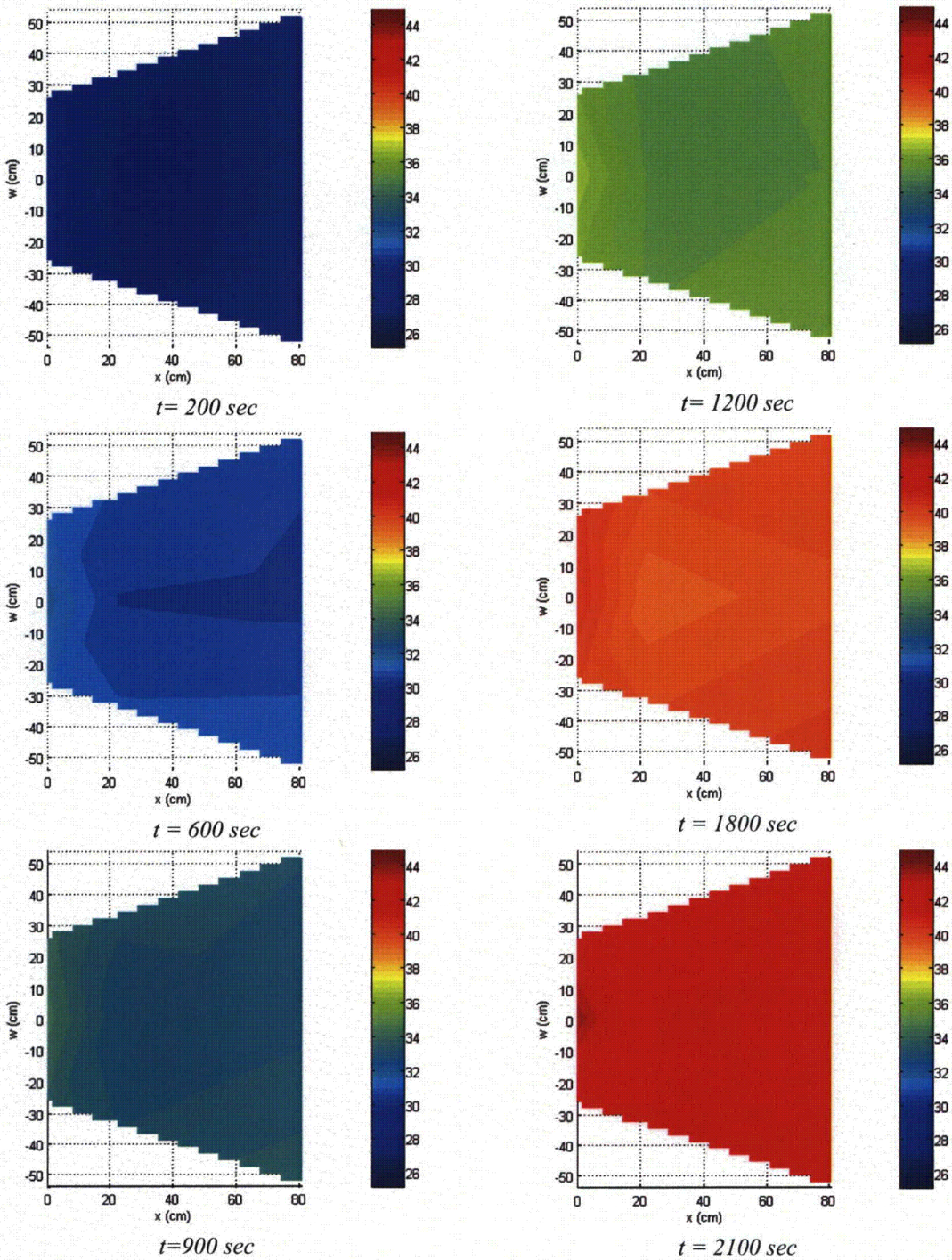

Figure 7.50 Temperature profile development along the pool surface for case T3-30

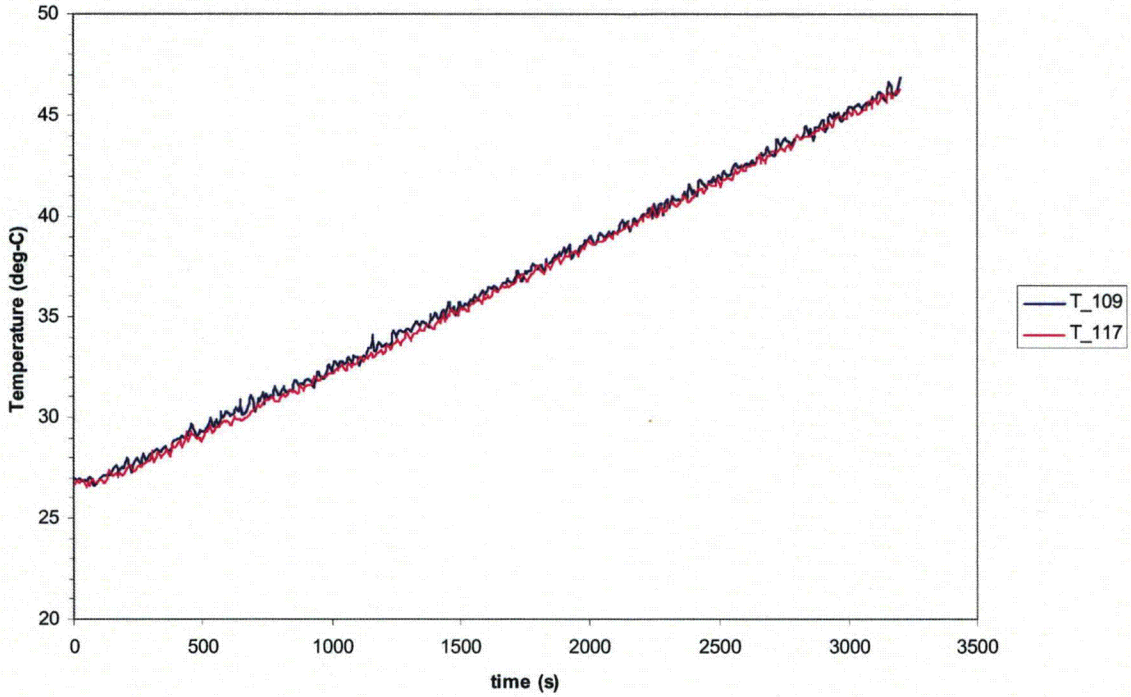

Figure 7.51 Real-time temperature data at the water surface for case T3-51†
†Refer to Table 7.2 for test conditions

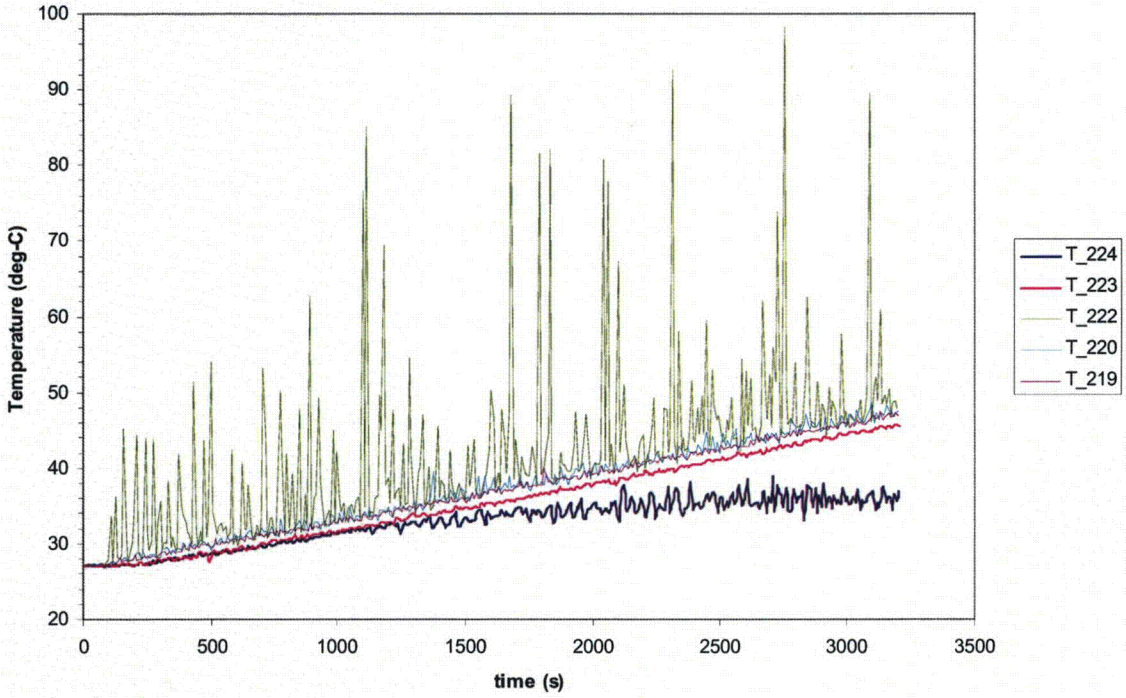

Figure 7.52 Vertical temperature distribution along the vent side centerline for case T3-51†

†Refer to Table 7.2 for test conditions

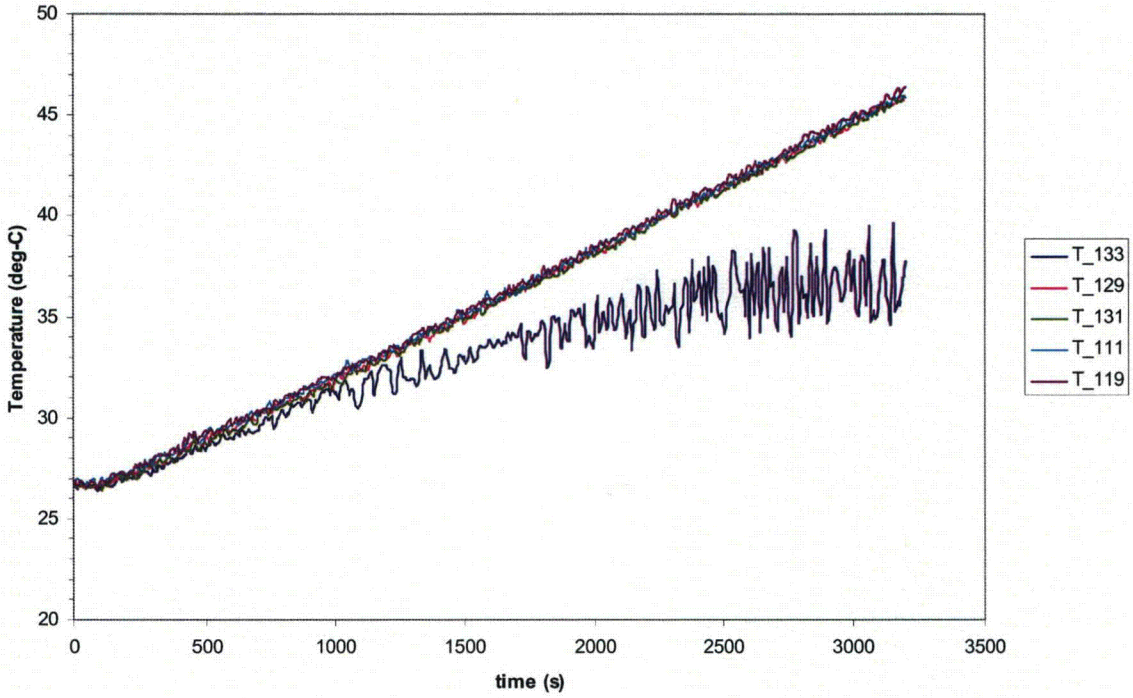

Figure 7.53 Vertical temperature distribution along the pool side centerline for case T3-51†

†Refer to Table 7.2 for test conditions

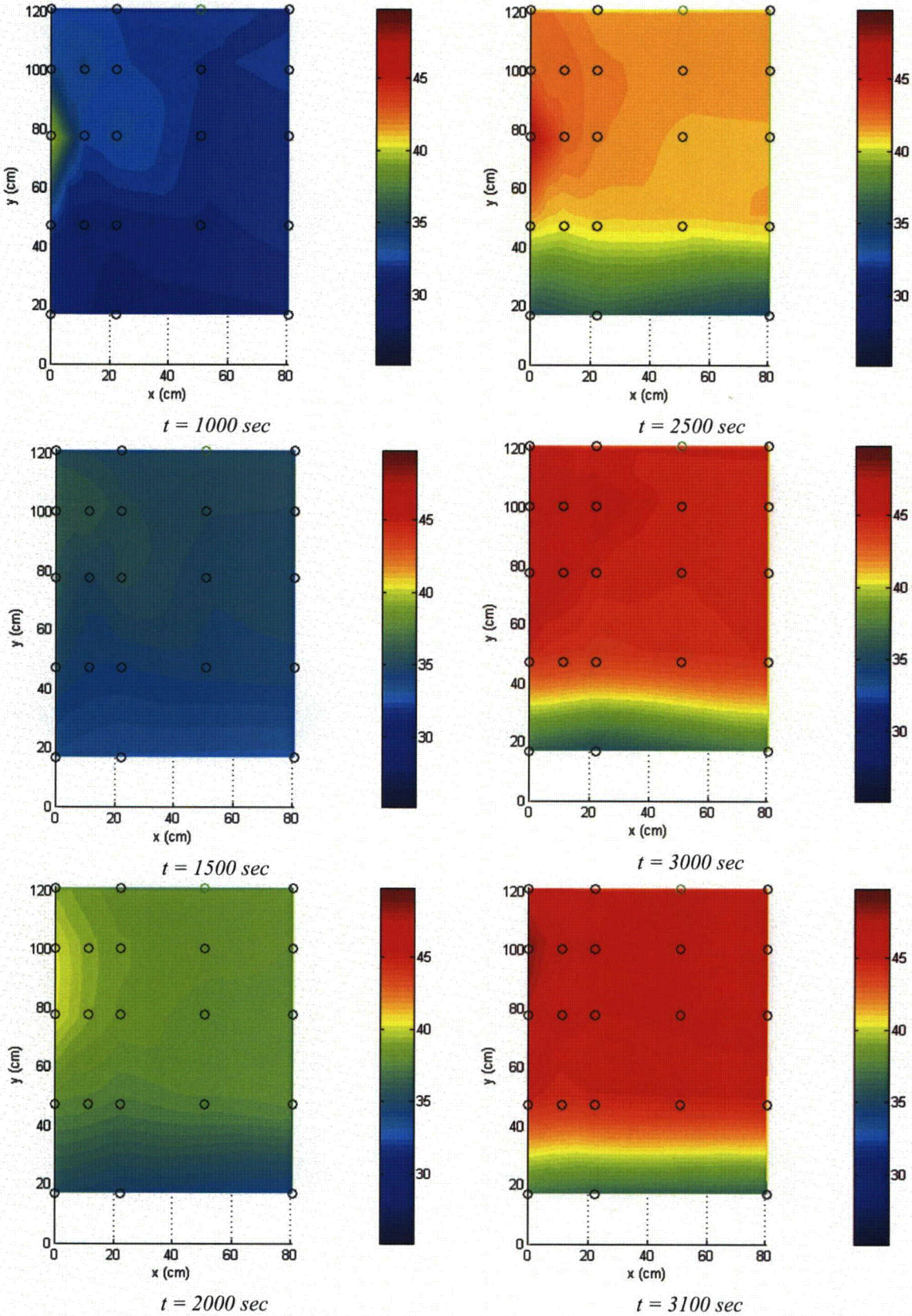

Figure 7.54 Temperature profile development along the pool vertical center plane for case T3-51

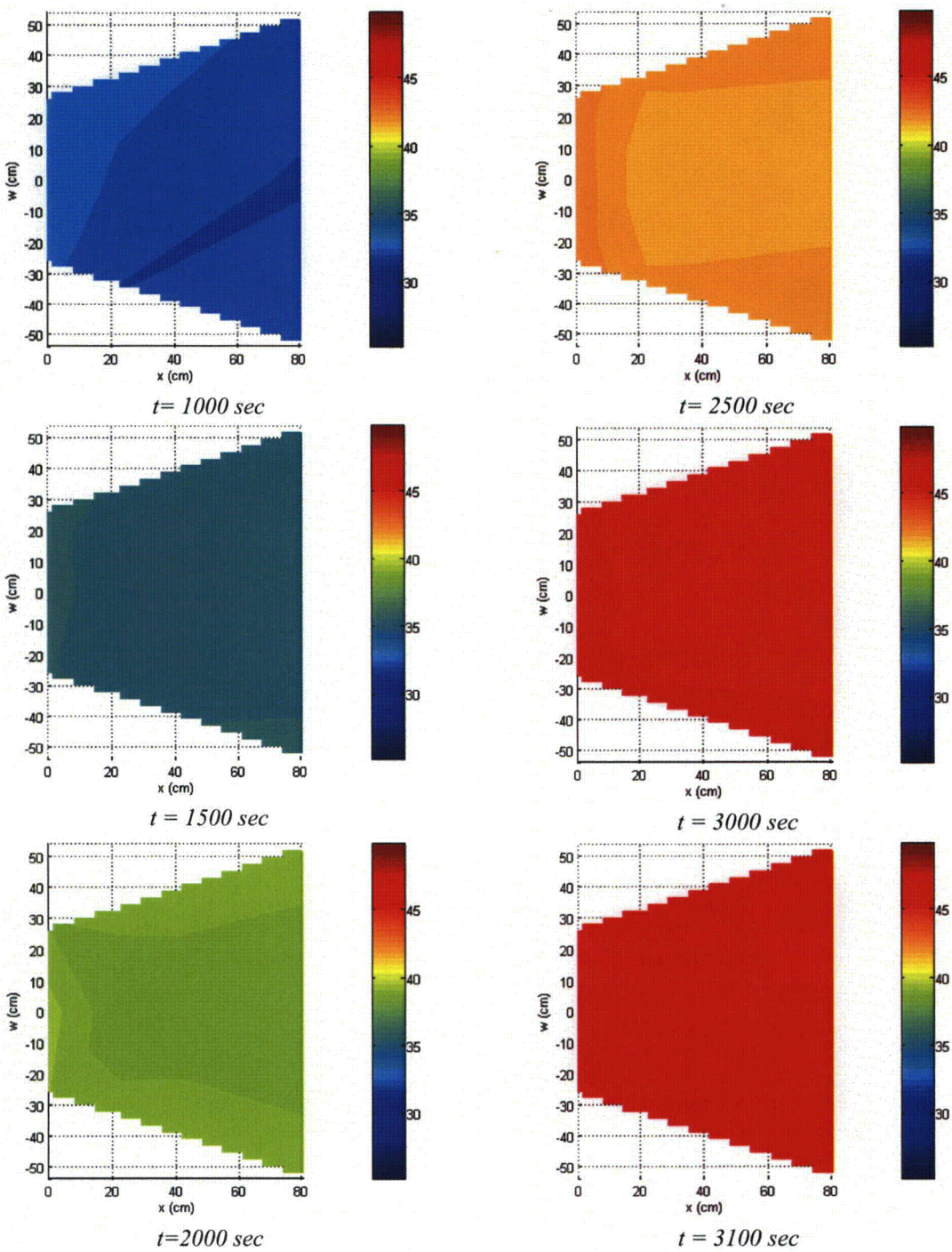

Figure 7.55 Temperature profile development along the pool surface for case T3-51

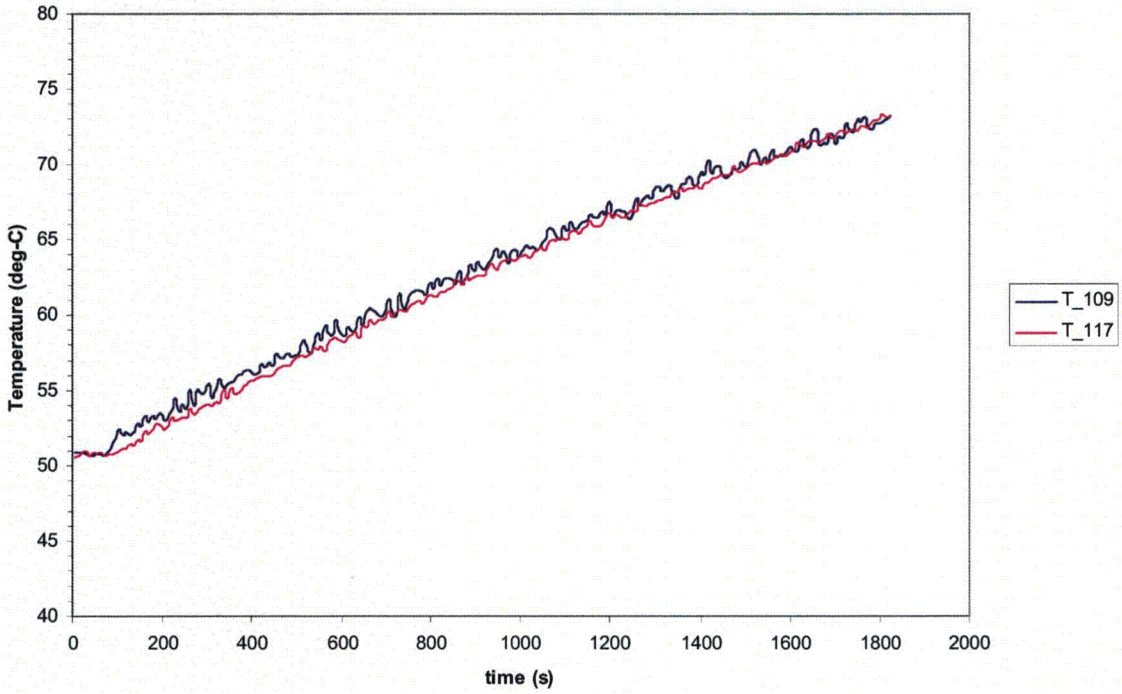

Figure 7.56 Real-time temperature data at the water surface for case T3-26†
†Refer to Table 7.2 for test conditions

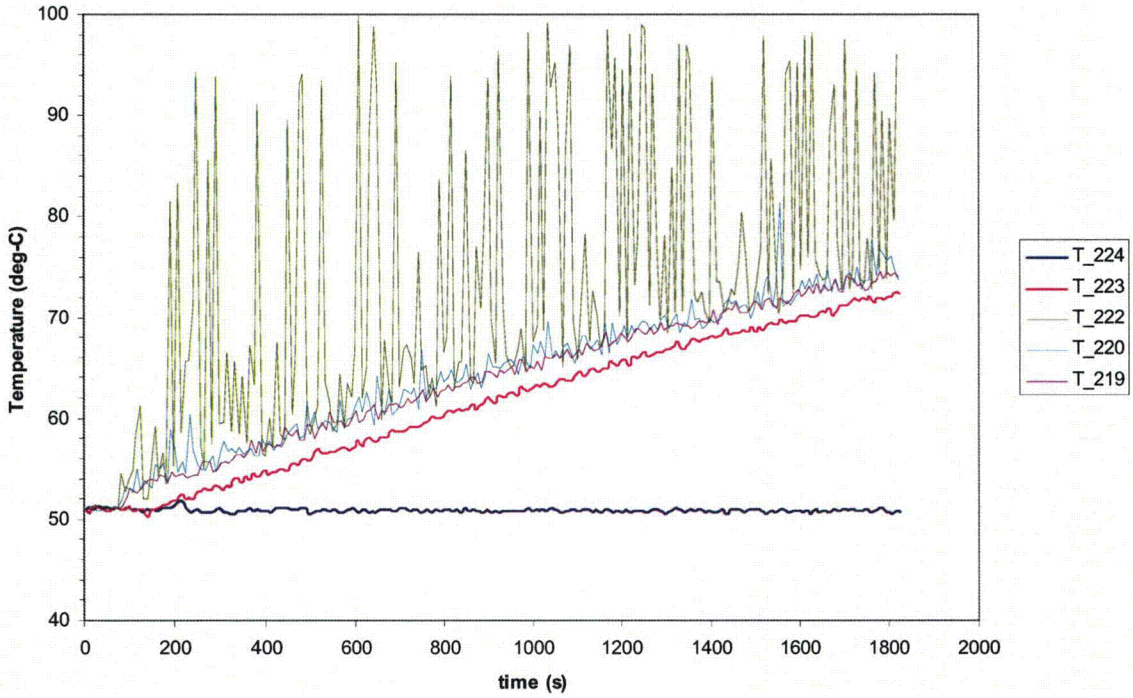

Figure 7.57 Vertical temperature distribution along the vent side centerline for case T3-26†

†Refer to Table 7.2 for test conditions

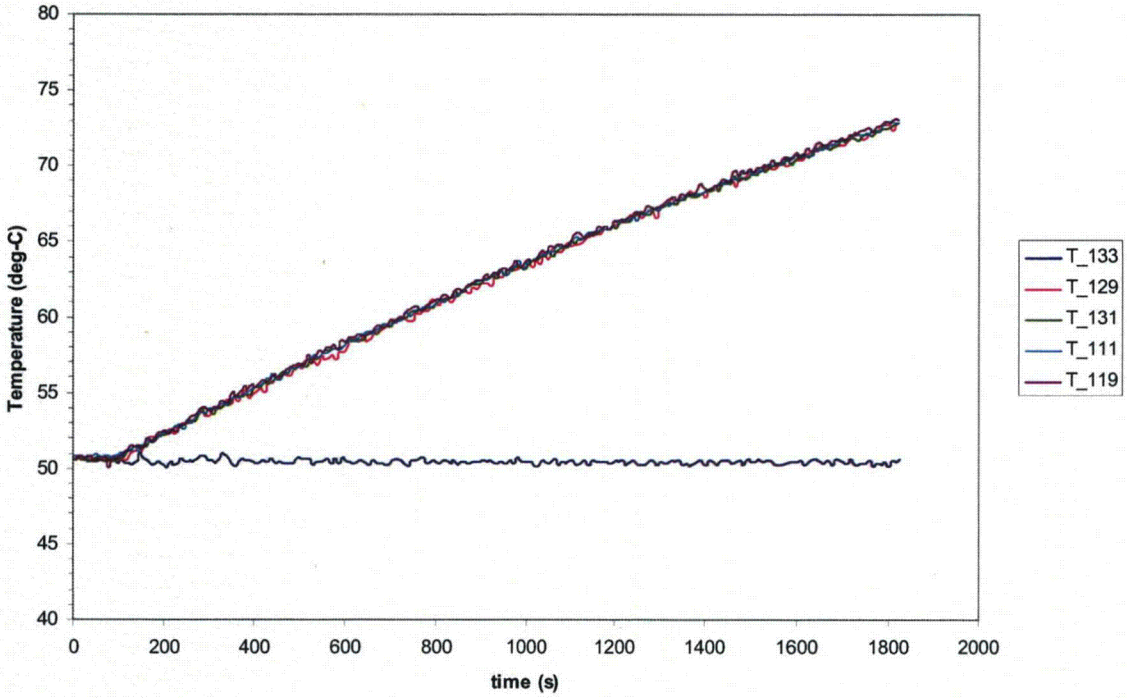

Figure 7.58 Vertical temperature distribution along the pool side centerline for case T3-26†

†Refer to Table 7.2 for test conditions

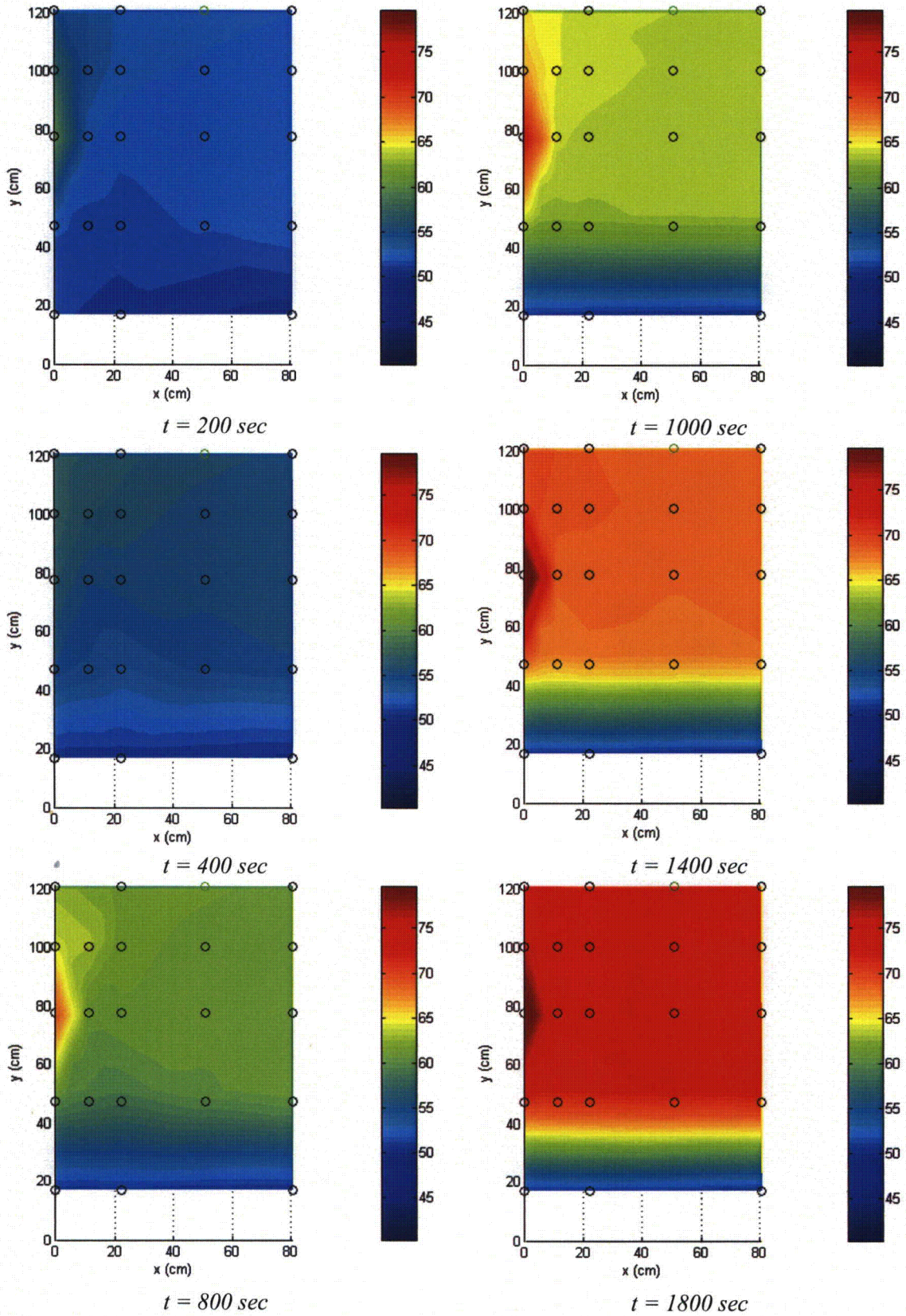

Figure 7.59 Temperature profile development along the pool vertical center plane for case T3-26

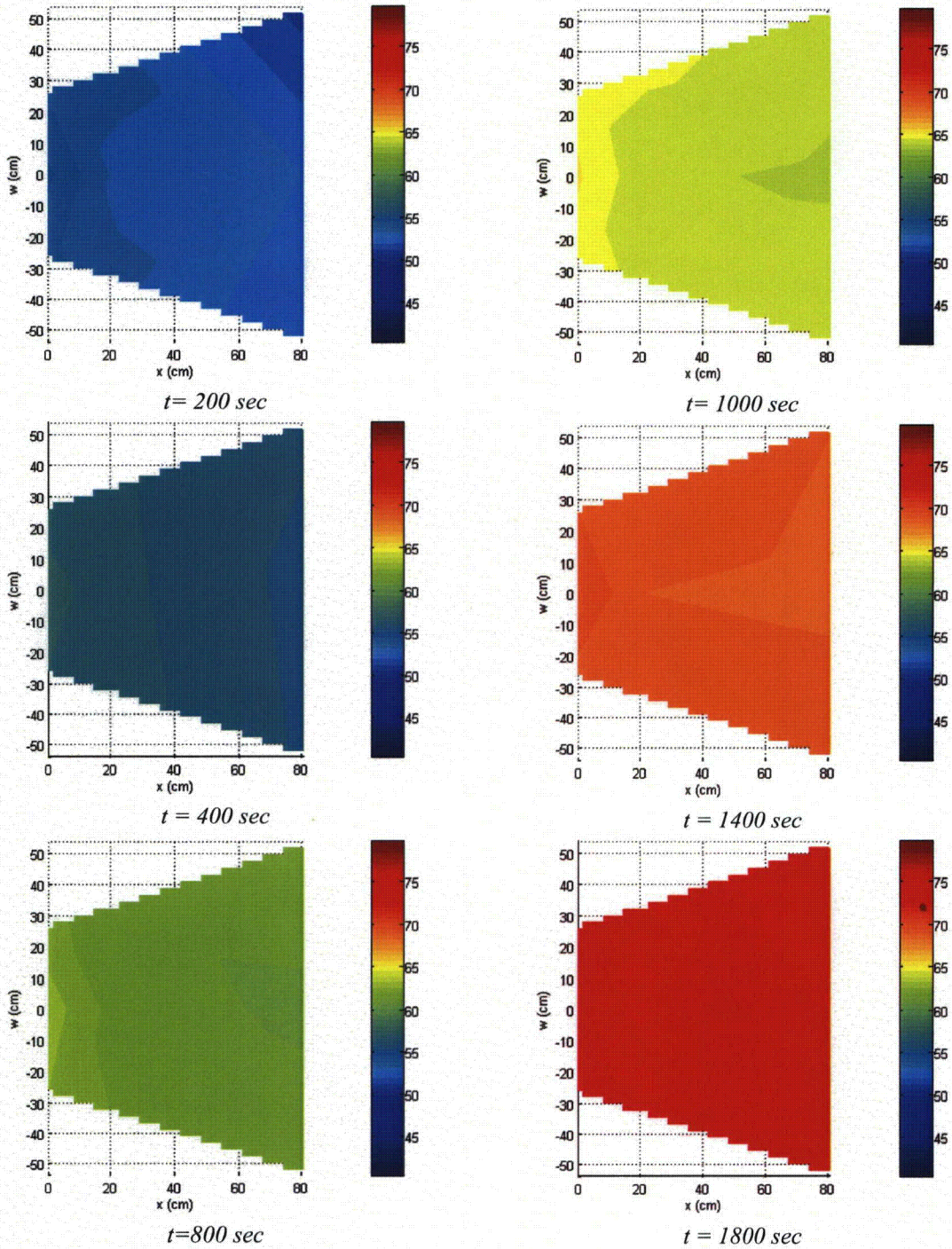

Figure 7.60 Temperature profile development along the pool surface for case T3-26

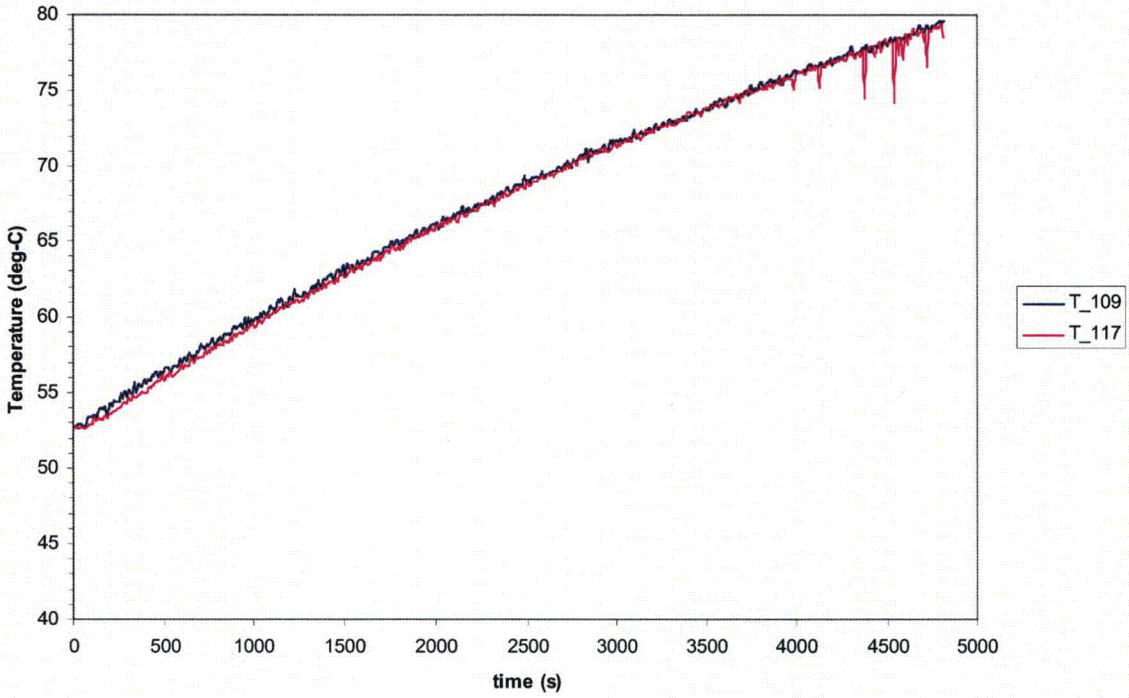

Figure 7.61 Real-time temperature data at the water surface for case T3-38†
†Refer to Table 7.2 for test conditions

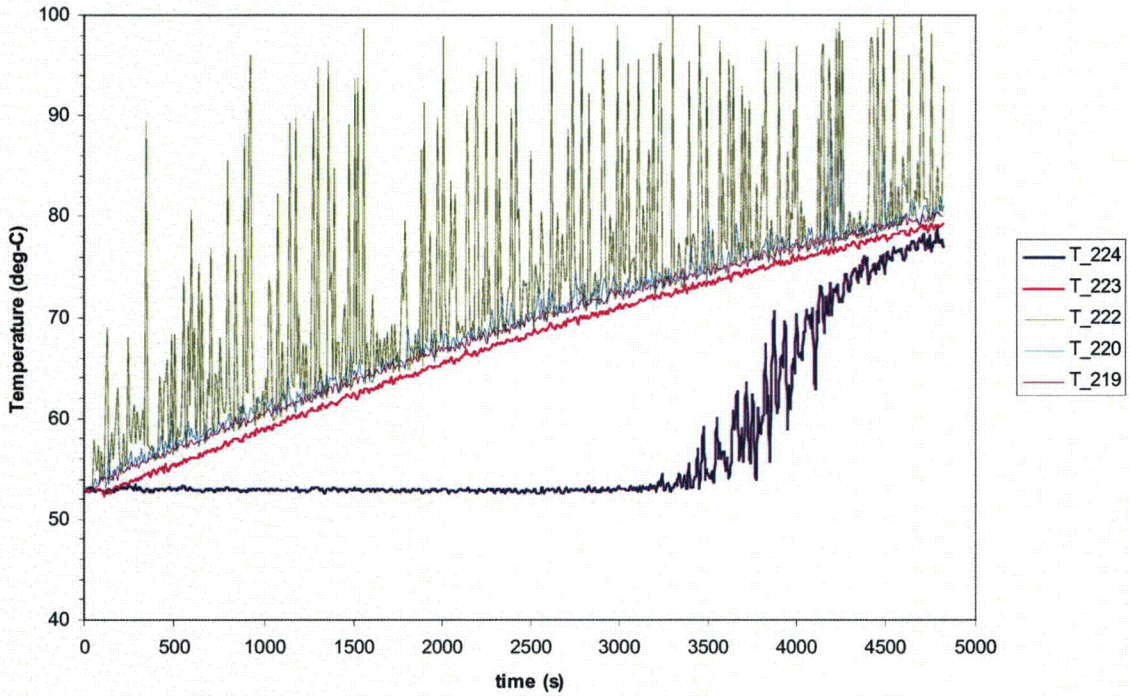

Figure 7.62 Vertical temperature distribution along the vent side centerline for case T3-38†

†Refer to Table 7.2 for test conditions

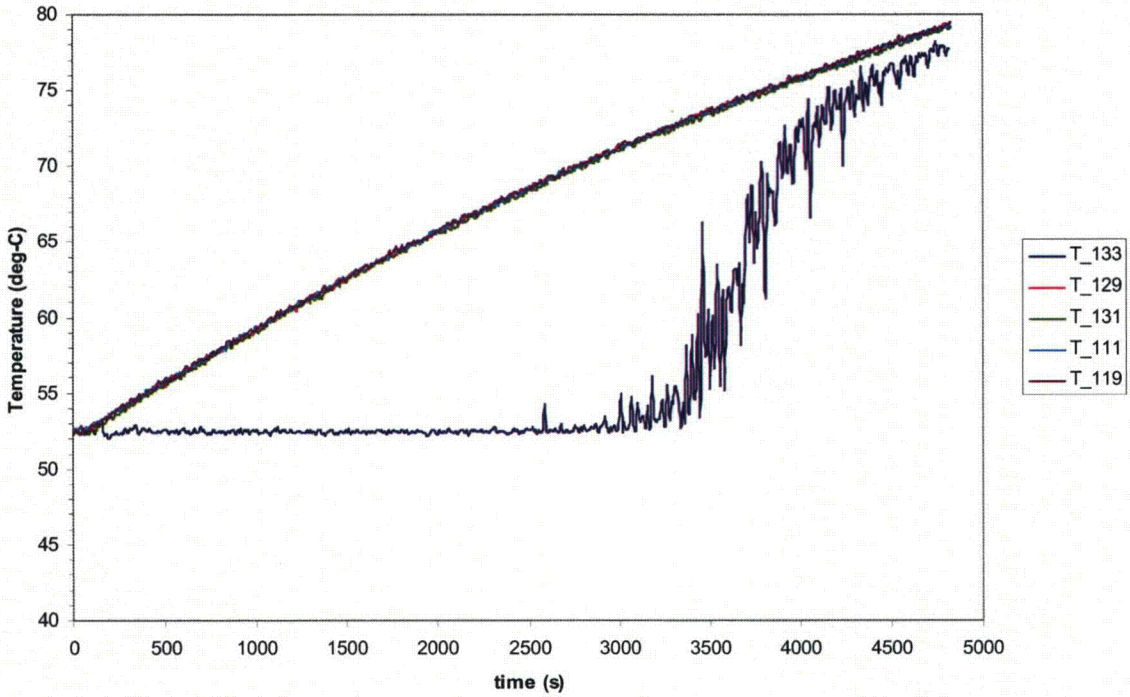

Figure 7.63 Vertical temperature distribution along the pool side centerline for case T3-38†

†Refer to Table 7.2 for test conditions

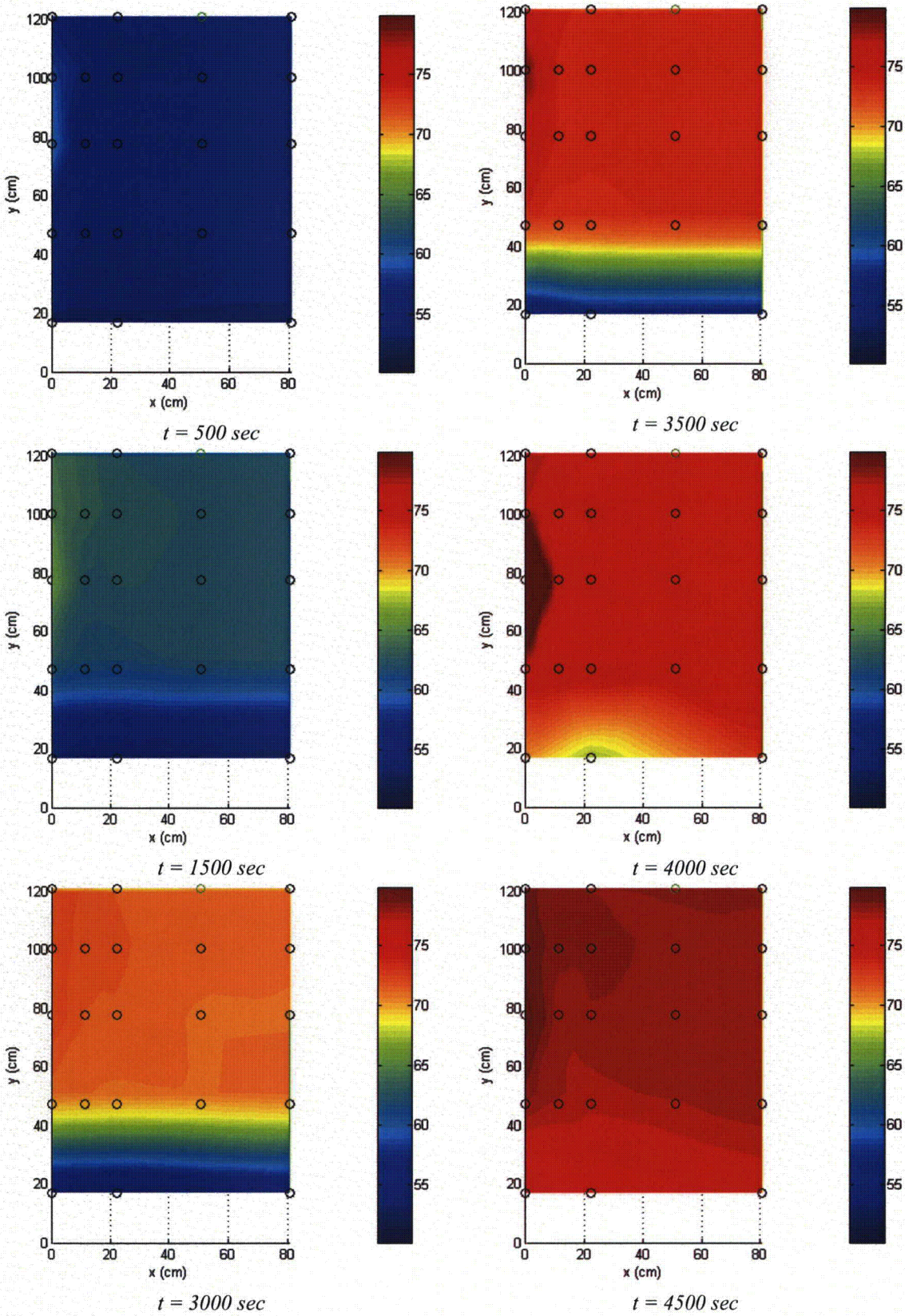

Figure 7.64 Temperature profile development along the pool vertical center plane for case T3-38

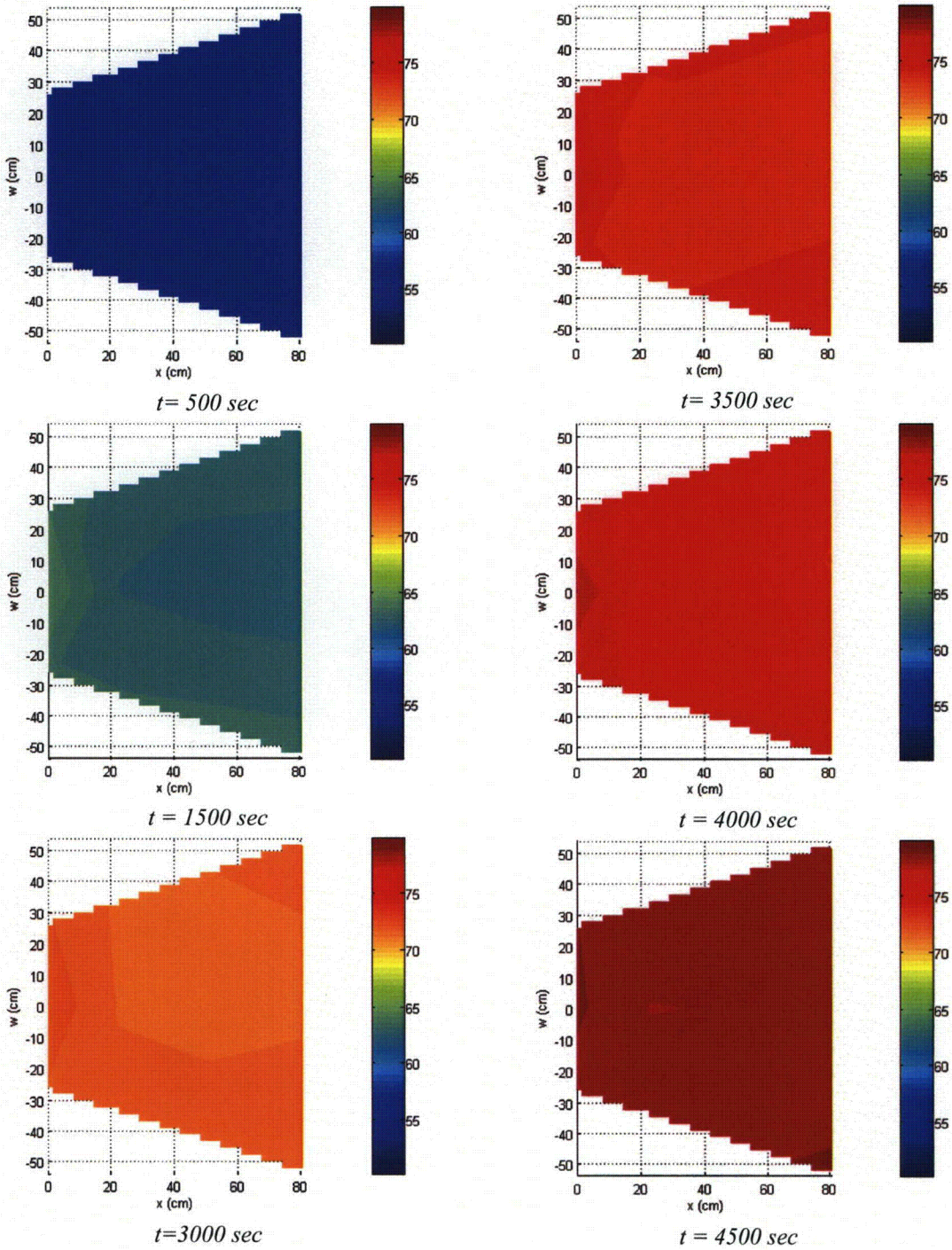

Figure 7.65 Temperature profile development along the pool surface for case T3-38

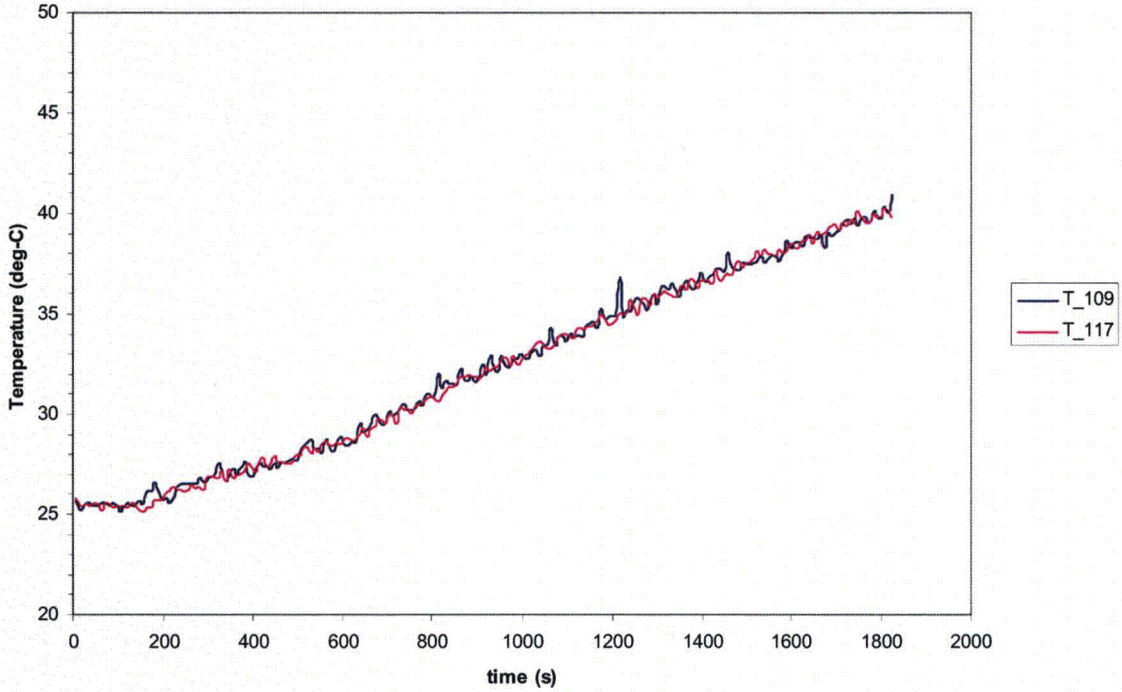

Figure 7.66 Real-time temperature data at the water surface for case T3-53†
†Refer to Table 7.2 for test conditions

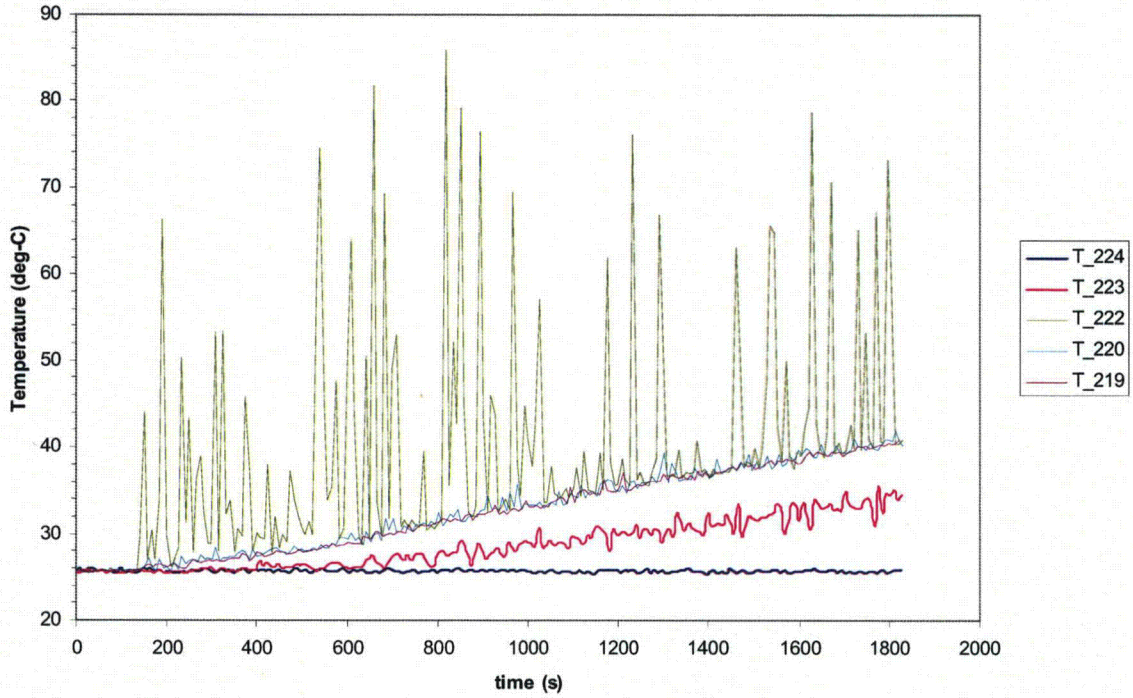

Figure 7.67 Vertical temperature distribution along the vent side centerline for case T3-53†

†Refer to Table 7.2 for test conditions

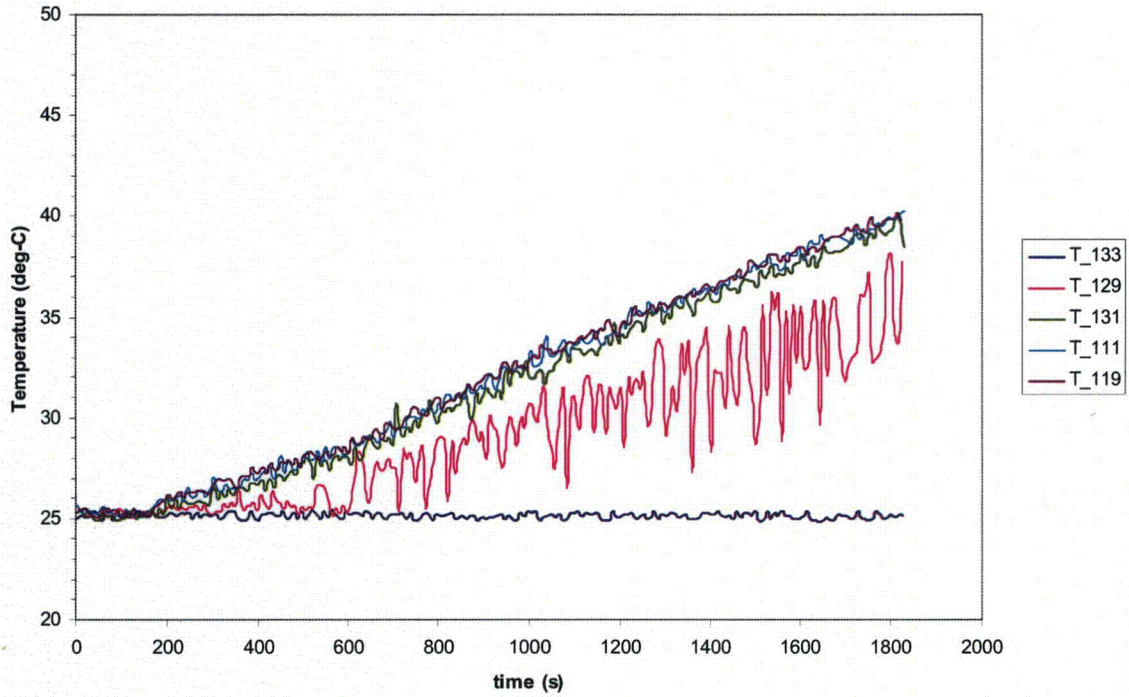

Figure 7.68 Vertical temperature distribution along the pool side centerline for case T3-53†

†Refer to Table 7.2 for test conditions

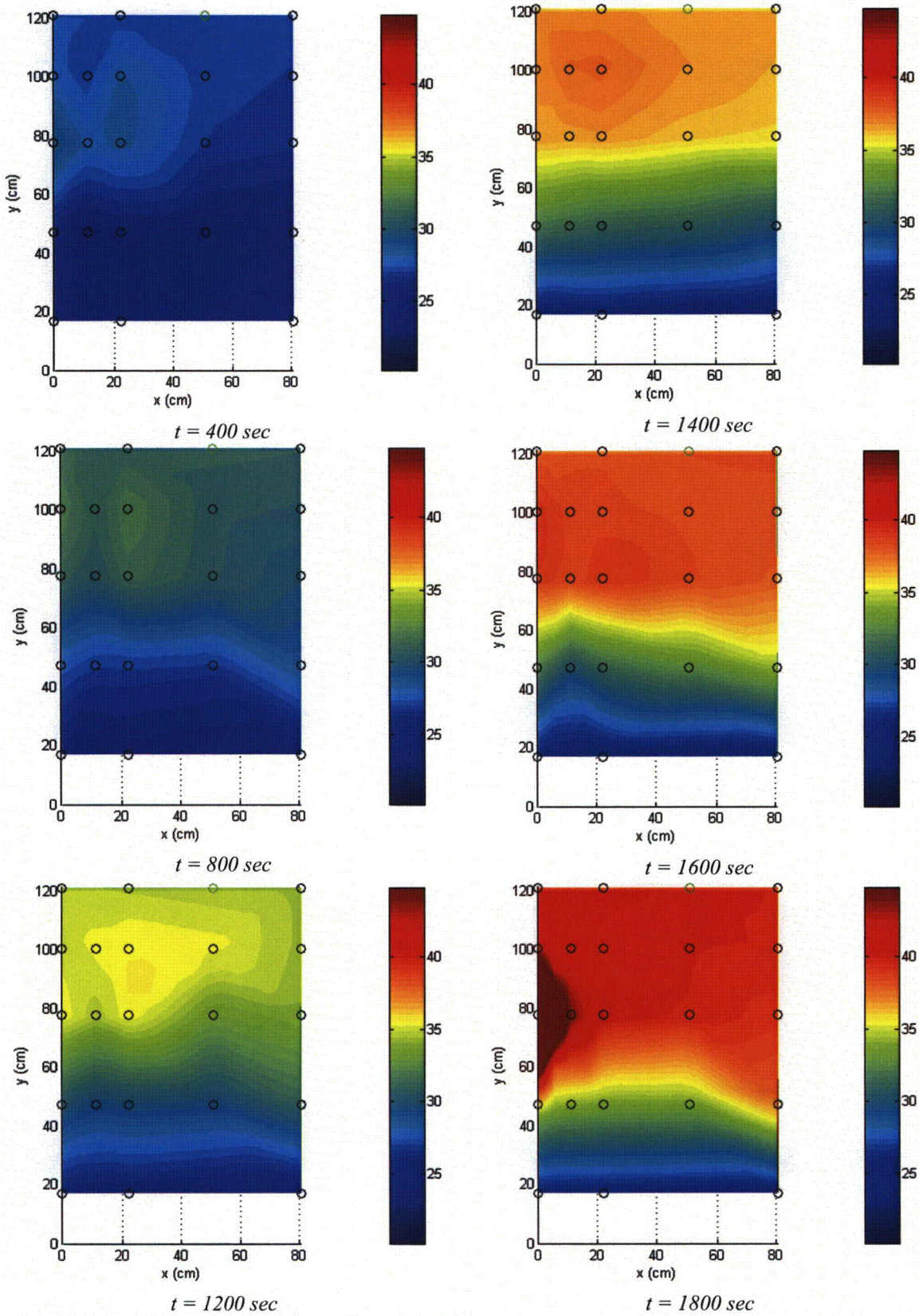

Figure 7.69 Temperature profile development along the pool vertical center plane for case T3-53

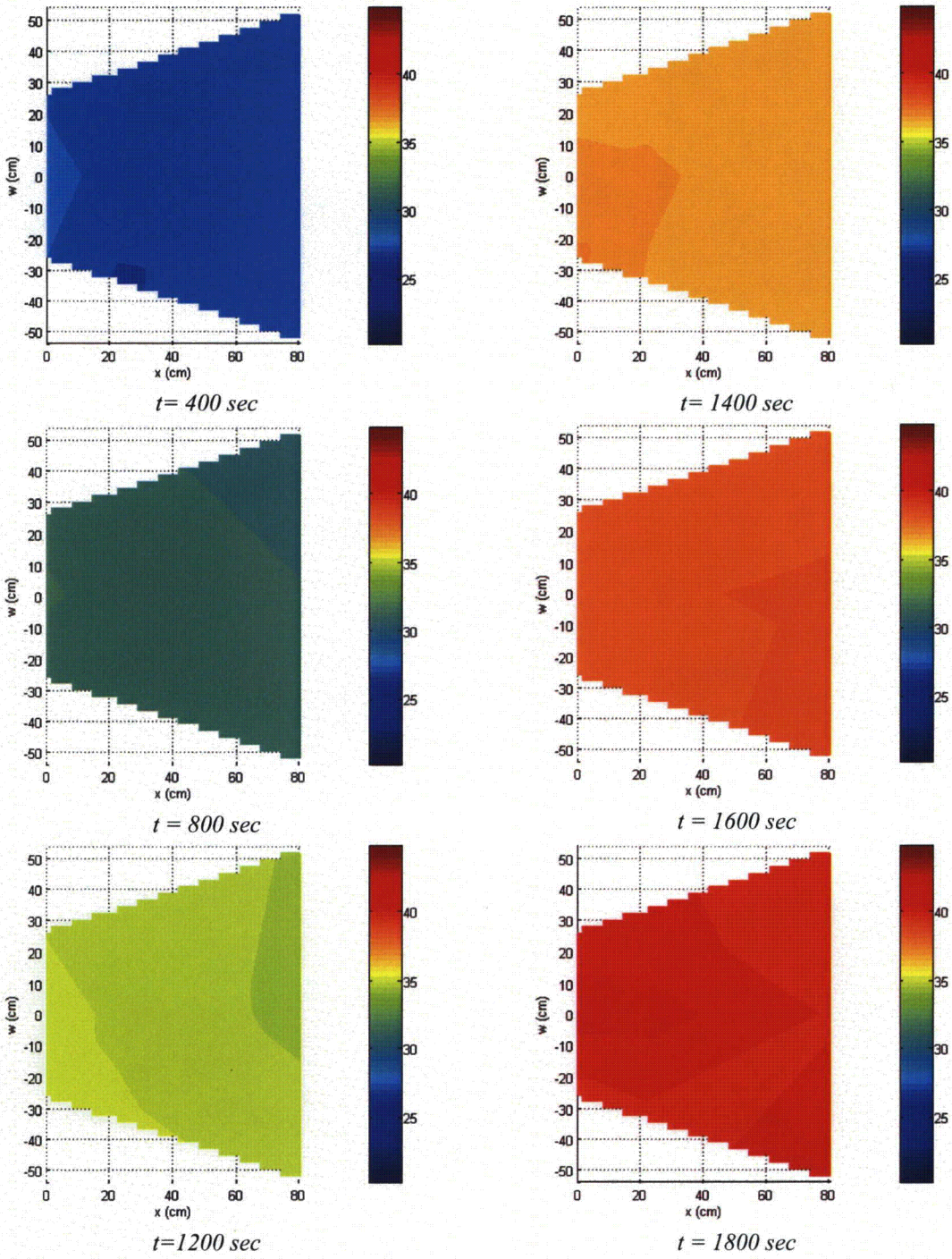

Figure 7.70 Temperature profile development along the pool surface for case T3-53

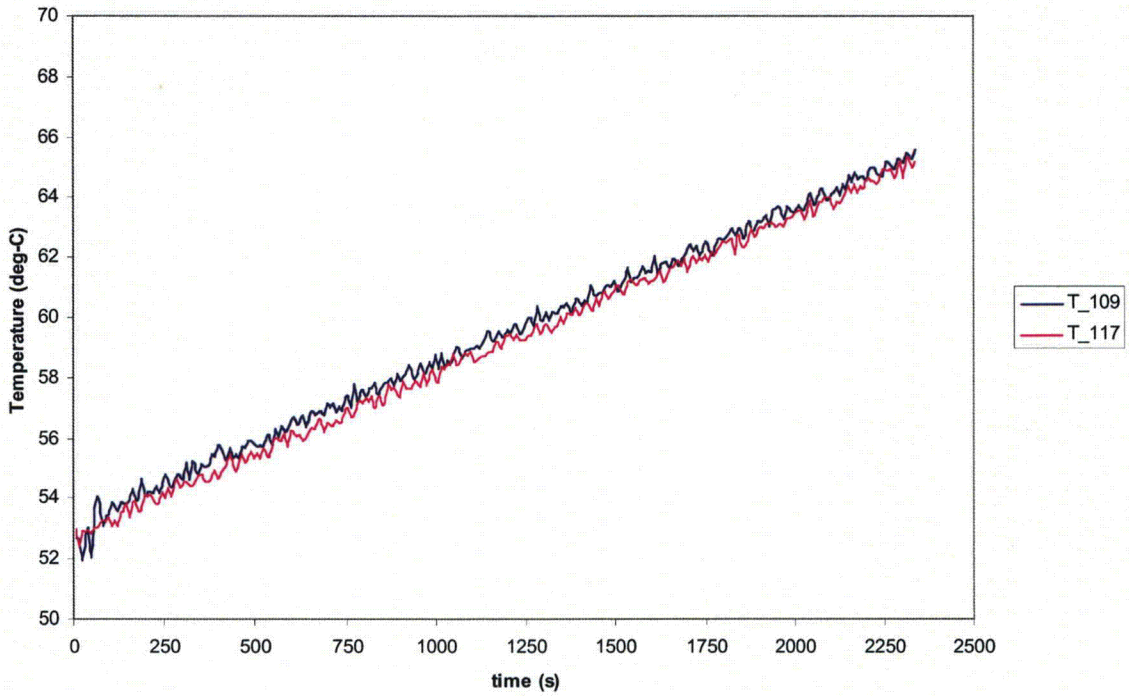

Figure 7.71 Real-time temperature data at the water surface for case T3-55†
†Refer to Table 7.2 for test conditions

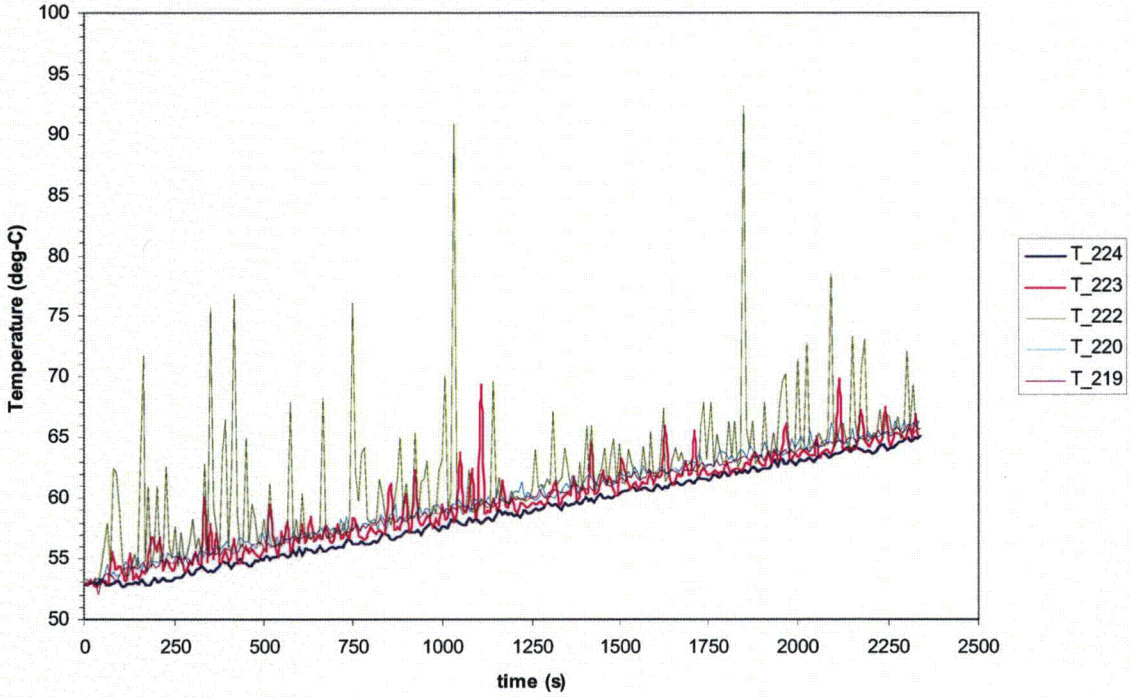

Figure 7.72 Vertical temperature distribution along the vent side centerline for case T3-55†

†Refer to Table 7.2 for test conditions

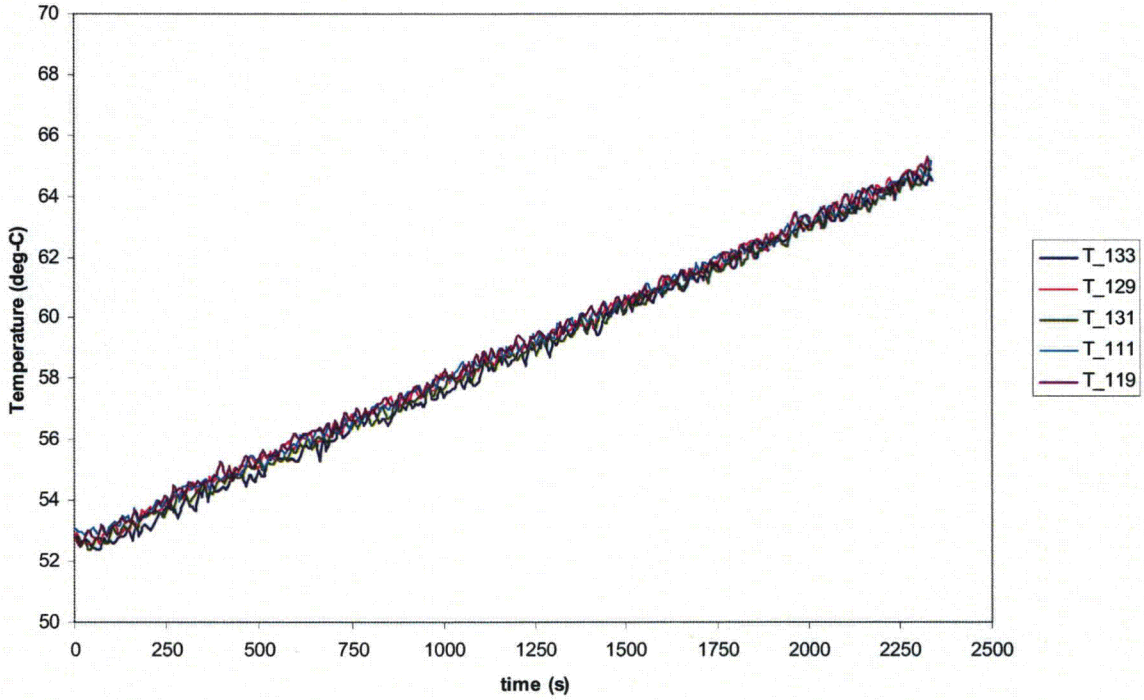

Figure 7.73 Vertical temperature distribution along the pool side centerline for case T3-55†

†Refer to Table 7.2 for test conditions

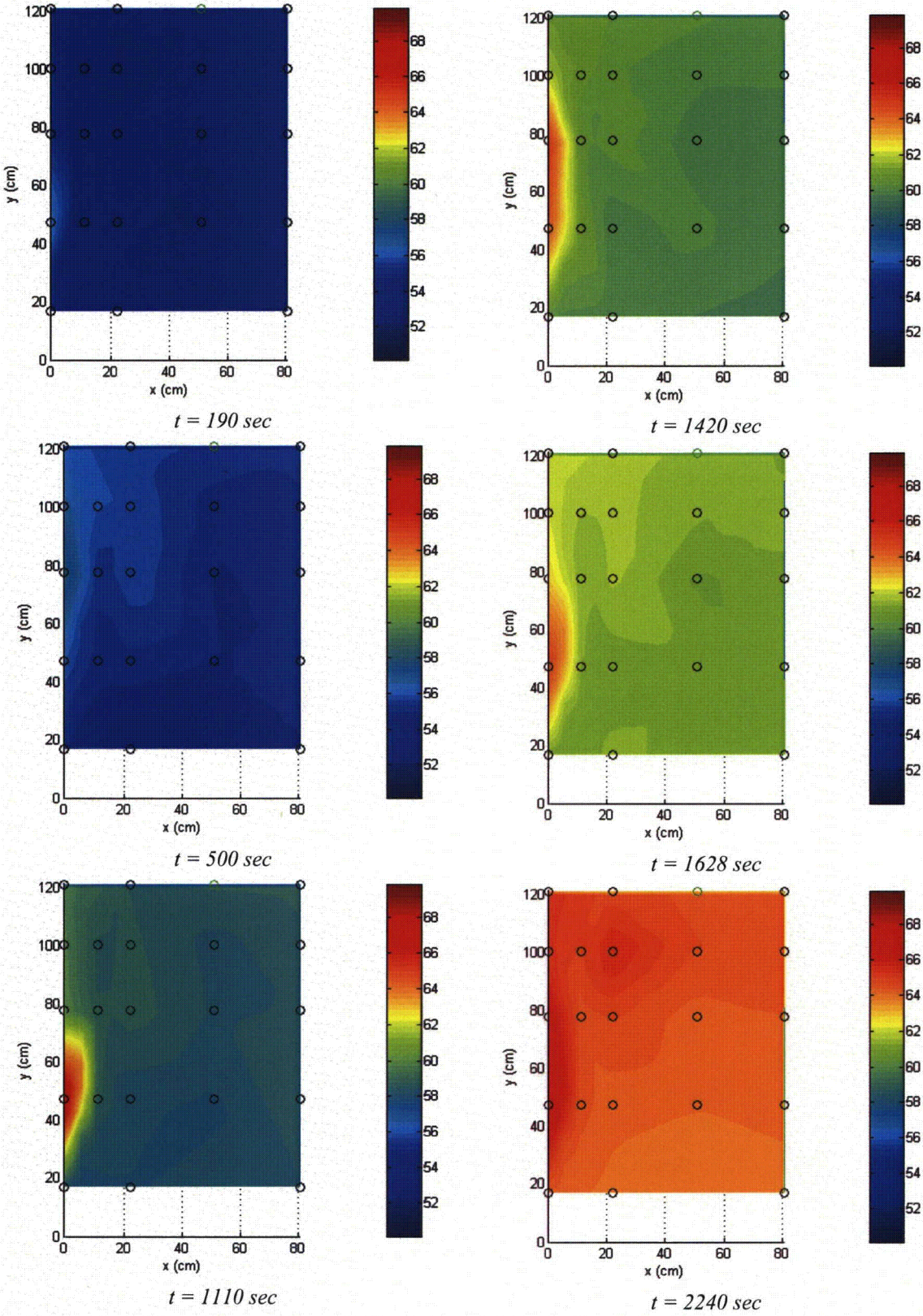

Figure 7.74 Temperature profile development along the pool vertical center plane for case T3-55

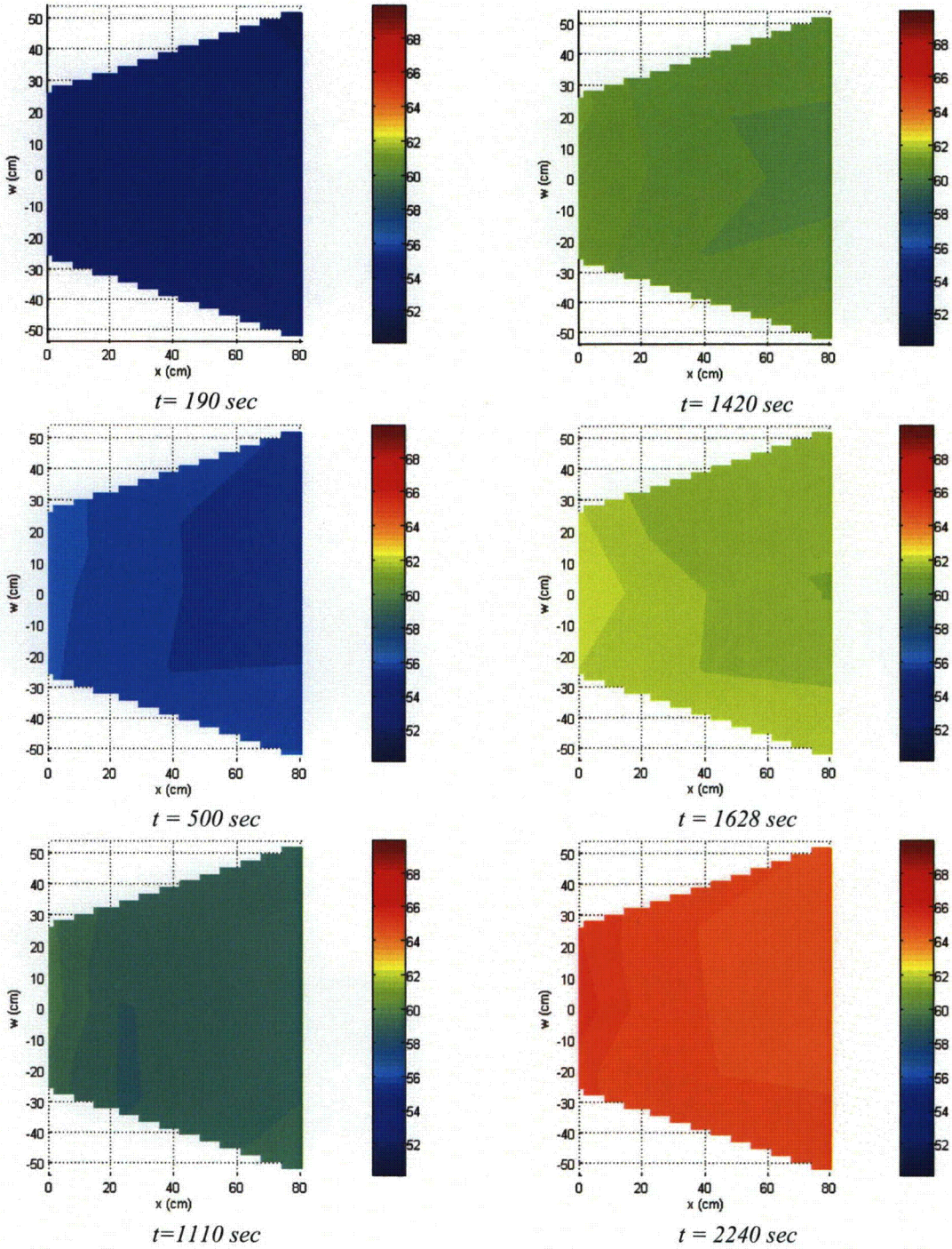

Figure 7.75 Temperature profile development along the pool surface for case T3-55

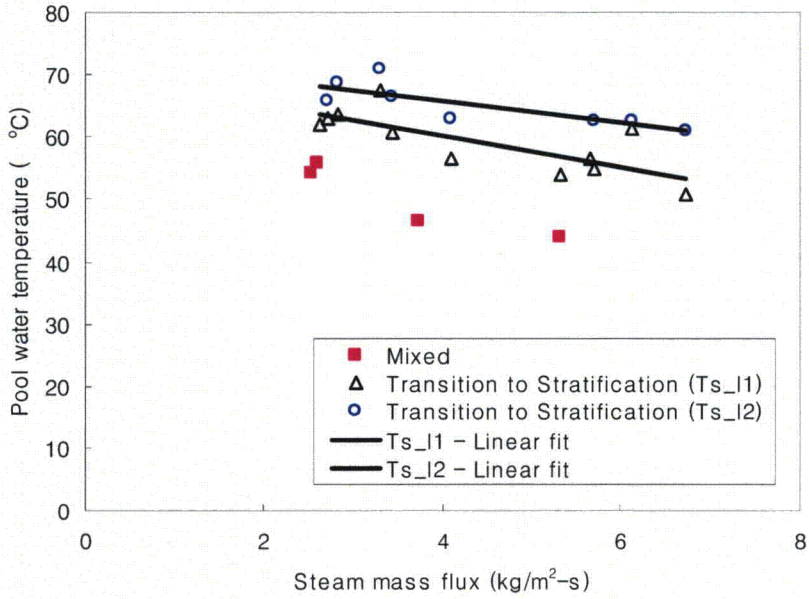

(a)

$$Fr = \frac{\rho_f \upsilon_m^2}{\left(\rho_f - \rho_m\right) g D}$$

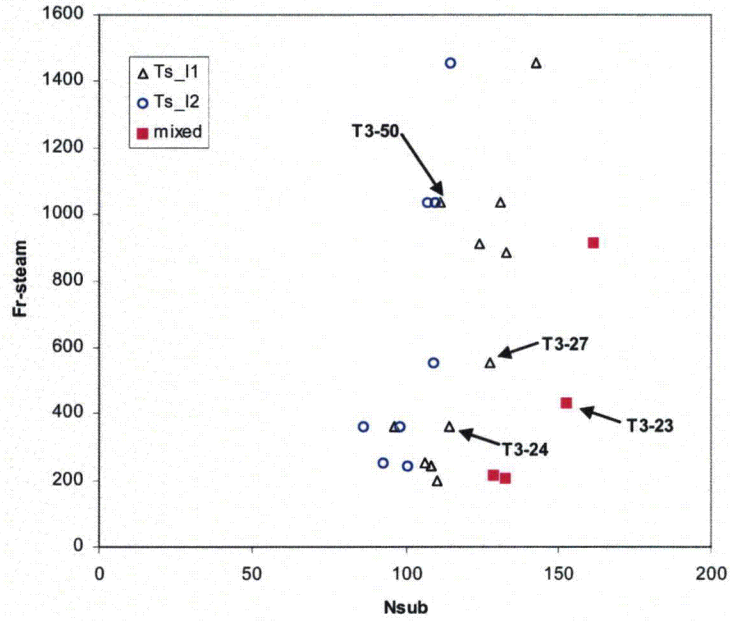

$$N_{sub} = \frac{\Delta\rho}{\rho_m}\frac{\Delta h_{sub}}{\Delta h_{fg}} = \frac{\Delta\rho\ c_{p,f}\Delta T_{sub}}{\rho_m \Delta h_{fg}} = \left.\frac{\Delta\rho}{\rho_m}\right|_{p_{in}} \frac{c_{p,f}\left(T_{sat}\big|_{-}T_{f,in}\right)}{\left.\Delta h_{fg}\right|_{p_{in}}}$$

(b)

Figure 7.76 The transition from the mixed to stratified conditions for pure steam injection cases (a) steam mass flux versus inlet pool temperature (b) Subcooling versus Froude number

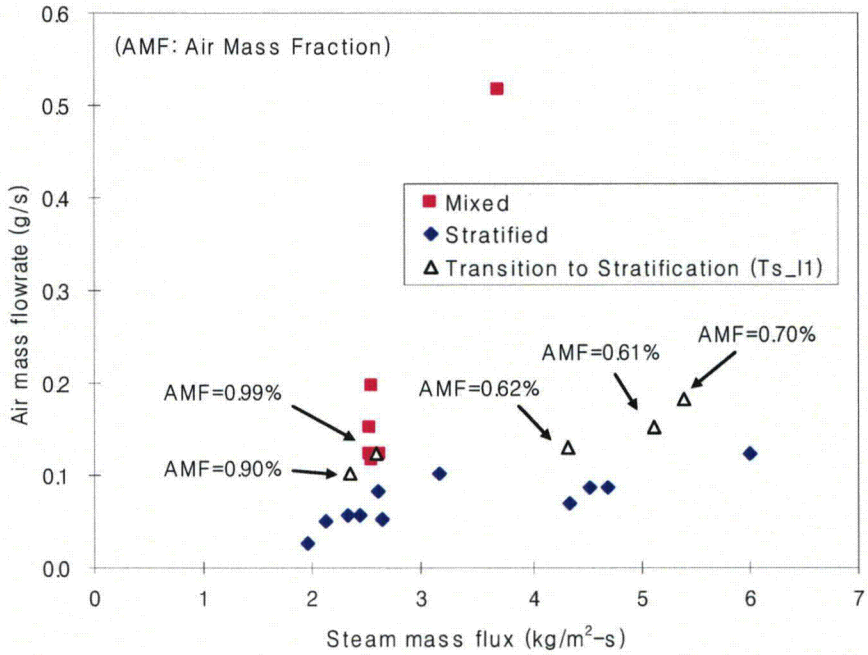

Figure 7.77 The transition from the mixed to stratified conditions for steam-air injection cases (steam mass flux versus air mass flow rate)

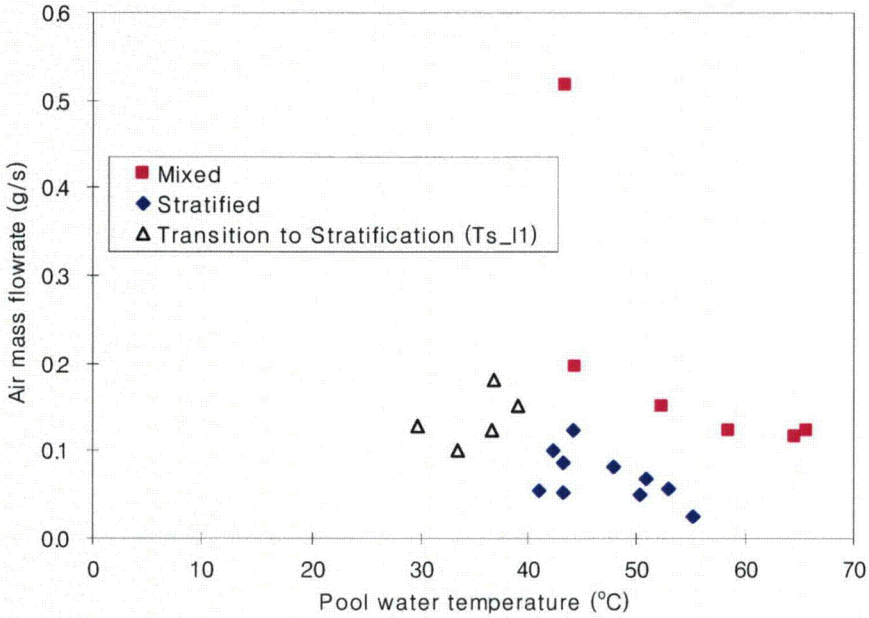

Figure 7.78 The transition from the mixed to stratified conditions for steam-air injection cases (pool water temperature versus air mass flow rate)

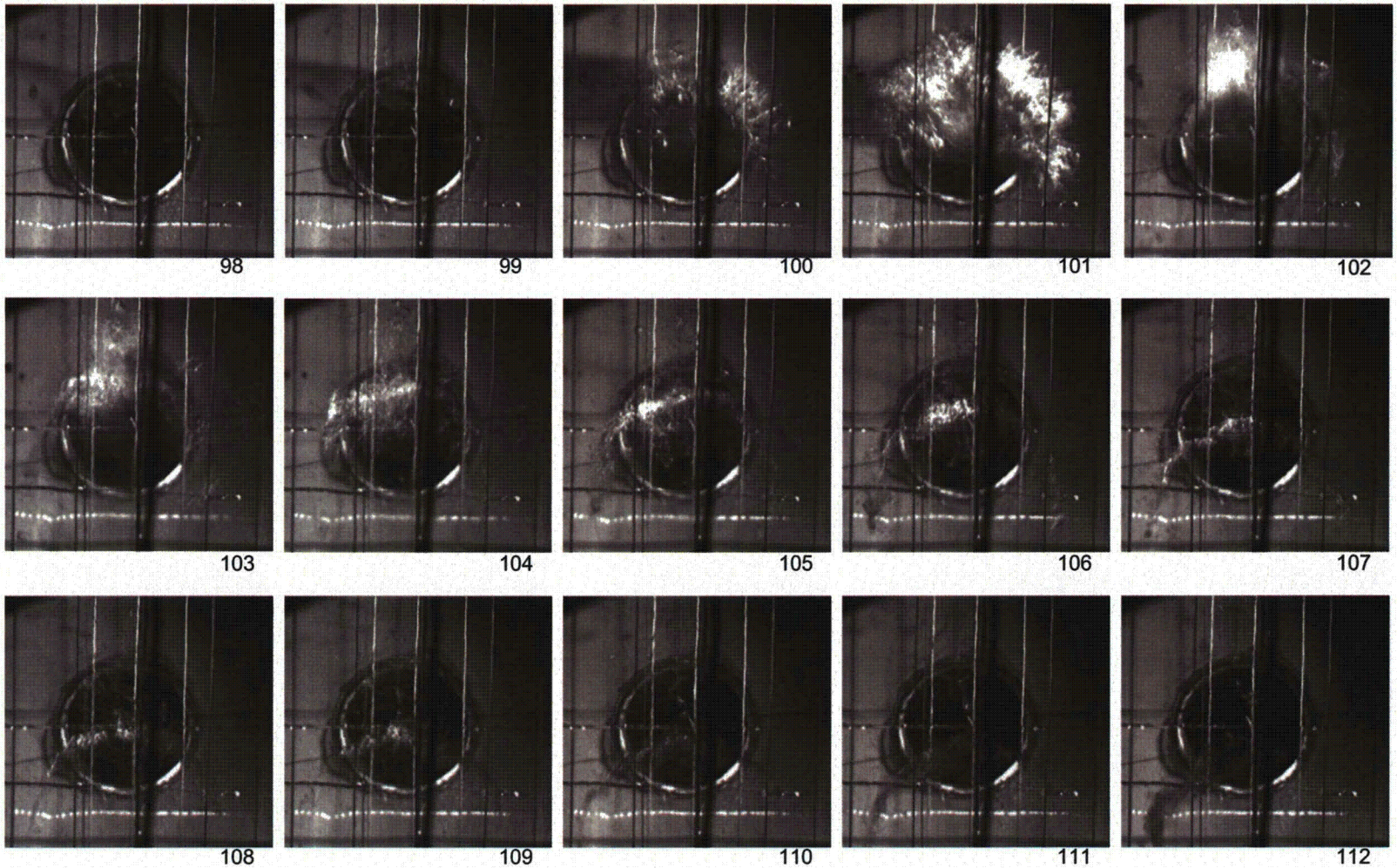

Camera is pointing downward towards vent for 3-inch vent diameter case. Visualization at window 8.

Figure 7.79 Venting images of steam mass flow rate of 17.8 g/s with no air. 0.033 seconds between frames.

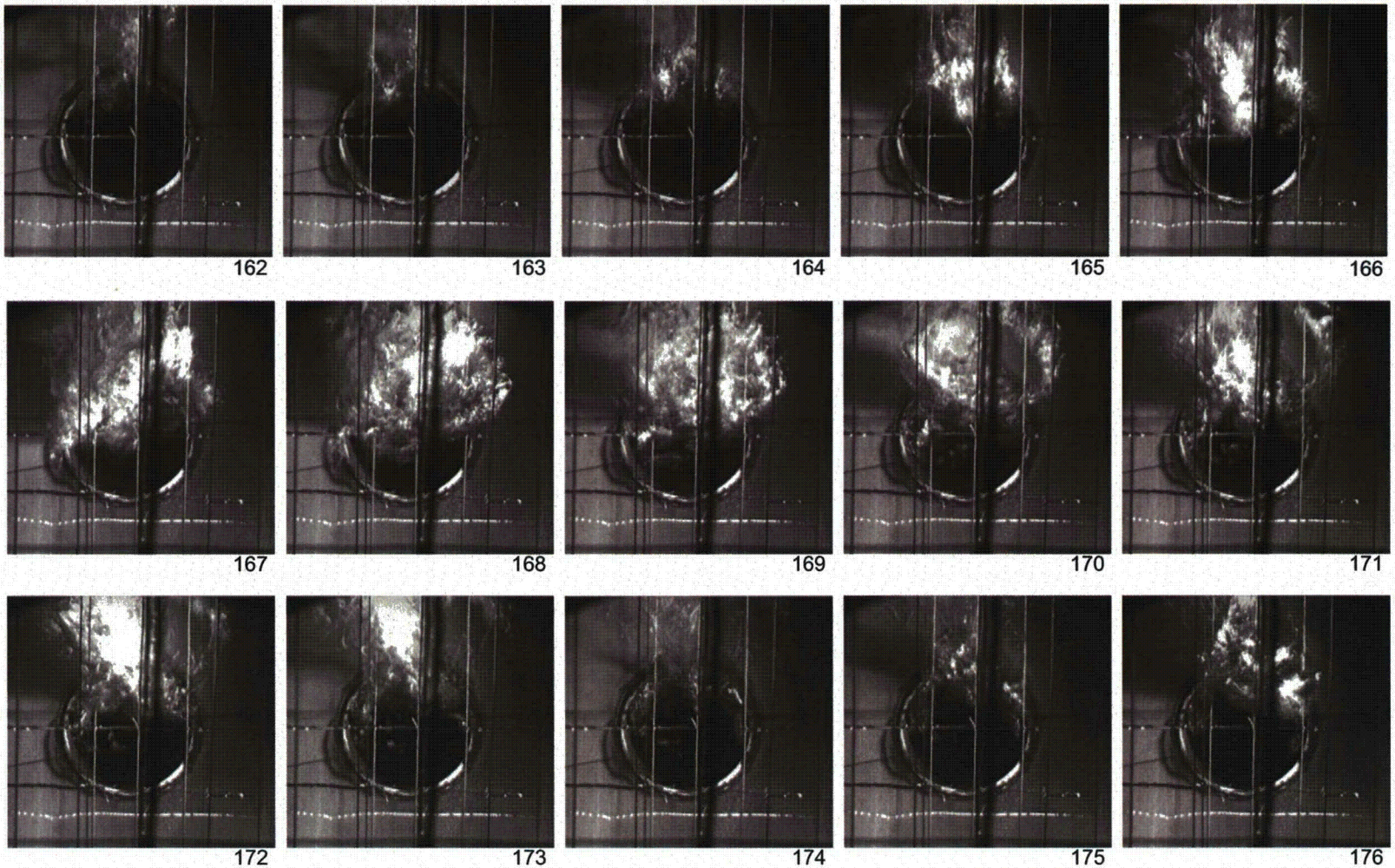

Camera is pointing downward to vent for 3-inch vent diameter case. Visualization at window 8.

Figure 7.80 Steam mass flow rate is 17.8 g/s with 0.5 % air. 0.033 seconds between frames.

7.4 References

Holland, F. A., & Bragg, R. (1995). Fluid Flow for Chemical Engineers. Retrieved, Oct. 2005. http://www.knovel.com/knovel2/Toc.jsp?SpaceID=10125&BookID=412

Norman, T. L., Park, H. S., Revankar, S. T., Ishii, M., Vierow, K., & Kelly, J. M. (2005). Steam-air mixture condensation in a subcooled water pool, Facility design and scoping tests. PU/NE-05-19.

Norman, T. L., Park, H. –S., Revankar, S. T., Ishii, M. & Kelly, J. M. (Nov. 5-10, 2006). Thermal stratification and mixing in an open water pool by submerged mixtures of steam and air. *In Proceedings of the IMECE 2006*, Chicago IL.